UNIVERSITÀ DEGLI STUDI DI SALERNO


UNIVERSITÀ DEGLI STUDI DI SALERNO

Dipartimento di Farmacia


PhD Program

in **Drug Discovery and Development**

XXXIII Cycle — Academic Year 2020/2021

***PhD Thesis in***

# *Application of Artificial Neural Networks to the design and optimization of superhydrophobic coatings*


Candidate

*Francesco Marrafino*

Supervisor

Prof. Dr. *Stefano Piotto*

PhD Program Coordinator: Prof. Dr. *Gianluca Sbardella*

*Dedicated to Simona, the beacon that lights my path.*

# ABSTRACT

Marrafino, Francesco, *Application of Artificial Neural Networks to the design and optimization of superhydrophobic coatings*, Ph.D. program in Drug Discovery and Development, 2021, University of Salerno.

Recently, considerable attention has been devoted to developing superhydrophobic surfaces due to their advantageous antimicrobial and self-cleaning properties. While significant effort has been devoted to their fabrication, very few polymeric superhydrophobic surfaces can be considered durable against externally imposed stresses. This work focuses on developing a coating with strong superhydrophobic properties and abrasion resistance, using a simple and scalable preparation process. Pyrogenic hydrophobic silica nanoparticles were used to confer superhydrophobic properties to the coatings. 450 samples were prepared using a layer-by-layer approach, deposing an epoxy resin or PDMS layer as adhesive on a substrate (PC/ABS), followed by one or more layers of silica nanoparticles or silica-resin mixed layers. The coating with the best properties shows a contact angle of 157° and a tape peeling grade resistance. The developed preparation method involves the spray deposition of a multilayer coating composed of four layers. Layers 1-3 are 1) silica nanoparticles, 2) epoxy resin, and 3) silica nanoparticles, followed by partial curing of the coating (15 minutes, 70°C); another silica layer is then sprayed on the surface and is cured for 10 minutes. In the second part of the work, the focus shifts to optimizing the coating and preparation process using Artificial Neural Networks. Given the high number of parameters involved, process optimization is a complex operation. Artificial Neural Networks are the best tool to deal with multivariate analysis problems. For this reason, data from all the prepared samples were collected into a dataset used to train a neural network capable of predicting the degree of hydrophobicity and abrasion resistance of a silica nanoparticles-based coating. The algorithms were used to prepare an optimized coating with a contact angle >160° and a high degree of abrasion resistance, currently under patent evaluation for potential application in antibacterial surfaces.

Finally, the application of Artificial Neural Networks to develop two bioinformatics predictive tools will be very briefly discussed.

KEYWORDS: Superhydrophobic, Artificial Neural Network, Antimicrobial, Antifouling, Self-cleaning, Surfaces.

# PREFACE

My three-year Ph.D. course in Drug Discovery and Development at the University of Salerno started in November 2017 under the supervision of Prof. Dr. Stefano Piotto as an industrial Ph.D. in the framework of "PON - Programma Operativo Nazionale Ricerca e Innovazione 2014-2020".

During the first year, the research mainly focused on developing a durable superhydrophobic coating to prepare antimicrobial surfaces. I worked on different preparation methods, used several materials, collected data, and built an extensive dataset.

I spent six months at SmartVASE Srl, a spin-off of the University of Salerno, learning the Artificial Intelligence techniques needed to optimize the coatings and the preparation processes utilizing the data acquired during the preparation of the coatings. The main objectives of the project were achieved ahead of time. A superhydrophobic coating with a fair degree of resistance to abrasion, and two predictive algorithms for the optimization of the process, were developed by the end of the second year. The algorithms have been used to obtain an optimized coating under patent evaluation at the time of writing. The acquired techniques were used to develop several projects, particularly for the development of two bioinformatics software applications based on Artificial Neural Networks, in collaboration with SoftMining Srl. The Artificial Intelligence applications ultimately led to identifying two selective antimicrobial peptides, under patent evaluation at the time of writing, which could be used as lead compounds for novel, selective antimicrobial drugs.

At the beginning of the third year of the Ph.D. program, I left for my six months internship at Prof. Caflisch's research group, University of Zurich, Department of Biochemistry, to further improve the Artificial Intelligence tools under development and to start the development of an AI-based software application for small molecules hit discovery and drug repurposing, interfacing classical *in silico* drug discovery methods with Artificial Neural Networks. I was at the beginning of my internship in Zurich when the pandemic of COVID-19 began, forcing a shift in the research efforts. Along with the aforementioned projects, which were slowed down due to quarantine and lockdown procedures, I collaborated with Prof. Caflisch's group in a project for the identification of SARS-CoV-2 $3CL^{pro}$ inhibitors, the main protease of the novel coronavirus responsible for viral replication. I was in charge of the virtual screening of a library of compounds already approved in therapy for other diseases. Of the 12 compounds that were ultimately selected, two showed potent inhibition of the virus at micromolar concentration.

**List of publications related to the scientific activity performed during the three years Ph.D. course in Drug Discovery and Development**

## Papers:

1) Diana, R.; Panunzi, B.; Concilio, S.; **Marrafino, F.**; Shikler, R.; Caruso, T.; Caruso, U. The Effect of Bulky Substituents on Two π-Conjugated Mesogenic Fluorophores. Their Organic Polymers and Zinc-Bridged Luminescent Networks. *Polymers* 2019, 11, 1379.
2) Diana, R.; Panunzi, B.; **Marrafino, F.**; Piotto, S.; Caruso, U. Novel Dicyano-Phenylenevinylene Fluorophores for Low-Doped Layers: A Highly Emissive Material for Red OLEDs. *Polymers* 2019, 11, 1751.
3) **Marrafino, F.**; Iannelli, P.; Di Martino, M.; Concilio, S.; Piotto, S. Superhydrophobic Coatings and Artificial Neural Networks: Design, Development and Optimization. In *Advances in Bionanomaterials II. BIONAM 2019. Lecture Notes in Bioengineering*; Piotto S., Concilio S., Sessa L., Rossi F., Eds.; Springer, Cham., 2020; pp 32–40.
4) Sessa, L.; Nardiello, A.M.; Di Martino, M.; **Marrafino, F.**; Iannelli, P. Molecular Dynamics Simulation of Antimicrobial Permeable PVC-Based Films. In *Advances in Bionanomaterials II. BIONAM 2019. Lecture Notes in Bioengineering*; Piotto S., Concilio S., Sessa L., Rossi F., Eds.; Springer, Cham., 2020; pp 111–119.
5) Di Martino, M.; **Marrafino, F.**; Diana, R.; Iannelli, P.; Concilio, S. Fluorescent Probes for Applications in Bioimaging. In *Advances in Bionanomaterials II. BIONAM 2019. Lecture Notes in Bioengineering*; Piotto S., Concilio S., Sessa L., Rossi F., Eds.; Springer, Cham., 2020; pp 243–258.
6) Pohl, M. O.; Busnadiego, I.; **Marrafino, F.**; Wiedmer, L.; Hunziker, A.; Fernbach, S.; Omori, E.; Hale, B. J.; Caflisch, A.; Stertz, S. Combined computational and cellular screening identifies synergistic inhibition of SARS-CoV-2 by lenvatinib and remdesivir. *bioRxiv 2021.03.19.435806.*

## Patents:

1) **Marrafino, F.**; Piotto, S.; Concilio, S.; Sessa, L. Superhydrophobic, self-cleaning coating optimized by means of Artificial Intelligence and methods for producing the same. EP patent, 2021. *Patent application under evaluation.*
2) Piotto, S.; **Marrafino, F.**; Concilio, S.; Sessa, L. Novel selectively targeted antimicrobial peptides. EP patent, 2021. *Patent application under evaluation. Patent evaluation consulting application number 37760CFD.*
3) Piotto, S.; **Marrafino, F.**; Concilio, S.; Sessa, L. Novel selectively targeted antimicrobial peptides and use thereof. EP patent, 2021. *Patent application under evaluation. Patent evaluation consulting application number 7179B419.*

## Conference proceedings:

**Marrafino. F**; Presented at the BIONAM 2019, 3rd International Conference on Bio and Nanomaterials, Genoa (IT). MSC cruise, Mediterranean Sea, September 29 – October 3, 2019.

# Table of Contents

# INTRODUCTION

# CHAPTER 1
# Superhydrophobic materials

### 1.1 Superhydrophobic materials

Nature has always been an inexhaustible source of inspiration for the development of science and technology. Many functional biological surfaces in nature, e.g., lotus leaves, rose petals, butterfly wings, or water striders, have unique wetting properties[1]. Superhydrophobic (SH) materials draw inspiration from these surfaces.

Surfaces with unique wetting characteristics, such as lotus leaves (*Nelumbo nucifera*), have attracted significant scientific interest thanks to their peculiar self-cleaning capabilities. The properties of lotus leaves are due to their low surface energy and the hierarchical roughness granted by micro/nanostructures[2] (Figure 1), developed on two overlapping layers of the leaf[3]. The lower layer of the leaf consists of epidermal cells forming papillae or protuberances of varying height but similar shape, approximately 10-15 μm apart; the upper layer is characterized by nanometer-sized hydrophobic wax protuberances covering the lower layer. The surface roughness caused by unique micro/nanostructures and the surface chemistry are two significant factors that affect surface wetting properties[4].

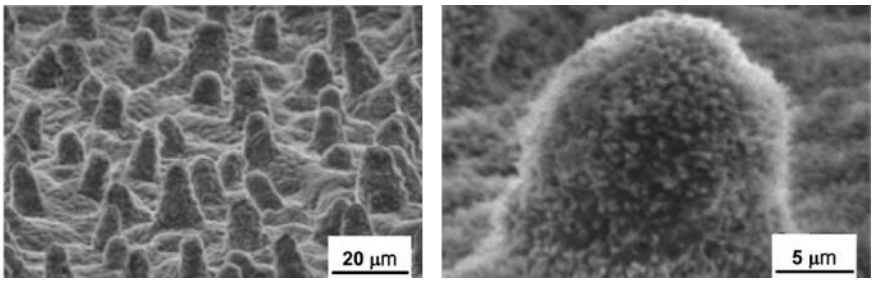


*Figure 1: Scanning electron microscope (SEM) micrographs of Nelumbo nucifera (lotus) leaf surface show hierarchical roughness[2].*

When raindrops fall on lotus leaves, they do not penetrate the roughness but immediately behave like spheres that roll rapidly over the surface, picking up dirt and debris (Figure 2) and granting lotus leaves their characteristic self-cleaning property. Self-cleaning surfaces show non-wetting properties owing to a water contact angle greater than 150° and an effortless rolling-off of water droplets. The occurrence of this effect, called the "lotus effect", is due to the grooves between the papillae of the leaf surface, which are too small for dirt particles to enter, so they allow the dirt to remain suspended on the papillae and, if the surface is sloping, sliding off. These grooves give the surface of the lotus leaf a marked roughness, and for these characteristics, the lotus leaf is classified as a superhydrophobic surface[5].

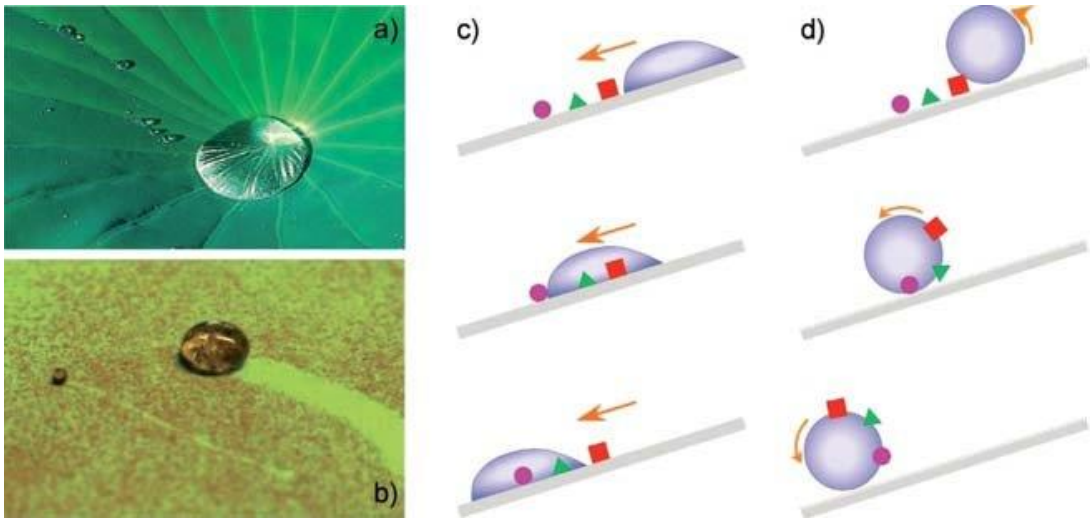


*Figure 2: a) Water drops on the surface of a lotus leaf; b) water drop cleaning a surface with self-cleaning properties; c) schematic representation of a drop sliding on a dirty, non-rough surface; d) schematic representation of a drop sliding on a dirty, rough surface*[6].

Lotus leaf with naturally developed superhydrophobic and self-cleaning effects has received significant interest from researchers, and led to biomimicking in coatings to develop materials with self-cleaning[7-13], anti-corrosion[14-18], anti-icing[10,19-23], anti-fogging[7,10,24-28], anti-fouling[11,22,29-32], and other properties[30,33-36].

In the last 15 years, the interest in SH materials has grown considerably[33], and today it is an even more interesting topic, with potential application to fight the spread of epidemics like COVID-19[37-39]. A query with the keyword "superhydrophobic" on ScienceDirect would give only 38 results in 2005, with the number slowly increasing to less than 300 references in 2010. The number of published articles steadily increased, mirroring the continually rising interest in the field, with more than two thousand published articles in 2020 only (Figure 3).

The increasing need for antibacterial materials has focused the attention of biomedical research on superhydrophobic surfaces[39,40]. For SH materials to see a practical application in the biomedical sector, however, it is necessary that the main limitations, first of all durability, as will be discussed later, are overcome. This work follows this trend, with the main objective of obtaining a surface with strong SH characteristics, therefore self-cleaning and antibacterial, with increased resistance to external stress for biomedical field applications.

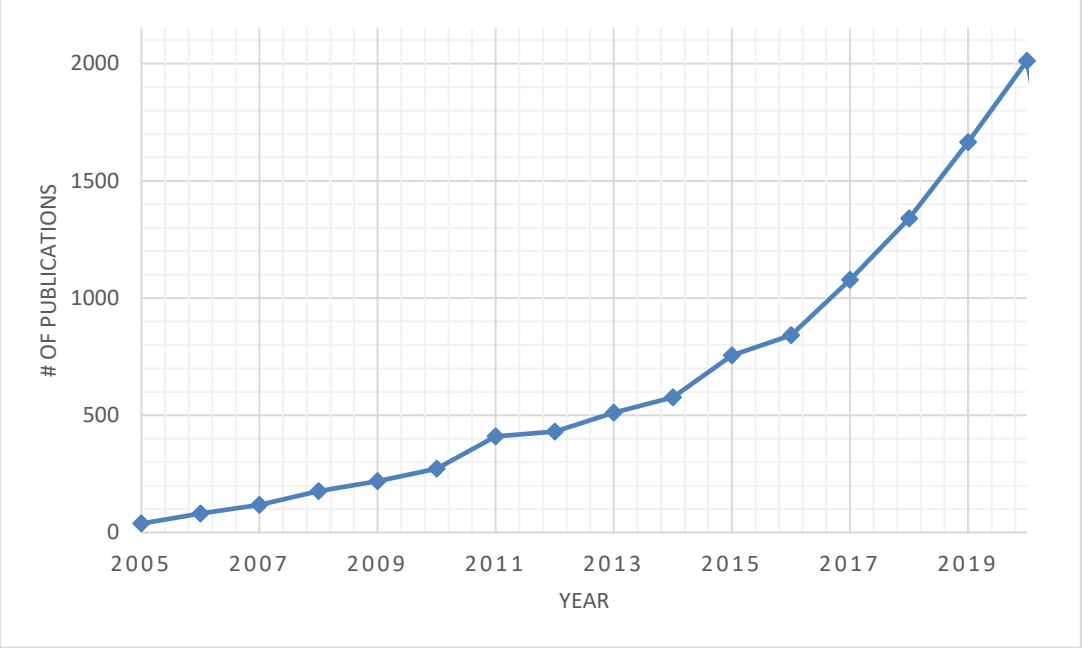


*Figure 3: Number of publications on ScienceDirect for the years 2005-2020 using the keyword "superhydrophobic" for the query.*

To be defined as superhydrophobic, a surface must have a water contact angle (CA) higher than 150°[10]. Superhydrophobicity is based on two principles[2,41]: low surface energy of the solid surface and increased surface roughness.

### 1.2 Wettability models and contact angle

A fundamental property of SH surfaces is wettability, i.e., the degree to which a liquid placed on a surface can adhere to the surface itself and the surrounding air. Wettability is defined as the ability of a liquid to maintain contact with a solid surface[42]. It mainly depends on the terminal groups of the molecules at the interface of the solid and the structuring of the surface[43] and is controlled by the balance between the intermolecular interactions of the adhesive type (liquid to surface) and cohesive type (liquid to liquid) (Figure 4).

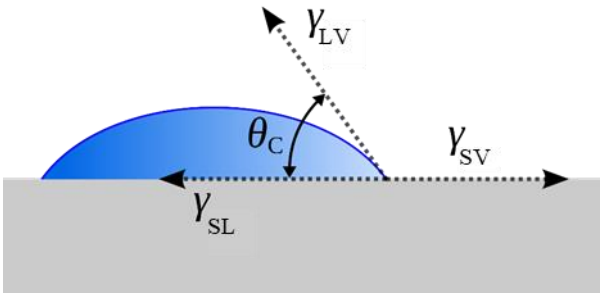


*Figure 4: Scheme of a liquid droplet showing a contact angle $\theta_C$. $\gamma_{SV}$ is the solid-gas interfacial tension, $\gamma_{SL}$ is the solid-liquid interfacial tension, and $\gamma_{LV}$ is the liquid-gas interfacial tension[43].*

Surfaces can be classified, based on wettability, into hydrophilic or hydrophobic by two basic parameters: static contact angle and roll-off angle.

### 1.2.1 Static contact angle

The static contact angle (or contact angle, CA) is defined as the angle between the solid-liquid tension direction and the liquid-vapor tension direction, tangent to the outer surface of the droplet, with the vertex at the three-phase liquid-solid-vapor point (Figure 4). The angle is measured immediately after the liquid droplet has been deposited on the substrate to be examined, and thermodynamic equilibrium has been reached between the solid, liquid, and vapor phases. Therefore, the static contact angle is an effective measure of the hydrophilicity or hydrophobicity of any surface: the greater the contact angle, the more spherical the droplet, and the more hydrophobic the surface; the smaller the contact angle, the more flattened the droplet and the higher the hydrophilicity of the material.

Surfaces with different wettability levels show different contact angle ranges (Figure 5). This angle depends on several factors, including surface energy and surface roughness. If the liquid wets the surface (hydrophilic surface), the value of the static contact angle is $0 \leqslant \theta \leqslant 90°$, whereas if the liquid does not wet the surface (hydrophobic surface), the value of the contact angle is $90° < \theta \leqslant 180°$. Surfaces with a contact angle of less than 5° are called superhydrophilic, while surfaces with a contact angle between 150° and 180° are called superhydrophobic[44].

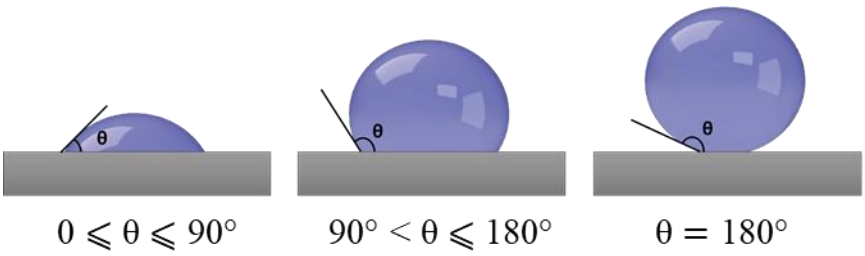


*Figure 5: Schematic representation of the profile of a water droplet on a surface. Hydrophilic surfaces have contact angle θ: $0 \leqslant \theta \leqslant 90°$; hydrophobic surfaces have contact angle θ: $90° < \theta \leqslant 180°$. θ = 180° represents a perfectly non-wettable surface[45].*

The contact angle for which the system assumes the absolute minimum of surface free energy is called the equilibrium contact angle. Due to the different initial conditions (e.g., the way the droplet is deposited or the inclination of the surface), many different metastable equilibria arise, to which the droplet shape can remain bound and which correspond to different values of contact angles. The highest value is usually referred to as the advancing

contact angle and the lowest value as the receding contact angle (dynamic contact angle, Figure 6).

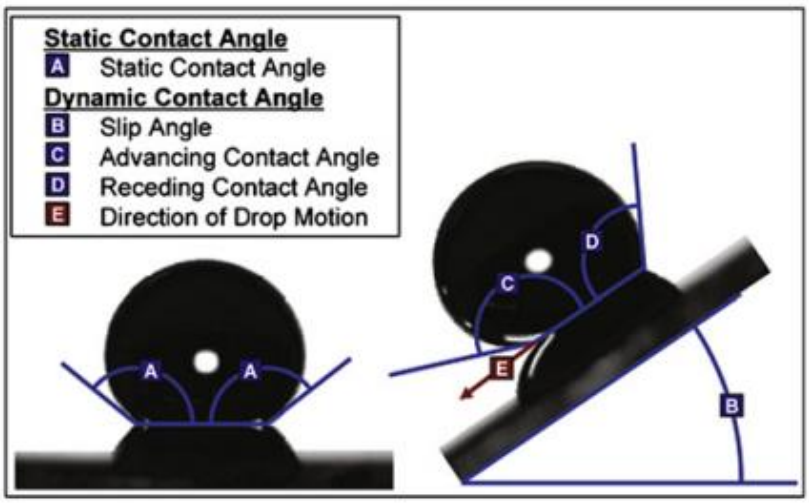


*Figure 6: Diagram of static contact angle and dynamic contact angle[46,47].*

When the value of the recession contact angle is different from the advancing contact angle, contact angle hysteresis (CAH) occurs. The latter is a measure of energy dissipation during the motion of a droplet along a solid surface. At a low CAH value, droplets can roll past the surface, facilitating the removal of contaminant particles. Surfaces with CAH less than <10° are called self-cleaning surfaces[13,44].

### 1.2.2 Roll-off angle

While the static contact angle provides information about the static equilibrium of the surface, it is essential in some situations that the liquid can flow away quickly. The angle at which a water drop rolls off a tilted surface is known as the roll-off angle ($\theta_R$)[48,49]. The roll-off angle is the minimum angle to which a surface must be tilted for the droplet to start moving. This measurement can also be used to classify surfaces, but the result does not necessarily coincide with what is obtained by measuring only the contact angle. SH surfaces show a static contact angle ≥ 150° and a roll-off angle ≤ 10°.

To date, however, there is still no set of requirements that represent the necessary and sufficient conditions for a surface to exhibit SH characteristics. Some studies have highlighted the main properties that an SH surface should possess to be defined as such. The main features are the very high static contact angle and a low CAH[22]. These characteristics would allow the droplet to bounce off the surface and then roll away. Another necessary characteristic, as mentioned above, is the presence of hierarchical surface roughness, characterized by geometric micro-imperfections intrinsic or consequent to mechanical

processing; these can take the form of grooves, scratches, or roughness of variable shape, depth, and direction[50].

### 1.2.3 Young's model

Young's model is used to describe the wettability of an ideal surface[51], assuming it is solid, smooth, rigid, chemically homogeneous, insoluble, and nonreactive[52] (Figure 8). The contact angle ($\theta$ between $\gamma_{SL}$ and $\gamma_{LV}$) can be defined by Young's equation (Equation 1):

$$\cos\theta = \frac{\gamma_{SV} - \gamma_{SL}}{\gamma_{LV}}$$

*Equation 1: Young's model equation.*

Where $\gamma_{SV}$ is the surface tension between the solid and vapor phases, $\gamma_{SL}$ between the solid and liquid phases, and $\gamma_{LV}$ between the liquid and vapor phases. $\gamma$ is also often referred to as the surface energy or Gibbs surface free energy, which is the amount of energy useful for breaking chemical bonds. Molecules that do not form chemical bonds on the surface tend to have a higher surface free energy than those that form chemical bonds more readily either with other molecules or with the surface itself.

For the study of SH surfaces, the surface tension corresponds numerically to the surface free energy per unit area under constant pressure and temperature conditions. Furthermore, a fundamental requirement for surface tension and surface free energy to be considered numerically equivalent is to assume no adsorption at the interfaces. For this reason, as shown in Figure 7, solid surfaces with very low surface tension will present a very low degree of wettability and consequently can be considered hydrophobic or superhydrophobic depending on the contact angle[43,44].

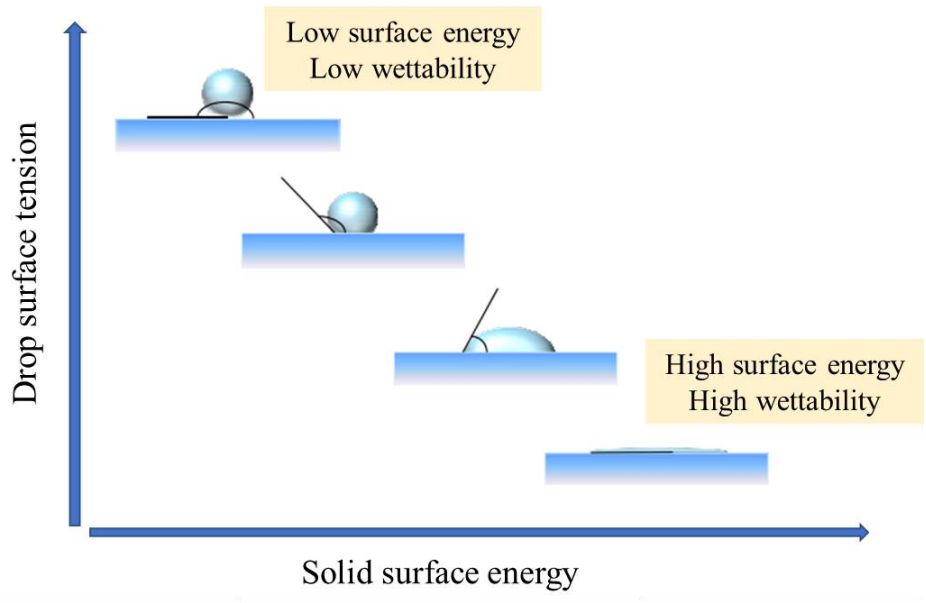


*Figure 7: Correlation between solid surface energy and droplet surface energy resulting in a difference in wettability.*

Surface tension is used for liquids, while surface free energy is a more general term for solids. Young's equation is mainly used for ideal solid surfaces. For heterogeneous surfaces, the three phases at the interface (solid, liquid, and vapor) and the surface roughness should be considered.

### 1.2.4 Wenzel and Cassie-Baxter models

As described above, Young's equation applies only to perfectly smooth and rigid surfaces, referred to as ideal surfaces. In nature, surfaces are far from this condition, so the Wenzel and Cassie-Baxter models describe real systems that are not perfectly smooth and rigid[53].

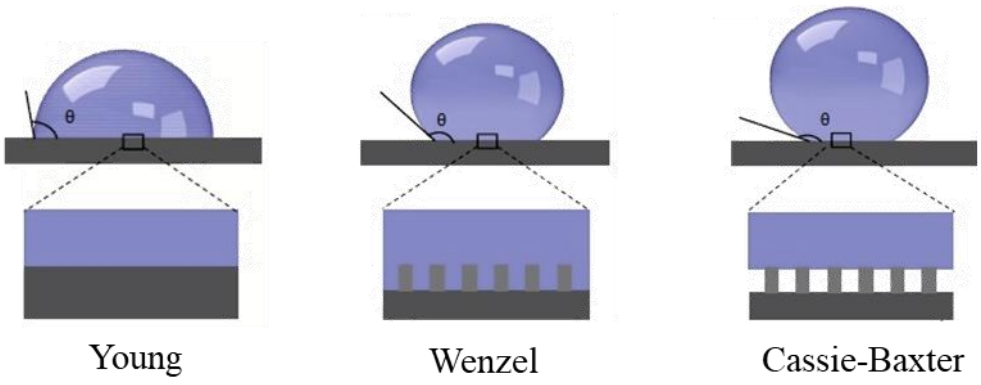


*Figure 8: Young's, Wenzel's, and Cassie-Baxter's models representation. Young's model represents the wetting of an ideal smooth surface; Wenzel's model represents the homogeneous wetting of a rough surface; Cassie-Baxter's model describes the wetting of a heterogeneous rough surface[45,53].*

If a drop is deposited on a rough horizontal surface, it will be necessary to consider the unevenness and defects of various types of the surface itself responsible for the different degrees of wettability of the surface. Generally, the projected (or apparent, or geometric) surface area is defined as the projection of the drop on the geometric plane of the surface, i.e., the area that macroscopically appears to be wetted by the drop. On the other hand, the true surface area is defined as the surface area wetted by the drop, considering its roughness. The parameter describing this system is the ratio between the true and projected surface area, denoted by *r*. According to Wenzel's model (Figure 8), the liquid droplet is in contact with all points of the underlying surface, and the true surface area is greater than the apparent surface area, i.e., $r > 1$. The extent of the static contact angle varies according to Wenzel's equation (Equation 2):

$$\boldsymbol{\cos\theta_W = r * \cos\theta}$$

*Equation 2: Wenzel's model equation[53].*

Where θ is Young's angle (defined by Young's equation, Equation 1) and $\theta_W$ is Wenzel's angle (or apparent angle). Wenzel's model describes the homogeneous wetting of a surface.

In Cassie-Baxter's model (Figure 8), on the other hand, the droplet of liquid does not wet the entire underlying surface but settles only on the peaks of the surface roughness, leaving trapped air between them. The surface behaves as a heterogeneous surface composed of its material and air. Cassie-Baxter's model holds true even for heterogeneous surfaces composed of multiple materials. The static contact angle for Cassie-Baxter's equation is (Equation 3):

$$\boldsymbol{\cos\theta_C = f1 * \cos\theta_1 + f2\ \cos\theta_2}$$

*Equation 3: Cassie-Baxter's model equation[53].*

Where $\theta_C$ is the static contact angle of the liquid on the heterogeneous surface composed of the fraction $f_1$ of one chemical group and $f_2$ of the other, $f_1 + f_2 = 1$, while $\theta_1$ and $\theta_2$ are the static contact angles of the liquid on pure and homogeneous portions of 1 and 2, respectively[54]. Cassie-Baxter's model represents SH materials wetting and is defined as "fakir" state.

### 1.2.5 Cassie-Wenzel transition (wetting transition)

Energy barriers play a crucial role in both chemistry and physics, including the phase transition. It is because of an energy change that a fundamental transition for the wettability of a surface can occur: the transition from the Cassie-Baxter wettability state to the Wenzel wettability state[55] (Figure 9).

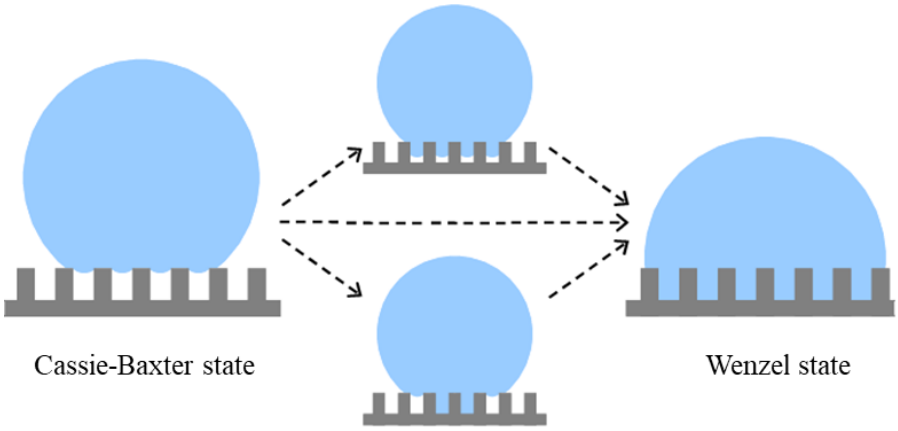


*Figure 9: Transition from the Cassie-Baxter state to the Wenzel state on rough surfaces[56].*

Typically, in the Cassie-Baxter state, the air is trapped between the grooves or scratches in the surface, resulting in a greater contact angle; conversely, in the Wenzel state, liquid enters the grooves resulting in greater wettability of the surface due to the increased contact area. The Cassie-Baxter is a metastable state that competes energetically with the Wenzel state[57]. To lock a surface into the Cassie-Baxter state, the energy barrier should be high enough to slow down the transition from the metastable state to the Wenzel state. An irreversible transition toward the more stable Wenzel state may occur. External stimuli such as mechanical impact, compression, or thermal perturbation trigger this transition. It has been shown that this transition occurs when the energy barrier of the Cassie-Baxter state is of the same order of magnitude as the external forces applied to the surface, especially pressure[55]. This transition is significant for SH materials. As this transition occurs, SH surfaces gradually lose their extreme water repellency features, eventually leading to the loss of the hydrophobic features and thus increasing the wettability of the material[56]. Aging and external stimuli can induce this transition in SH materials, posing a significant limit for the development of these surfaces.

## 1.3 Preparation methods

A vast array of techniques has been used to fabricate SH surfaces, such as lithographic processes, sol-gel methods, solvent casting, chemical vapor deposition (CVD), chemical

etching, electrospinning, dip-coating, and templating. These techniques show many drawbacks arising from complex and time-consuming planning procedures and costly facilities that prohibit such strategies from being implemented on a wide scale. Low-cost, easy-to-use methods for comprehensive applications are therefore required. Brush-coating, dip-coating, and spray-coating could meet the specifications. However, the mechanical softness of the surface microstructures restricts the application of SH coatings[58]. The major challenge is the design of a simple, scalable method leading to mechanically robust and chemically inert layers, and an even more significant challenge is the design of mechanically and thermodynamically durable, defect-tolerant SH surfaces[10,33,59].

Numerous scientific literature reviews describe the many preparation methods used to prepare SH coatings[10,20,22,33,34,57,60-62], and countless examples could be reported. Preparation methods are broadly divided into two main categories: top-down and bottom-up methods.

Top-down methods employ nanofabrication tools controlled by external experimental parameters to create nanoscale devices with desired shapes and characteristics starting from larger dimensions and reducing them to the values required to structure the material. These methods include but are not limited to plasma or chemical etching, laser patterning, templating, photo- and soft lithography techniques[61]. The main advantage of top-down methods is that they allow the preparation of surfaces with exact topography, resulting in excellent SH properties. These methods, however, are costly, the surfaces have little resistance to mechanical stress, and cannot be applied on a large scale.

The bottom-up approach aims to create complex, multilevel structures at the nanoscale through molecular or atomic components. Various materials can be deposited with this approach, including electrospinning techniques, sol-gel processes, and layer-by-layer deposition[61,63]. Bottom-up methods produce surfaces with good roughness, although not as precise as top-down methods, with the advantage that they are generally inexpensive, allow the preparation of more resistant surfaces, and are more easily scalable at the industrial level. Specifically, for the purpose of this work, i.e., the preparation of a durable SH coating using inexpensive and easily industrially scalable methods, layer-by-layer deposition methods will be used. These techniques have been widely employed to fabricate SH surfaces[60]. Several nano/micro-structures can be prepared using layer-by-layer techniques, a fundamental feature for SH coatings. Many raw materials can be used to fabricate multilayer assemblies: water-soluble polyelectrolytes, polymers and copolymers, and bio-macromolecules[63,64]. Layer-by-layer methods include dip-, spin- and spray-coating techniques.

### 1.4 Applications in the biomedical field

Thanks to their water-repellent and self-cleaning properties, superhydrophobic surfaces have a high potential for application in life sciences[10]. The possibilities are plenty, and a vast range of scientific papers describing possible uses of SH in the biomedical field are available.

Falde et al.[52] investigated the performance of SH surfaces in protein adsorption, blood compatibility, and bacterial interaction for diagnostic applications, drug delivery, and antibacterial surfaces. Ciasca, G. et al.[57] focused on applications involving extremely small quantities of molecules for high throughput cell and biomaterial screening. SH surfaces have great potential for application in microfluidics, microarrays, and micro-analytical devices, as discussed by Gogolides et al.[65]. Lima, A. C., and Mano, J. F. extensively described how SH surfaces interact with proteins and cells[45,66]. The application of advanced materials with antibacterial properties has also been studied extensively, and the design and preparation of effective antibacterial surfaces is still a very high priority[22,29,40,67].

As already mentioned, SH materials showed excellent self-cleaning[68], anti-biofilm, and anti-fouling properties[69-71], preventing protein adsorption, eukaryotic cellular adhesion and proliferation, platelet adhesion/activation, and blood coagulation[45,66], showing a high potential for application in many industrial fields and life sciences. SH materials would find possible use in developing antibacterial surfaces, diagnostic supports, textiles and nonwovens, antibacterial and anti-clogging implantable biomedical devices, and several other additional prospective uses. However, the effective application of SH surfaces in the biomedical field depends on enhancing existing surfaces to make them more robust and stable.

#### 1.4.1 Antibacterial surfaces

Among the many possibilities, perhaps the one of greatest interest is the development of antibacterial surfaces[29,44,72]. Pathogenic bacteria can cause severe infections and failure of biomedical or prosthetic devices. The growing use of antibiotics has turned infectious agents immune to medications, and new approaches to deal with them need to be developed[73,74]. Interest in antibacterial surfaces grew further following the outbreak of the COVID-19 pandemic, which greatly increased awareness of the need to prevent the spread of microorganisms[39]. The bacteria adhesion and proliferation on surfaces and the subsequent biofilm formation pose challenges in healthcare and industrial applications, such as medical

implants, petroleum pipelines, aquatic flow systems, textiles, food industry machinery[44,75,76], and public health.

There are two approaches to developing a bactericidal or bacteriostatic surface: the introduction of biocidal substances on the polymer surface or the development of a material unsuitable for the growth of microorganisms[67]. The former type materials are the most widespread[76-81] and require extreme caution to prevent the release of biocides into the environment. On the other hand, SH surfaces could offer an excellent solution to the limits of these methods, falling in the second category.

Classically, bacterial cells are treated as inert particles, and it is assumed that bacterial adhesion to a flat surface is determined by van der Waals interactions and repulsive interactions with the electrical bilayer of the cell and the surface. However, the interactions between cells and materials are much more complex, involving highly dynamic cells, an environment with many variables, and material surfaces affected by many different properties.

The formation of a mature biofilm caused by bacteria adhesion is generally divided into two stages (Figure 10). During Stage I, bacteria establish the first interactions with the surface materials; this Stage is rapid and reversible. Stage II involves specific and nonspecific interactions between the proteins on bacterial surface structures (pili or fimbriae) and the surface molecules; this Stage is generally considered irreversible.

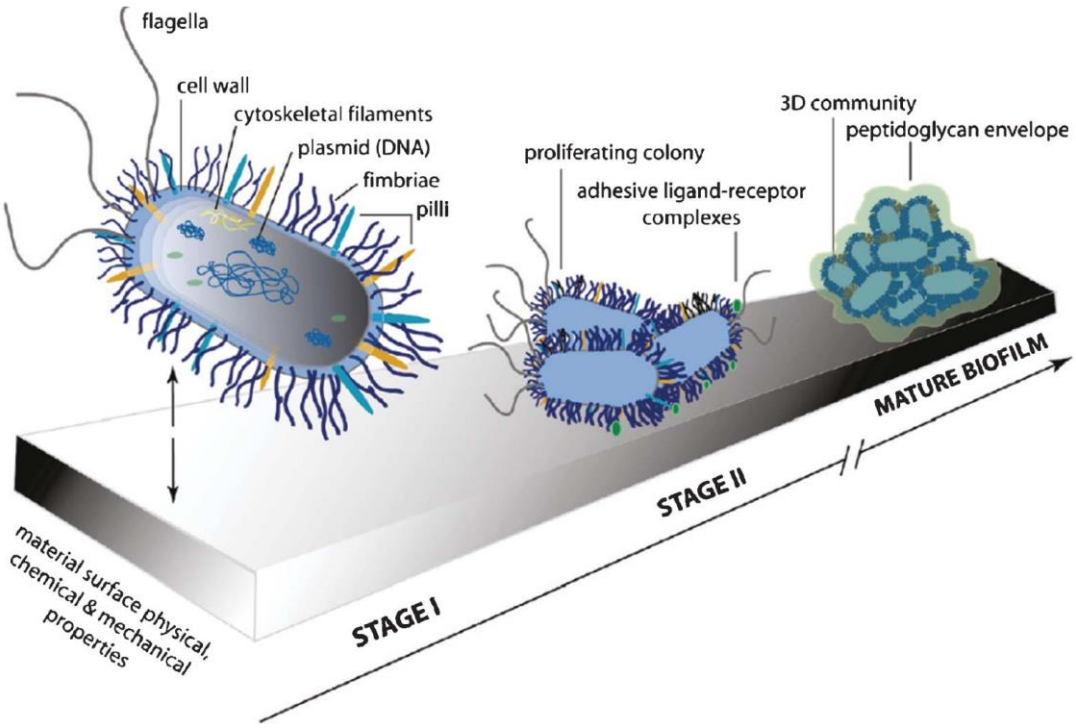


*Figure 10: Schematic representation of the two stages of bacterial biofilm formation[67].*

Bacterial adhesion to hydrophobic surfaces has been extensively studied and extended to superhydrophobic surfaces. Several researchers have investigated the possibility of using superhydrophobic surfaces to reduce bacterial adhesion[10,22,29,44,52,71,72,82].

The adhesion of bacteria to surfaces with different surface free energies has been extensively studied, and it has been shown that surface free energy can significantly affect the adhesion of bacteria. Surfaces with low surface energy have been shown to prevent bacterial adhesion effectively[83-85].

Several studies have also investigated surface wettability on bacterial adhesion, showing a good relationship between the two phenomena and that bacteria are attracted to hydrophilic surfaces with a contact angle of 40°-70°[86-90]. Low surface energy and very low wettability of SH surfaces are the main features that prevent bacterial adhesion.

Reduced protein adsorption also plays a role in antibacterial activity. Bacterial adhesion is established by different interactions, which can be nonspecific or specific, e.g., adsorbed protein membrane[29]. The formation of protective layers can promote bacterial adhesion and biofilm formation. It is generally believed that proteins adsorb more favorably on surfaces with a contact angle of 60-90° and hydrophobic surfaces[91]. On the other hand, superhydrophobic surfaces show low protein adsorption and easy protein removal, resulting in low bacterial adhesion[92-96].

### 1.5 Limitations of superhydrophobic materials

At the time of writing, the durability of most superhydrophobic surfaces still poses a great limit in their development. SH materials with poor durability tend to lose their extreme water-repellency properties even upon application of small stress. Faulty durability is due to either topography failure, failure of the low-surface energy coating, or failure of both[10]. The loss of SH features is described by the Cassie-Wenzel transition, as previously discussed.

SH surfaces are found in very a limited range of applications, and their use for surface development has been significantly slowed down due to short lifespans, low mechanical strength, inability to maintain surface properties under extreme environmental conditions, and due to difficult manufacturing processes involving the use of harmful chemicals, high costs, and long processing times[33], regardless of the high potential of application.

For these reasons, the research and production of surfaces with SH features and the improvement of the currently existing techniques are attracting great interest from the scientific community. The use of organic solvents and fluorochemicals or low volatile organic compounds should be minimized to avoid any possible environmental health

hazards. Novel preparation methods with cost-effective and high quality must be a continuous target for researchers and industry. However, the durability of superhydrophobic surfaces is considered the most important aspect that should be further strengthened in future works in this field. The short lifespan of these materials prevents any practical use, both in industrial and biomedical fields[10,33]. Finally, there are still no clear criteria for defining SH materials durability. For this reason, and thanks to the ever-growing attention that these materials are gathering from the scientific community, future research efforts from academia and industry will surely focus on the comprehension of all mechanisms involved and the testing methods in order to establish specific characterization standards[10,97].

To tackle all these issues, the main objective of this work is to obtain a durable superhydrophobic coating with self-cleaning and antibacterial properties for biomedical applications and an efficient, low-cost, easy-to-apply, and industrially scalable preparation method.

# CHAPTER 2
# Artificial Neural Networks

## 2.1 Machine Learning and Artificial Neural Networks: an overview

The concepts of Artificial Intelligence (AI), Machine Learning (ML), and Artificial Neural Networks (ANNs) are now known to the general public thanks to the attention that these methods have received in recent years. As technology has advanced ever faster, interest in and use of these methods has grown exponentially, and they are now applied in a wide range of fields, including speech and facial recognition, self-driving cars, email spam filtering, optical character recognition, weather and finance forecasts, smart houses, medical imaging and diagnosis, drug discovery and bioinformatics, and even creative arts[98]. The great success of these methods and their application in many areas of science is also linked to the availability of effective and easy-to-use software, which does not require in-depth knowledge of programming languages to train a neural network and obtain valid results. The growth of these methods is closely related to the increasing availability of big data and the ever-growing ability to organize and manage large datasets, all thanks to the increasing performance of computers, both in home-computing and high-performance computing. A plethora of articles, books, and courses are available in the literature that analyzes and deepens all aspects of this vast Computer Sciences branch. In this chapter, a brief overview of the main concepts related to Artificial Neural Networks is given. Artificial Intelligence methods were used in this work for the optimization of superhydrophobic coatings and the development of AI-based software for drug discovery.

## 2.2 Machine Learning

Machine Learning (ML) is a branch of Artificial Intelligence (AI), which studies computer algorithms that auto-improve by learning from experience[99]. Arthur Samuel, a pioneer in AI and computer gaming, coined the term *machine learning* in 1959[100].

In general, machine learning aims to understand the structure of data and fit that data into a model that can be understood and used. Machine learning algorithms create models based on sample data, known as training data, making forecasts and decisions without being specifically programmed. ML can also be defined as the process of solving a practical problem by collecting a data set and algorithmically building a statistical model from that data set to solve a practical problem. Therefore, ML involves computers learning from data provided so that they carry out certain tasks.

In computer programming, it is possible to program algorithms defining all the steps required that the machine should execute to perform a problem-solving task. In traditional

computing, the programming can be carried out entirely by humans, and no learning is required from the machine. For more advanced tasks, however, the creation of all the needed algorithms can be extremely challenging. In these cases, it can be more effective to guide the machine to develop its algorithms, rather than programming every step that the computers should perform. ML facilitates computers in building models from sample data in order to automate decision-making processes[101].

ML is a rapidly evolving science and has entered almost every technology field. Some of its applications are facial recognition software, optical character recognition (OCR), recommendation engines, or self-driving vehicles. ML methods have also been widely used in life sciences, medical imaging[102-104], electronic health records (EHR) for personalized medicine[105-107], drug design and bioinformatics[108-113], neuroscience[114], medical devices[115], and diagnosis[116].

### 2.2.1 Machine Learning Methods

In ML, learning tasks are generally divided into three broad categories: supervised, unsupervised, and reinforcement learning. These categories are based on how the learning signal is received or how feedback is given to the system.

- In supervised learning, example input and output data are appropriately labeled by humans and are used to train the machine to learn a general rule that maps inputs to outputs.
- In unsupervised learning, the learning algorithm does not have access to labeled data. With this method, the algorithms have to find structure within input data by themselves. Unsupervised learning could be used as a tool for solving a problem or discovering hidden patterns in data.
- In reinforcement learning, a software application has to perform a given goal by interacting with a dynamic environment. Performance feedback is given as the algorithms navigate the problem space, maximizing the rewards received when a correct operation is performed.

ML approaches are in continuous development and improvement. Some of the most used methods are k-Nearest Neighbor, Decision Trees, Linear and Logistic Regression, Naive Bayes, Support Vector Machine, Artificial Neural Networks, and Deep Learning.

Both supervised and unsupervised learning have their specific uses, varying according to the type of data available (discrete or continuous). The most common general applications of these two learning methods are generalized in Table 1.

| | **Supervised Learning** | **Unsupervised Learning** |
|---|---|---|
| **Discrete data** | Classification or categorization | Clustering |
| **Continuous data** | Regression | Dimensionality reduction |

*Table 1: General applications of supervised and unsupervised learning.*

#### 2.2.1.1 Supervised learning

In supervised learning, the computer is given sample labeled input data with the desired output. This method aims to learn by comparing the actual output with the trained data, detecting errors, and adjusting the model accordingly. Therefore, in supervised learning, patterns are used to predict label values on additional unlabeled data.

In supervised learning, classification is typically used to assign input-output labels, and classification algorithms are used to predict or classify discrete values (e.g., true/false, spam/not spam, cat/dog, etc.). On the other hand, regression is used to assign input data to continuous output, and regression algorithms are used to predict continuous values (price, age, salary, etc.). Because regression statistics can predict the dependent variable when the independent variable is known, regression provides forecasting power.

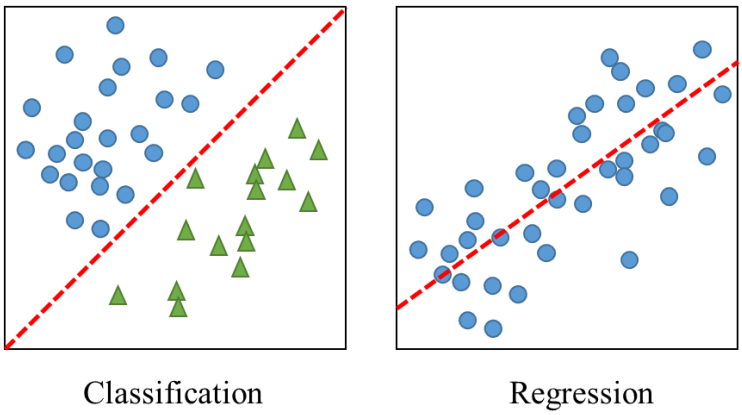


*Figure 11: Schematic representation of classification and regression algorithms. Classification is used to classify discrete data, while regression is used to predict continuous data.*

Popular supervised learning algorithms are Logistic Regression, Artificial Neural Networks, Naive Bayesian, Random Forests, and Support Vector Machines. The aim is to

find relationships or structures in the input data to efficiently generate the correct output in regression and classification. The training data completely determine the correct output. Noise or mislabeling of data reduces the effectiveness of the trained model.

In supervised learning, model complexity refers to the complexity of the function that the machine is trying to learn, similar to the degree of a polynomial. The nature of the training data generally determines the appropriate level of model complexity. A low-complexity model is preferred if the dataset is small or unevenly distributed across several possible scenarios. In this case, a high complexity model will overfit when applied to a small number of data points. Overfitting refers to training a feature that fits the training data very well but cannot be generalized to other data points.

#### 2.2.1.2 Unsupervised learning

In unsupervised learning, the data are unlabeled, so the learning algorithm must find matches between input data only. Because unlabeled data is more common than labeled data, machine learning techniques that enable unsupervised learning are particularly valuable. Unsupervised learning can discover hidden patterns in a data set or can be used for feature learning, which allows a computer to automatically discover the representations needed to classify raw data. Without getting the right answer, unsupervised learning techniques can look at complex, unstructured data to find potential meanings or correlations. Unsupervised learning is often used to detect anomalies, such as fraudulent credit card purchases or recommendation systems that suggest what products to buy next. A classic example in unsupervised learning is feeding unlabeled cat images to an algorithm that finds matches and classifies cat images.

Unsupervised learning is generally used for clustering, representation learning, and density estimation. The goal is to learn the inherent structure of the data without explicit labeling. Some commonly used algorithms are k-Means Clustering, Principal Component Analysis, and Autoencoding. There is no concrete way to compare model performance for most unsupervised learning methods since no labels are provided.

Two popular applications of unsupervised learning are dimensionality reduction and exploratory analysis. Dimensionality reduction, a method of representing data with fewer columns or features, can be achieved using unsupervised methods. Unsupervised learning is very useful in the exploratory analysis because it allows for the automatic determination of data structure and can provide initial insights that can then be used to test particular hypotheses.

### 2.3 Artificial Neural Networks

Artificial Neural Networks (ANNs) are ML systems loosely inspired by the biological neural networks of animal brains. Such systems learn to perform tasks by providing examples, usually without programming task-specific rules.

An ANN is a model based on a series of interconnected units or nodes, called artificial neurons, that loosely mimic the neurons in a biological brain. Each neuron is a node connected to other nodes by connections corresponding to biological axon-synapsis-dendrite connections. Each connection has a weight that determines the strength of influence of one node on another. An artificial neuron receiving a signal can process it and then pass it on to other artificial neurons connected to it.

In general ANN implementations, when artificial neurons are connected, the signal is expressed as a real number. Each neuron output is computed as a nonlinear function of the sum of its inputs. Artificial neurons are usually assigned weights that are adjusted as learning progresses. These weights increase or decrease the strength of the signal when connected. Artificial neurons may have a threshold so that a signal is only transmitted if the total signal exceeds that threshold.

Typically, artificial neurons are assembled in layers. Different layers can perform different types of transformations on their input data. Signals travel from the input layer to the output layer, generally passing through multiple hidden layers (Figure 12). The input layer takes the input data, performs computation through its neurons, and then passes the output data to the subsequent layers. Neurons are connected in different patterns so that the output of some neurons becomes the input of others. The output layer takes as input the data passed by the previous layers, performs computation through its neurons, and then computes the output. Hidden layers sit between the input layer and the output layer, hence the name. For the vast majority of problems, a single hidden layer is sufficient. Typically, each hidden layer contains the same number of neurons. The greater the number of hidden layers in a neural network, the longer the neural network produces outputs and the more complex problems it can solve.

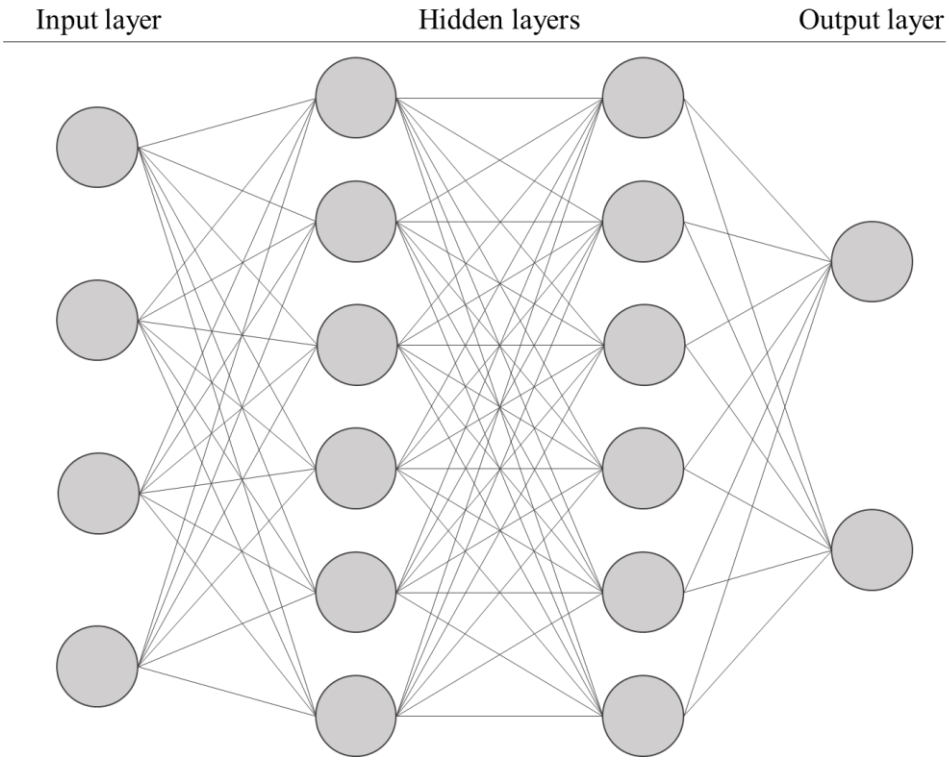


*Figure 12: Schematic representation of an ANN layout with two hidden layers.*

The ANN approach's original goal was to solve problems in the same way as the human brain and perform tasks where traditional algorithms were ineffective. Over time, however, the focus shifted to specific tasks, and ANNs quickly turned their attention to improving empirical results, largely abandoning attempts to stay true to their biological predecessors. Artificial Neural Networks are used for various tasks, including computer vision, speech recognition, machine translation, social network filtering, video games, and medical diagnostics.

The number of ANN types available is very high. Each type of ANN uses different principles and rules, each with its advantages and disadvantages. The main difference between ANN types is the different layout that connects the layers of the system, with different rules for learning, error propagation, weights, etc.

### 2.3.1 Training and learning

In this work, ANNs were trained using supervised learning since a labeled dataset containing known inputs and outputs was used.

Learning is the adaptation of a network to solve a problem more efficiently, given example observations. ANNs are trained by processing examples, each with known inputs

and outputs, and creating probability-weighted associations between them stored in the network data structure to increase the accuracy of the results.

When training the neural network on a given example, the difference between the processed output of the network and the target output is typically determined, and this difference is stored as an error. During training, the weights are adjusted to minimize the observed errors. The network then uses this error value to adjust its weighted associations according to the learning rule. Subsequent adjustments cause the neural network to produce an output that becomes increasingly similar to the target output. Once a sufficient number of such adjustments have been made, criteria-based learning can be discontinued.

Training is discontinued if learning additional observations do not significantly reduce the error rate. Even after training, the error rate usually does not reach 0. If the error rate is too high after training, the network usually needs to be redesigned. In practice, this is achieved by defining a cost function that is periodically evaluated during training. As long as the performance decreases, training is continued. The cost function can only be approximated. The output is numerical, so if the error margin is small, the difference between the output and the correct answer is small. Training tries to reduce the total difference between observations.

Backpropagation is a widely used algorithm for training ANNs. When adapting a neural network, backpropagation computes the gradient of the loss function for the network weights for a single input-output point and does so efficiently instead of computing the gradient directly for each weight separately. This efficiency allows gradient methods to train multilayer networks by updating the weights to minimize loss; gradient descent or variants, such as stochastic gradient descent, are often used. The algorithm calculates the gradient of the loss function for each weight using a chain rule, computing the gradient layer by layer and iterating from the last layer to the last to avoid unnecessary computation of intermediate terms in the chain rule.

# AIM OF THE WORK

**Aim of the work and thesis outline**

The main problems of the superhydrophobic surfaces developed so far are the high costs, low stability, the short-lived durability of the nanostructure, and the difficulty of large-scale application of the preparation processes. The main objective of the project was to develop coatings that met all the necessary standards to be defined as superhydrophobic through a simple, reproducible, and scalable approach. The coatings had to overcome the limits set by the old development strategies. The ultimate goal of the project was to obtain fluorine-free surfaces with antibacterial and antifouling properties for application in biomedical devices and antibacterial surfaces. Considering all the characteristics that these surfaces must possess and the limitations of the examples reported in the literature, optimizing the coatings was not a simple process. To help overcome these challenges, Artificial Neural Networks were employed to optimize coatings and preparation processes.

The project started with the preparation of superhydrophobic surfaces using plastic polymers (PLA, PC/ABS, ABS), coated with an adhesive layer of epoxy resin (DGEBA). Silica nanoparticles were used to confer the necessary characteristics to the surfaces. These nanoparticles can create a compact hydrophobic coating with a uniformly distributed, nano-structured roughness, thus providing the surface with strong superhydrophobicity. The second objective of the project was to build a dataset containing information on materials, processes, and operating parameters used to fabricate the coatings. The dataset was used to train an Artificial Neural Network, intending to optimize both the surfaces obtained and the preparation methods.

The first part of the work will discuss the design and preparation of the coatings, carried out through different procedures, using numerous materials, and varying the operating parameters of the preparation process. The materials used and the characterization tests performed will be described, and the process by which the coatings were prepared will be explained. The characterization of the best coating obtained, with strong superhydrophobic characteristics and a contact angle of 157°, will be described, and the possible applications of the coating itself will be briefly discussed.

In the second part of the work, the focus will be on the Artificial Neural Networks training process. The construction of the dataset will be outlined, and its structure will be clarified. The efficient predictive algorithms obtained, which allow determining the contact angle and the possible degree of resistance of a coating using user-defined composition and operational parameters, will be discussed. The algorithms were successfully used to prepare an

optimized, abrasion-resistant, self-cleaning coating with a contact angle >160°, under patent evaluation at the time of writing.

Finally, two Artificial Neural Networks applications carried out in parallel to the main project will be briefly discussed. The first application, a working prototype named NN-AMP, is a software application for predicting antimicrobial peptides activity and selectivity. NN-AMP can also generate new peptides starting from an input sequence, progressively increasing the sequence selectivity, and can predict entirely new antimicrobial sequences. This tool was used to generate two novel antimicrobial sequences, under patent evaluation at the time of writing, which will be used as potential lead compounds to develop selective antimicrobial peptides. The second application is an Artificial Intelligence-based tool for anti-cancer drug discovery and small molecule repurposing, which is still in the pre-prototype phase.

# RESULTS AND DISCUSSION

# CHAPTER 3
# Design and preparation of superhydrophobic coatings

### 3.1 Design of the superhydrophobic coatings

As discussed in CHAPTER 1

Superhydrophobic materials, there are countless examples of SH surfaces preparation by different methods in the scientific literature, with the focus often being on obtaining durable surfaces, which is still a significant problem[10,33,60]. Layer-by-layer methods were preferred for developing the SH coating of this work, mainly because of their ease of application, cost containment, and, most importantly, scalability of processes.

Moreover, many SH surfaces are prepared using fluorinated reagents. Fluorinated compounds with low surface free energy are used to enhance hydrophobic efficiency in the preparation of SH surfaces. These compounds, however, are expensive and toxic. Economical and environmentally safe fluorine-free materials, such as alkyl-silanes and long-chain organic compounds, have been used to fabricate water-resistant surfaces[58]. For this reason, in the design phase, in addition to the use of economic and scalable processes, the focus was on the use of non-fluorinated materials. The main inspiration for the design of the coatings were the works of Yilgor et al.[64] and Cholewinski et al.[117]

In their work, Yilgor et al. describe a simple and general method for the preparation of SH surfaces, using hydrophobic fumed silica and several polymers, including crosslinked epoxy resins. The SH surfaces are prepared using a simple, multistep spin-coating procedure. The first step is the deposition of a layer of the desired polymer (e.g., epoxy resin), followed by the deposition of two layers of hydrophobic fumed silica, using a THF dispersion of silica nanoparticles. Cholewinski et al. prepared, using a facile dip-coating process, a robust SH bilayer coating, using an epoxy resin adhesive layer as the base, and hydrophobic fumed silica to confer nanoscale roughness and thus SH properties to the surface. The coatings proposed by Yilgor et al. and Cholewinski et al. are of simple preparation, using low-cost and efficient materials and methods.

The coatings described in this work were prepared via multistep deposition (Figure 13), a layer-by-layer process. The coatings were developed according to the general scheme: 1) adhesive layer; 2) curing time t; 3) one or multiple silica or mixed layer(s). The first layer is the adhesive (epoxy resin), followed by one or more layers with superhydrophobic or protective properties. The layers were deposited via spray coating to improve on the works that inspired the process. Curing was carried out in a laboratory drying oven at different temperatures, based on the coating mixture components and the substrate.

*Figure 13: Multistep deposition scheme. The first step is the deposition of the adhesive layer, followed by the deposition of one or more layers with superhydrophobic properties.*

The design of the SH coatings followed an iterative process. During the design phase, the primary focus was to use materials and methods that were inexpensive and easily scalable on an industrial level and techniques that could be easily automated. It was decided to apply an iterative process for the design of the coatings, i.e., several tests were carried out by varying substrates, methods, coating composition, and operating parameters to have sufficient data to build a dataset suitable for the training of an Artificial Neural Network, which could then be used for the optimization of the processes and the coatings. The general workflow for the preparation of coatings is described in Figure 14.

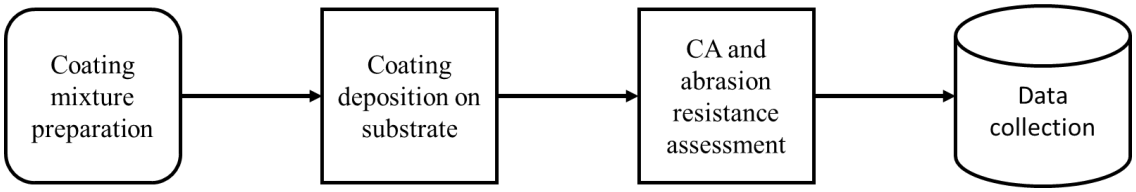


*Figure 14: General workflow for the preparation of the coatings. The first step is the preparation of the coating mixture, followed by the deposition on the solid substrate. After the curing of the coating, contact angle and mechanical resistance tests are carried out. Data are then collected for future use in ANN training.*

More than 450 samples were prepared during the project, varying:

- deposition substrate
- silica layer composition
- crosslinker for epoxy resin
- number of layers
- curing times

The techniques and materials used during the project are described in 3.2 Materials and Methods. The schemes used to prepare the coatings are described in a 3.3 Preparation of an abrasion-resistant superhydrophobic coating.

## 3.2 Materials and Methods

### 3.2.1 Substrates

A few polymeric materials, commonly used to produce plastic objects and surfaces, were selected for coating deposition. These materials were chosen with biocompatibility in mind. Four polymers were initially compared:

- Polylactic Acid (PLA)
- Polystyrene (PS)
- Acrylonitrile Butadiene Styrene (ABS)
- Polycarbonate/Acrylonitrile Butadiene Styrene (PC/ABS).

PLA was considered for the biodegradability. Given the operating conditions to which the samples were subjected, PC/ABS was selected as substrate, as it was the only material that did not show signs of degradation to the temperatures and solvents used. Cross-linking tests were carried out on all samples with an epoxy resin and a cross-linker, the adhesive layer base components. Since the complete cross-linking of the resins requires curing in a drying oven at relatively high temperatures (60°-80°C), the best results were obtained using the PC/ABS polymeric alloy. PLA, PS, and ABS showed different degrees of deformation or degradation when in contact with the solvents used for the resin-crosslinking agent mixtures and the silica particle suspensions. The substrate materials were cut into squares of 20x30x4 mm ca. for all the samples prepared during the project.

#### 3.2.1.1 Polylactic Acid

Polylactic acid (PLA)[118,119], or polylactide, is a polymer of lactic acid. It is a thermoplastic aliphatic polyester produced by fermentation of non-toxic, renewable raw materials, natural organic acids, or sugars derived from renewable resources such as sugar cane. PLA is a biodegradable polymer under high humidity conditions (>20%) and temperatures above 60°C. The mechanical properties of PLA vary from those of an amorphous polymer to those of a semi-crystalline polymer. The glass transition temperature is higher than room temperature; transparent materials are obtained. PLA becomes biodegradable upon hydrolysis at temperatures greater than 60°C and humidity greater than 20%. The general operating temperatures of PLA are between -20° and 60°C.

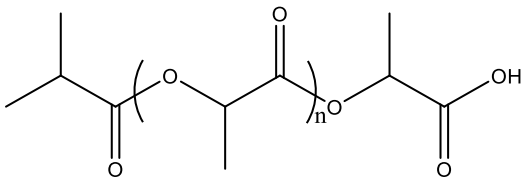


*Figure 15: Polylactic Acid polymer structure.*

A solid surface of PLA 4030D was used, on which wettability test and CA measurement were performed. The surface was found to be wettable with a measured static CA of approximately 45°. PLA was discarded from sample preparation because it underwent deformation at operating temperatures and surface degradation using solvents.

### 3.2.1.2 Polystyrene

Polystyrene is a polymer of styrene[120,121]. It is a thermoplastic aromatic polymer with a linear structure. At room temperature, it is a glassy solid; above its glass transition temperature, about 100 °C, it acquires plasticity; it begins to decompose at a temperature of 270 °C. Expanded polystyrene comes in the form of a very light white foam, often shaped into spheres or chips, and is used for packaging and insulation. It is chemically inert and is soluble in chlorinated organic solvents (dichloromethane and chloroform), acetone, and some aromatic solvents such as benzene and toluene.

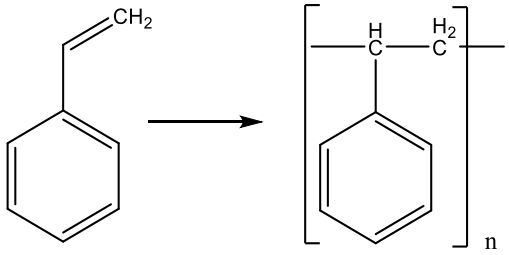


*Figure 16: Styrene polymerization scheme.*

A solid surface of PS was used, on which wettability test and CA measurement were performed. The surface was found to be wettable with a measured static CA of approximately 32°. Notably, the polymer showed significant degradation using organic solvents required to prepare the epoxy resin mixtures and the silica nanoparticles suspension.

### 3.2.1.3 Acrylonitrile-Butadiene-Styrene

Acrylonitrile-Butadiene-Styrene[122-124] is a common thermoplastic copolymer derived from styrene polymerized together with acrylonitrile in the presence of polybutadiene. Its most important mechanical properties are impact resistance and hardness. Several modifications

can be made to the polymer to improve impact resistance, hardness, and heat resistance. Impact strength, for example, can be expanded by increasing the amount of polybutadiene over styrene and acrylonitrile. Generally, ABS operating temperatures range between -20° and 80°C. ABS is resistant to solvents, alkalis, concentrated hydrochloric and phosphoric acids, alcohol, and oils. It is soluble in esters, ketones, 1,2-dichloroethane, and acetone.

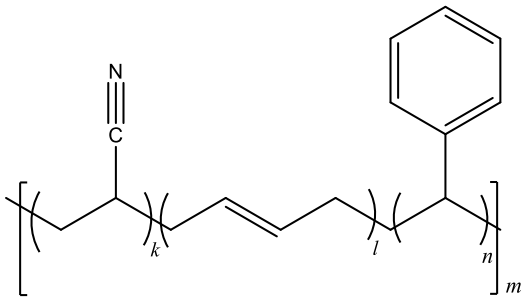


*Figure 17: ABS structure.*

An ABS solid surface was used, on which wettability test and CA measurement were performed. The surface was found to be wettable at a measured static CA of approximately 62°. The ABS showed slight deformation at operating temperatures.

#### 3.2.1.4 Polycarbonate/Acrylonitrile-Butadiene-Styrene

Polycarbonate/Acrylonitrile-Butadiene-Styrene[122] resins are amorphous resins produced by mixing PC and ABS. The combination of the two polymers enhances most of the desirable properties of both resins: the excellent processability of ABS[125] and the excellent mechanical and thermal properties of PC[126]. Operating temperatures range from -30°C to 80-90°, and heat resistance can reach 140°C. The ratio of polymers determines its final characteristics. It is resistant to solvents, alkalis, concentrated hydrochloric and phosphoric acid, alcohol, and oils. It is soluble in esters, ketones, 1,2-dichloroethane, and acetone.

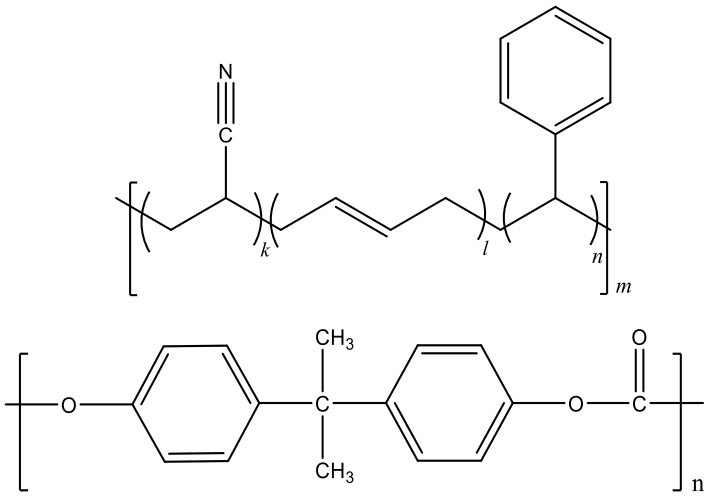


*Figure 18: ABS structure (above) and PC structure (below).*

A PC/ABS solid surface was used, on which wettability test and CA measurement were performed. The surface was found to be wettable at a measured static CA of approximately 62°. PC/ABS is the only polymer that did not show degradation or deformation at the operating conditions.

### 3.2.2 Coating materials

The coatings prepared during the project consist of three main components: an epoxy resin, which acts as an adhesive and provides resistance to abrasion; a cross-linking agent to ensure the proper curing of the epoxy resin; silica nanoparticles, to give SH properties to the coatings. The principal materials tested during the project are outlined below.

#### 3.2.2.1 Epoxy resin

Epoxy resins represent a versatile class of thermosetting polymers, widely used in various industry sectors, from aerospace to sports goods. Epoxy resins are reactive intermediates, crosslinked using hardeners (curing agents) like polyamines, aminoamides, and phenolic compounds. Epoxy resins present one or more epoxy groups in their structure. The epoxy group is a three-membered cyclic ether group, also referred to as 1,2-epoxide or oxirane. These functional groups are characterized by a high ring tension and consequently react easily with nucleophilic agents[127-129].

The most used epoxy resins are diglycidyl ethers of bisphenol A (DGEBA), produced by condensation of epichlorohydrin and bisphenol-A (IUPAC name: 2-[[4-[2-[4-(Oxiran-2-ylmethoxy)phenyl]propan-2-yl]phenoxy]methyl]oxirane) in an alkaline environment. This reaction (Figure 19) is still the most common method for their production[127,128,130,131].

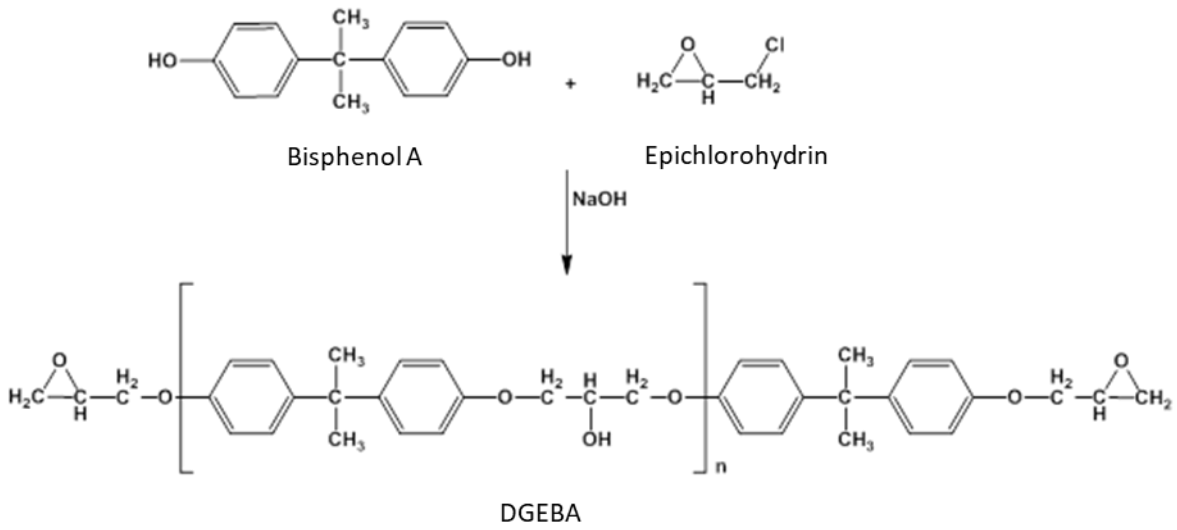


*Figure 19: Production of epoxy resins from bisphenol-A and epichlorohydrin in alkaline environment*[127,129].

DGEBA is a colorless solid that melts slightly above room temperature. Bisphenol-A moiety confers excellent characteristics to DGEBA (toughness, rigidity, and high-temperature performance), while the ether linkages confer chemical resistance, and the hydroxyl and epoxy groups confer adhesive properties. A parameter of interest for epoxy resins is the epoxide content, handy to calculate the mass of needed cross-linking agents. It is expressed as the Epoxy Equivalent Weight (EEW), which is the weight of resin in grams that contain the one-gram equivalent of epoxy (g/eq)[132], or as the equivalent weight, which is the weight in grams of resin containing 1 mole equivalent of epoxide (g/mol)[127,133].

DGEBA has been used as the adhesive layer of the coatings, thanks to its advantageous properties. The product used is Araldite GY2600 (Huntsman), an unmodified, high-viscosity epoxy resin based on bisphenol-A with extremely low chlorine content and excellent mechanical and chemical resistance in solvent-free coatings. EEW of Araldite GY2600 is 184-190 g/eq.

### 3.2.2.2 Cross-linking agents

Epoxy resins alone generate brittle films, so it is necessary for the epoxy monomer to react with a cross-linking agent, called a curing agent or hardener. The curing agent affects the viscosity, the reactivity of the mixture, and the type of bonds formed and allows to obtain structures with a high degree of cross-linking. Epoxy resins contain two chemically reactive functional groups: epoxy and hydroxyl groups. Cross-linking process involves the epoxide group reaction with cross-linking agents such as aliphatic or aromatic amines, anhydrides, carboxylic acids, and polyamides. Generally, electron-withdrawing groups near the epoxy

ring increase the resin reactivity for nucleophilic reagents, while for electrophilic ones, there is a decrease in the crosslinking rate[127-129,134].

The most used hardeners are aliphatic and aromatic amines. Primary amines, having two hydrogen atoms available, can react with two epoxy groups, while secondary amines can react only with a single epoxy group. Tertiary amines cannot react with the epoxy group but can act as catalysts[130,134]. Figure 20 shows the general reaction scheme between a primary or secondary amine and the resin epoxy group.

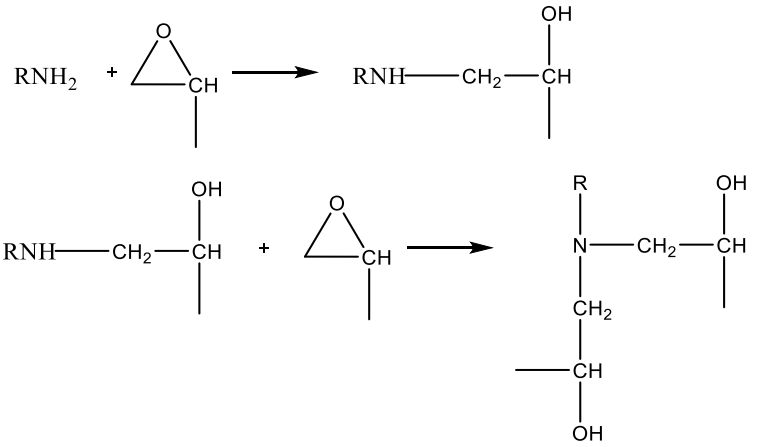

*Figure 20: General reaction scheme between primary amines and epoxy group (above) and secondary amines and epoxy group (below)[127,129].*

Primary amines react faster than secondary amines[135]. The epoxy group reaction with a primary amine initially produces a secondary alcohol and a secondary amine, which can react with another epoxy group to give a tertiary amine and two secondary hydroxyl groups[136]. The reaction proceeds through the formation of a trimolecular activated complex (Figure 21).

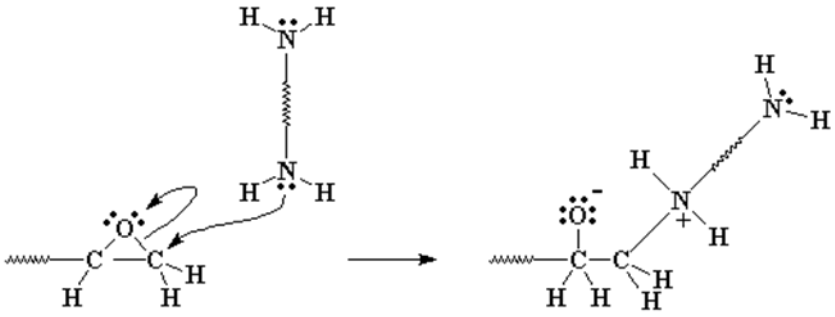

*Figure 21: Chemical structure of the activated trimolecular complex formed during the opening reaction of an epoxy ring by an amine[136].*

Electrons from the diamine attach the carbon atom near the epoxy oxygen, providing a negative charge to the oxygen and a positive charge to the nitrogen. If the epoxy monomer

and the amine are multifunctional, the resulting product possesses a three-dimensional lattice.

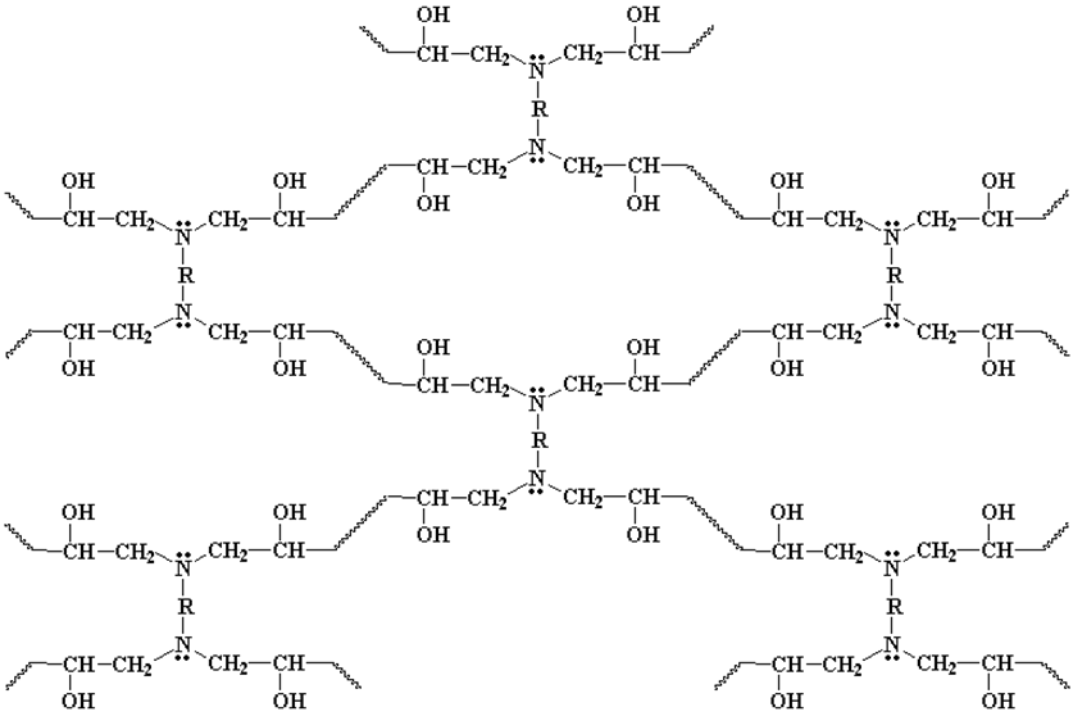

*Figure 22: Representation of the three-dimensional lattice of an epoxy resin[136].*

The amine hydrogen equivalent weight (AHEW) is the weight of amine in grams that contain the one-gram equivalent of active hydrogens (g/eq) and represents the hydrogen content of a cross-linking agent. It is used to calculate the mass of amine needed for complete epoxy curing.

During the project, three different cross-linking agents were used: Jeffamine D230, Jeffamine D400, and Jeffamine EDR148 (Huntsman). Jeffamine D series products (D230 and D400) are amine-terminated polyoxypropylene glycols (Figure 23). The amines have low viscosity, color, and vapor pressure and are miscible with various solvents. Table 2 shows the main properties of Jeffamine D230 and D400.

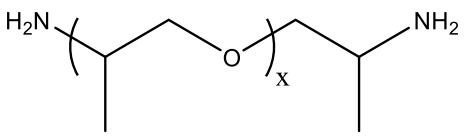

*Figure 23: Jeffamine D series products general structure.*

| | **AHEW (g/eq)** | **Molecular weight (MW)** | **x (repeated unities)** | **Curing time and temperature** |
|---|---|---|---|---|
| **D 230** | 60 | 230 | ~2,5 | 60° - 40min |
| **D 400** | 115 | 430 | ~6,1 | 75° - 24h |

*Table 2: Jeffamine D230 and D400 properties.*

Jeffamine EDR series products (EDR148) are more reactive than other Jeffamine diamines and triamines due to their linear PEG-based structure (Figure 24).

Jeffamine EDR148 polyetheramine has been formulated to cure at room temperature with long times and rapidly complete curing at medium temperatures. It has, besides, excellent resistance to thermal shock.

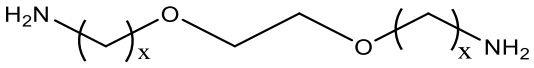


*Figure 24: Jeffamine EDR series products general structure.*

| | **AHEW (g/eq)** | **Molecular weight (MW)** | **x (repeated unities)** | **Curing time and temperature** |
|---|---|---|---|---|
| **EDR148** | 37 | 148 | 2 | 55/60° - 20min |

*Table 3: Jeffamine EDR148 properties.*

Accelerator 400 (Huntsman) curing promoter was tested during the project. Accelerator 400 comprises 1-(2-Aminoethyl)piperazine (Figure 25) and is an epoxy curing promoter designed for use with amine hardeners. The product was developed specifically for use with Jeffamine curing agents, but it is compatible with most amine-cured epoxy systems. Table 4 shows the main properties of Accelerator 400.

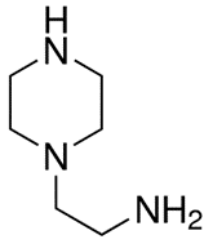


*Figure 25: Accelerator 400 structure.*

| | **AHEW (g/eq)** | **Molecular weight (MW)** |
|---|---|---|
| **Accelerator 400** | 145 | 192 |

*Table 4: Accelerator 400 properties.*

Formulation of epoxy resins with amine cross-linking agents is calculated using parts per hundred of resin (phr) values. This value represents the curing agent parts needed to cure 100 parts of epoxy resin for a 1:1 stoichiometric ratio. Phr is calculated as follows, based on a resin quantity of 100 grams:

$$phr = \frac{AHEW\ of\ curing\ agent}{EEW\ of\ epoxy\ resin}\ x\ 100$$

To calculate the accelerator mass, it is convenient to estimate the accelerator usage in phr and then calculate the amount of amine hardener needed to attain a 1:1 stoichiometric ratio. The calculation is done as follows, based on a resin quantity of 100 grams:

$$Grams\ of\ curing\ agent\ = \left\{\frac{100g\ of\ epoxy\ resin}{EEW\ of\ epoxy\ resin} - \frac{phr\ of\ Accelerator\ 400}{AHEW\ of\ Accelerator\ 400}\right\}\ x\ AHEW\ of\ curing\ agent$$

Different coating preparation schemes were applied during the project. At the same time, various cross-linking tests were performed at different temperatures, using the reported hardeners. As a result of the analyses, it was decided to use Jeffamine EDR148 to prepare the coatings due to the advantageous curing temperature and the shorter curing time compared to the other two Jeffamine products. Jeffamine D400 was excluded because the high temperatures and long curing times caused deformation of the PC/ABS substrate, while Jeffamine D230 was excluded because it required much longer curing times than EDR148.

Finally, blends of hardeners + Accelerator 400 were also tested. The curing acceleration effect is remarkable in the blends D230/D400 + Accelerator 400, although it did not result in times comparable to curing with EDR148 alone. On the other hand, for the mixture with EDR148, no increase in curing times was observed to justify the use of Accelerator 400, which was ultimately discarded from the preparation of the final coating.

#### 3.2.2.3 Hydrophobic silica nanoparticles

Silica (silicon dioxide, $SiO_2$) is a silicon oxide that, due to its characteristics, is suitable for the synthesis of nanoparticles. Mesoporous Silica Nanoparticles (SNPs) have pores ranging from 2 to 50 nm and have several applications, including drug encapsulation, controlled drug release[137-140], can be used as insulators, as a refractory or reinforcing material[141], or as UV protective material[142]. SNPs main advantages are the low production cost, ultra-high specific surface area, good dispersal ability, strong adsorption, high chemical purity, and excellent stability[143].

Hydrophobic SNPs have been widely used to prepare superhydrophobic surfaces for various applications (e.g., antifouling, anti-icing, drag reduction, bacteriostatic coatings) thanks to their potential to create hydrophobic surfaces with uniformly distributed roughness[20,22,30,33,64,117,144]. Two commercial pyrogenic silica were used for the coatings prepared during the project: Aerosil R202 (Evonik), nanoparticles diameter approx. 11 nm, and Aerosil R504 (Evonik), amine-modified surface, nanoparticle diameter approx. 9 nm.

Aerosil R202 fumed silica (Figure 26) is composed of SNPs (11 nm diameter) treated with polydimethylsiloxane (PDMS). The silicone oil treatment guarantees marked hydrophobia of the product. It is highly efficient in the thickening of complex polar liquids, such as those based on epoxy or polyurethane, it improves the water-resistance of moisture-sensitive formulations, such as cosmetic preparations, the anti-sedimentation behavior of pigments and resistance in epoxy coatings, improves the fluidity of powders and slows down corrosion processes. The high hydrophobicity of these PDMS-treated SNPs makes them particularly useful in achieving good flowability.

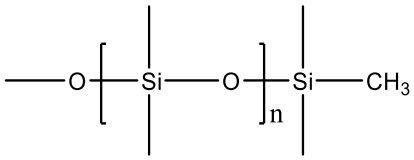


*Figure 26: Aerosil R202 NPs surface.*

Aerosil R504 fumed silica consists of high purity hydrophobic SNPs (9 nm diameter) treated with hexamethyldisilazane and aminosilane to functionalize it with organic amino groups (Figure 27).

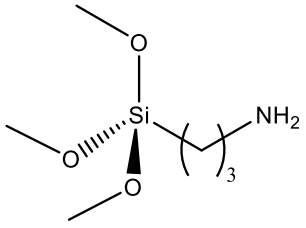


*Figure 27: Aerosil R504 NPs functionalized surface.*

Both R202 and R504 gave excellent results in terms of SH properties, resulting in surfaces with very high CAs (>150°). SNPs can reach extremely high CAs when deposited on a clean substrate; however, the layer has no resistance by itself and can be removed easily with a finger swipe since there is no adhesion on the substrate. Amino-functionalized Aerosil R504 was used to test the possibility of having a covalent bond between the nanoparticles and the underlying adhesive to improve coating resistance since epoxy resin readily reacts with amino groups (Figure 21). However, the amino group of R504 seems to have little to no

influence on resistance (i.e., there should be no covalent bonding) while resulting in slightly lower CAs compared to R202, as outlined in 3.3 Preparation of an abrasion-resistant superhydrophobic coating.

### 3.2.3 Coating preparation methods

As already mentioned, layer-by-layer methods were selected for coating preparation, given the ease of application and cost-effectiveness of these processes. In particular, spray-, spin-, and dip-coating techniques were tested. After carrying out tests on several samples using the three deposition techniques, it was decided to adopt the spray-coating method as the standard procedure.

Indeed, spray-coating has proved to be the best method to prepare homogeneous and compact coating surfaces or films on the entire surface of the samples (Figure 28a). Moreover, spray-coating resulted as the most suitable of the three tested methods to be applied on large surfaces, thus allowing for easier industrial-level scalability. Using spin-coating (Figure 28b), it was impossible to obtain complete surface coating since the mixture was distributed only near the center of the sample and in the areas surrounding the deposition point. The dip-coating technique (Figure 28c), on the other hand, coated the surface entirely, but the layers were excessively thick (causing incomplete curing) and not homogeneous due to the formation of air bubbles during the extraction of the samples from the solution/mix.

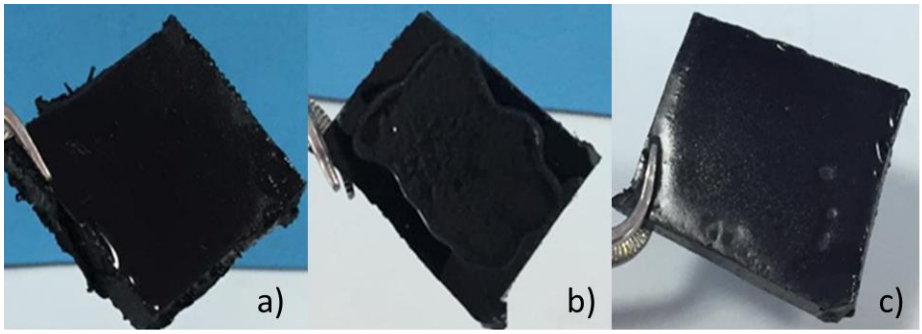


*Figure 28: a) Spray-coated ABS-PC sample; b) spin-coated ABS-PC sample; c) dip-coated ABS-PC sample.*

A commercial airbrush was used to coat the samples. The samples were clamped under a fume hood at 15 cm distance from the airbrush. Each layer was deposited with a single spray from the airbrush, performing a hand motion at standard speed from right to left. Naturally, the manual nature of the process involves a certain degree of variation, but a standard speed of deposition on the sample was maintained as far as possible to keep this variation at a minimum and to avoid the deposition of excessively thick layers.

### 3.2.3.1 Spin-coating method

Spin coating is a process used to apply a uniform thin film to a flat solid substrate[145]. An excess amount of a very dilute solution of the coating materials, such as a polymer or silica mixture, is deposited on the substrate, which is then set into rapid rotation by a special rotor to distribute the solution over the substrate by centrifugal force uniformly. The solvents used are usually very volatile, so the film thins during the process also due to the evaporation of the solvent. The spin is stopped as soon as the desired thickness is reached, which can be below 10 nm. The spin coating process is generally divided into three main steps (Figure 29):

1) Deposition of the solution on the substrate.
2) Acceleration of the substrate up to the chosen spin speed.
3) Rotation of the substrate at constant speed and evaporation.

Spin-coating generally allows obtaining homogenous coatings with variable thickness. The control of film thickness can be achieved by altering spinning speed and time, while the spinning device restricts the size of the substrate. The method is low cost but cannot be scaled given the limitation imposed by the spinning device[146].

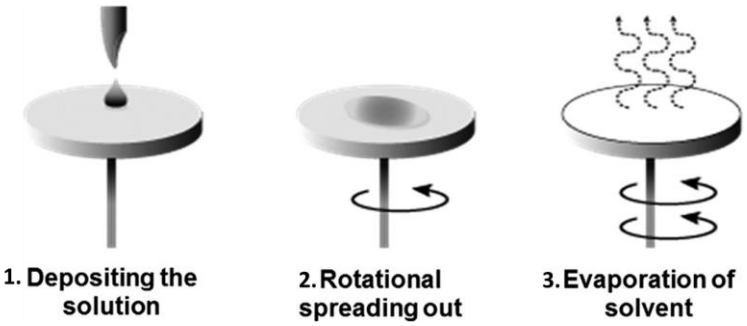


*Figure 29: Spin-coating method steps[147].*

### 3.2.3.2 Dip-coating method

Dip-coating is a method used to deposit thin film onto a solid surface by dipping the substrate in a tank containing a solution of the coating to be deposited, followed by induced drying or baking. The dip-coating process can be accomplished in four steps (Figure 30):

1) Preparation of the precursor solution. The solution is mixed in a tank of appropriate dimensions.
2) Immersion. The substrate is immersed in a solution containing the substance to be deposited at a steady speed, preventing rapid agitation.

3) Time in contact with the solution. The layer stays fully submerged in order to allow the coating substance to be deposited.
4) Removal of the sample. The substrate is drained from the solvent at a steady pace, preventing rapid agitation, and is left to dry.

The method is easy to apply and allows the control of the thickness of the coating by varying the viscosity of the solution. Coating thickness, however, can vary at different sections of the surface, and the distribution of the layers can be uneven[146,148]. The process can be automated, is fast, and low-cost. However, scaling the method up for large surfaces could prove difficult due to the intrinsic limits of the method, requiring specific dipping speeds and tanks.

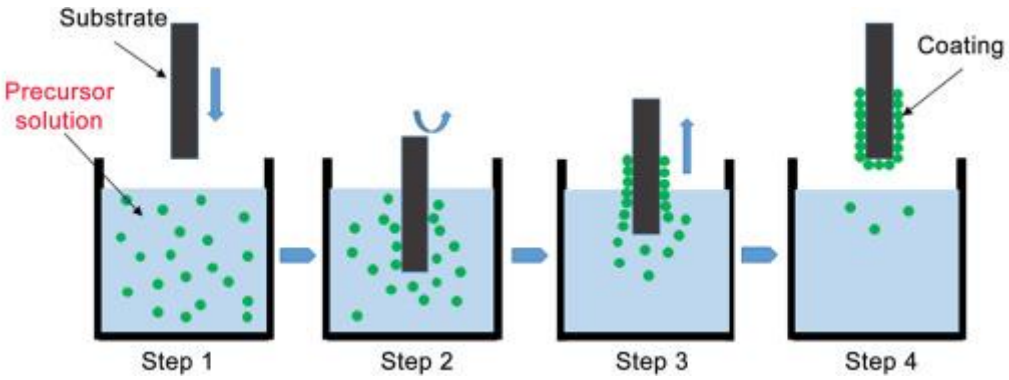


*Figure 30: Sequential steps of the dip-coating method[149].*

### 3.2.3.3 Spray-coating method

Spray-coating is a process used for the deposition of materials in solution on suitably prepared substrates. In general, during spray processes, particles typically between 1 - 100 μm in diameter, contained in special tanks, are sprayed onto the substrate by a flow of gas (usually air or nitrogen) with suitable pressure and velocity. These particles are deposited on the surface of the substrate through a nozzle of variable size. Upon impact, each droplet is distributed over the substrate and rapidly solidifies to form a lamella. The materials used are polymers and composites. Deposited film thicknesses vary from about 20 μm to several mm depending on the spray process and the characteristics of the raw material used, whether in powder or solution form. High cooling rates cause a single flake to solidify before a subsequent flake impacts the substrate at the same point. The random succession of particle adhesion to the substrate leads to the formation of the typical lamellar microstructure of coatings. The main feature of sprayed coatings is the creation of rough and irregular surfaces on a micrometer scale. Spray-coating strategies have the advantages of easy application,

scalability, speed, low cost, and are compatible with many type substrates, facilitating large-scale fabrication[147].

### 3.2.4 Surface characterization methods

During the project, various characterization tests were carried out on the used materials and prepared coatings to test their structural behavior, performance, and characteristics, verify the desired properties (high CA, abrasion resistance), and define their usability limits[150,151].

#### 3.2.4.1 Contact angle

The evaluation of the wettability of the surfaces was carried out by measuring the static contact angle of a sessile drop through an optical tensiometer[152]. To measure the CA of a drop, the optical tensiometer records the images of the drop, placed on an appropriate plain surface, and automatically analyzes the shape of the drop. Modern optical tensiometers use digital cameras and automatically send the snapshots to the connected computer hardware. The captured image is analyzed with a drop profile fitting method to determine the CA, using the Young-Laplace equation, with the tangent line drawn from the baseline to the edge of the drop[153,154]. The surface tension of the liquid, gravity, and the solid substrate properties influence the drop shape. The tensiometer syringe dispenses a given volume of water on the surface, and after a brief, gentle contact between the tip of the needle and the surface of the sample, the syringe tip is pulled away, leaving the drop on the surface. Contact angle measurements were carried out by dropping a 10.0 µl water droplet on the samples, adequately placed on a flat surface. All CA values reported in this work are the average of five measurements.

As reported in 3.2.1 Substrates, the CA analysis was performed on the substrate polymers. Figure 31 shows a clean PC/ABS sample with a contact angle of approximately 62°.

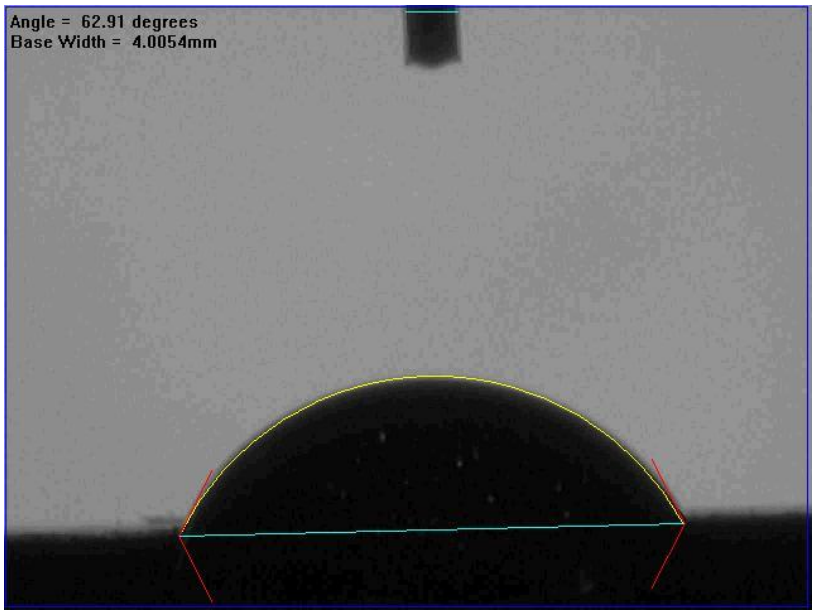


*Figure 31: Snapshot of a sessile drop on a PC/ABS surface, taken with an optical tensiometer.*

Substrates wettability was tested after the deposition of a single layer of cross-linked epoxy resin. Since the other substrates were discarded, only PC/ABS CA measurement is reported. Figure 32 shows the CA measurement of a PC/ABS sample coated with a single layer of Araldite GY2600 epoxy resin, cross-linked with Jeffamine EDR148. The CA of the coated polymer is approximately 86°, showing a CA increase of around 24° compared to the clean PC/ABS surface.

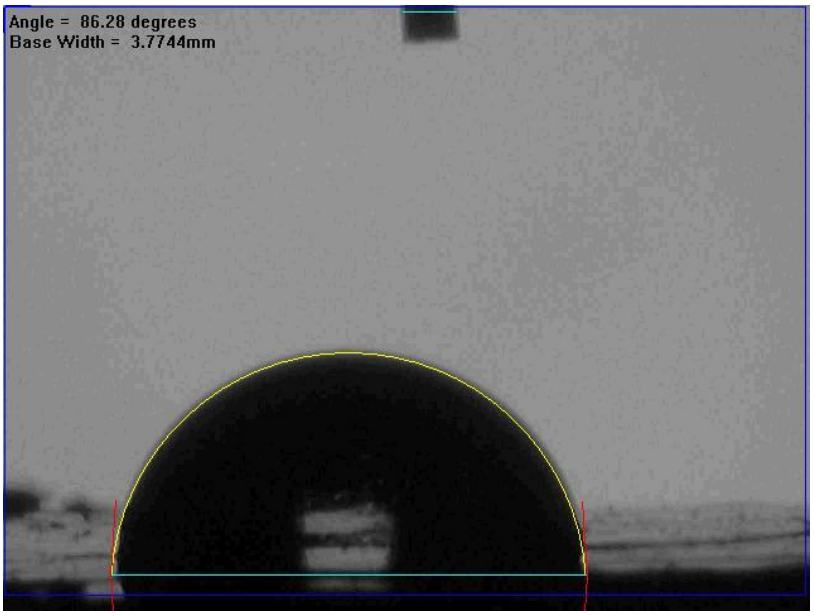


*Figure 32: Snapshot of a sessile drop on a PC/ABS surface coated with a single layer of Araldite GY2600 crosslinked with Jeffamine EDR148, taken with an optical tensiometer.*

The described procedure has been applied to measure the CA of the numerous samples prepared during the project. The use of a layer of pyrogenic silica involves a significant

increase in CA compared to epoxy resin alone, with values generally never below 140° (Figure 37).

#### 3.2.4.2 Surface roughness

As described in CHAPTER 1

Superhydrophobic materials, the presence of micro/nanoscale roughness is paramount for a surface to exhibit SH properties[62]. Scanning Electron Microscopy (SEM) is a type of electron microscopy that does not use light as a source of radiation but a beam of focused, high-energy primary electrons that strike the sample and can be used to observe a surface at the microscale[155]. The beam is generated by a tungsten electron source, which emits a stream of primary electrons. When the electron beam strikes the sample surface, it penetrates the sample to a depth of several microns, depending on the accelerating voltage and the density of the sample, producing secondary electrons and characteristic X-rays. One or more detectors collect these signals to form images that are then displayed on a computer screen. Although not capable of providing atomic resolution, some scanning electron microscopes can achieve a resolution of less than 1 nm. Typically, modern full-size SEMs offer a resolution between 1 and 20 nm, while desktop systems can provide a resolution of 20 nm or higher. This technique is a powerful tool to investigate inhomogeneous solids at the microscopic scale[156].

SEM analysis has been performed on several of the developed superhydrophobic samples and on the PC/ABS substrate to inspect the surface roughness. PC/ABS SEM images at 20µm, 10µm, and 2µm magnifications are shown in Figure 33, Figure 34, and Figure 35, respectively. SEM images show that the tested PC/ABS surface has some minor roughness and imperfections. However, it lacks the micro/nanoscale roughness and hierarchical structures necessary to ensure high CAs to a surface, which can be observed in Figure 38 and Figure 39 for the S0189 sample, coated with a SH coating.

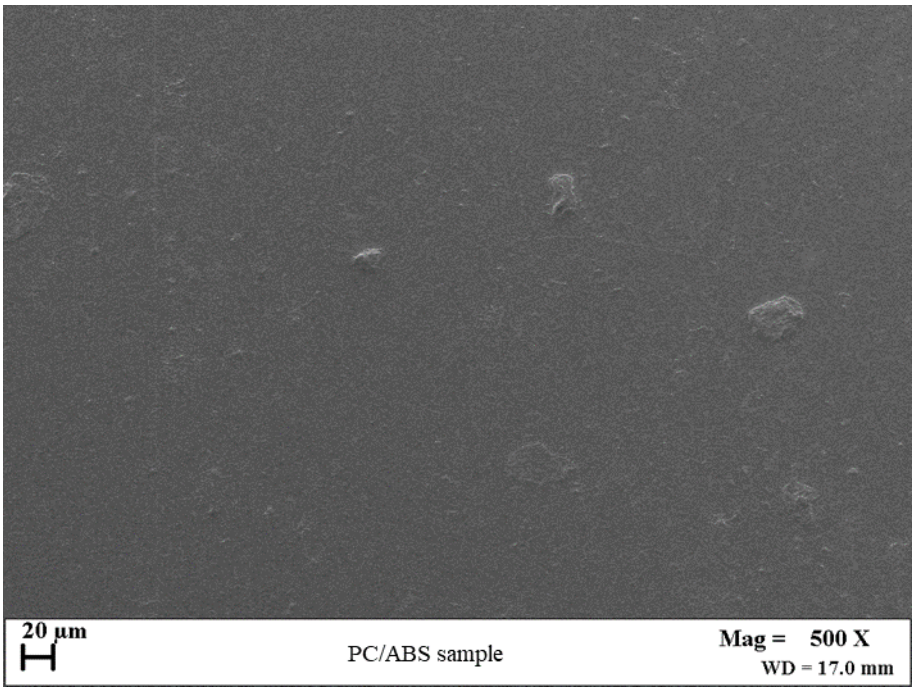


*Figure 33: SEM image of a PC/ABS clean sample at 20µm resolution.*

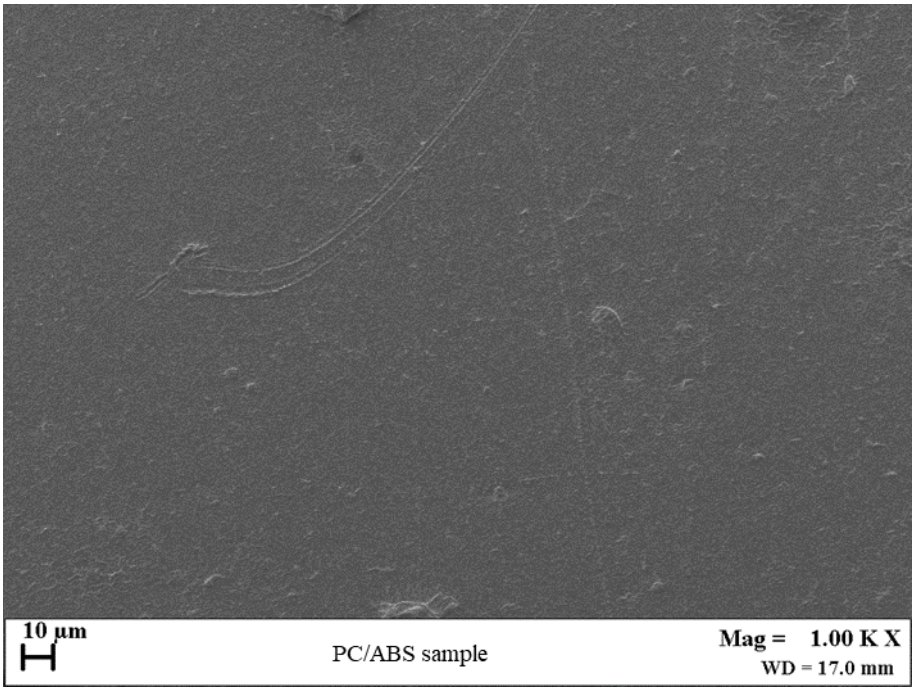


*Figure 34: SEM image of a PC/ABS clean sample at 10µm resolution.*

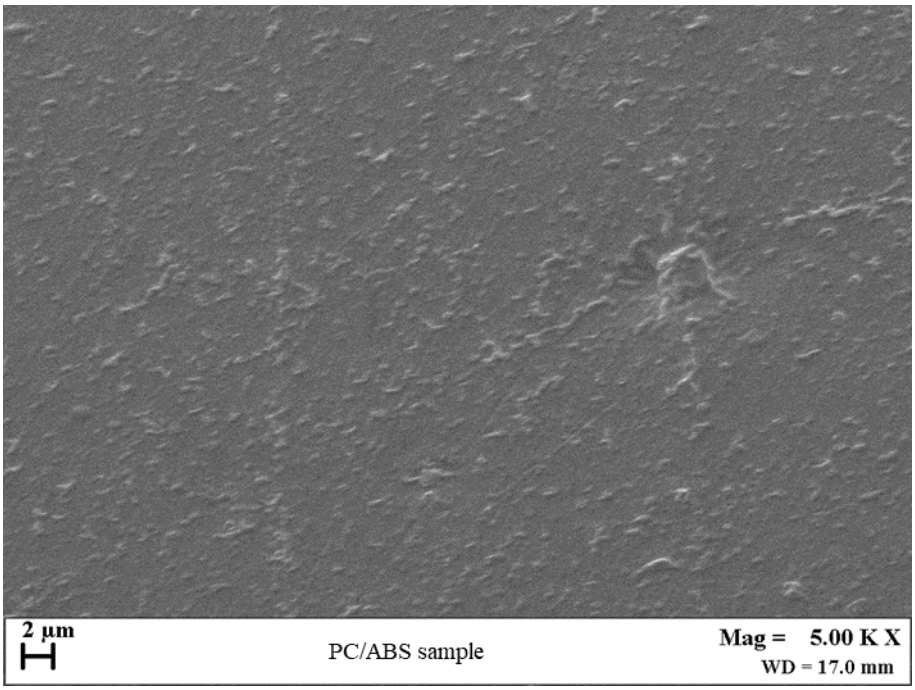


*Figure 35: SEM image of a PC/ABS clean sample at 2µm resolution.*

### 3.2.5 Coating abrasion resistance tests

The abrasion resistance of SH coatings, as previously discussed, is one of the most critical aspects of these materials. The preparation of multiple samples, aimed at collecting data for preparing a training set to be submitted to ANN, required the use of rapid and practical tests to evaluate mechanical strength to cut the time and costs associated with the preparation of each sample. The tests selected for the samples prepared during the project were finger scratch and tape peeling tests. These techniques are widely used for the assessment of abrasion resistance of SH coatings.

#### 3.2.5.1 Finger scratching test

A scratch is a sliding indentation on the surface of a material. The scratch phenomenon has many facets to its nature and requires a great deal of attention regarding testing and evaluation. This becomes especially important when a scratch behavior on a polymer or polymer-coated surface is considered, as in the present work[157,158].

The scratch test was introduced by Heavens[159] in the 1950s as a qualitative method for evaluating the adhesion and mechanical resistance of a coating and has been developed and automated over the years. Today, the test is widely used in academic and industrial settings as a measurement tool and in Quality Control[160].

The finger scratch test is a simplified variation of the scratch test and consists of scratching the surface with a finger to see whether the coating adheres to the underlying surface. The finger scratch test was used as a first quick test to verify the resistance of the samples prepared during the project. This extremely rapid test allowed to evaluate the abrasion resistance of the samples with immediacy, allowing them to quickly classify the non-resistant samples in the preparation of the dataset to be submitted to ANN and drastically cutting the time needed to perform mechanical stress tests.

#### 3.2.5.2 Tape peeling test

The tape peeling test is used to evaluate the adhesion of a coating to a substrate[117]. The main application strategy exploits repeated peeling on the same area of a surface to highlight the possible detachment of the coating layers of the evaluated material. The procedure is the following:

1. adhesive tape is applied to an area of the coating
2. the tape is pressed onto the surface and left to adhere
3. the tape is removed from the surface

The test is successful if the coating is not removed by tape when it is peeled away from the surface. However, data reported in the literature have indicated that the results are highly dependent on the quality of the adhesive tape, the roughness of the tested surface, the rigidity of the tape, and, to a lesser extent, the attachment pressure and the speed of removal of the tape[161,162].

The tape peeling test was used on all samples that responded positively to the finger scratching test, evaluating the CA variation at each subsequent tape peeling cycle. The most stable coatings prepared during the project do not show significant changes in CA and therefore in SH properties after 8+ cycles of tape peeling.

### 3.3 Preparation of an abrasion-resistant superhydrophobic coating

Several procedures were developed during the project, following different preparation schemes and using various materials. The processes were designed incrementally, targeting the detected problems to improve the coating properties continually and iteratively, to have a range of materials and operating parameters useful to build a solid dataset. All tested mixtures were prepared in triplicate samples (and in five replicates for the more durable coatings) to ensure that the results were reproducible.

The first procedure designed for coating preparation, Procedure A, is represented by the scheme: 1) adhesive layer; 2) curing time t; 3) silica or mixed layer. The general composition of the layers is reported in Table 5.

| | |
|---|---|
| **Substrate** | PLA, PS, ABS, or PC/ABS; dimensions: 20x30x4mm |
| **Adhesive layer** | GY2600 + hardener (1:1) |
| **Curing time t** | 1, 2, 4, 6, 8, 10, 16, or 18 hours |
| **Silica layer** | solvent + Aerosil R504 or R202 (2.5% wt) |
| **Mixed layer** | [solvent + Aerosil R504 or R202 (2.5% wt)] + [GY2600 + hardener (0.25% wt of the total mass)] |

*Table 5: Layer compositions and curing times for the coatings prepared according to Procedure A.*

In the first batch of tests, the coatings were deposited on various substrates, as described in 3.2.1 Substrates. PLA, PS, and ABS underwent deformation and degradation with high temperatures, making the polymers unsuitable for coating deposition. For this reason, PC/ABS was used as substrate. Various samples were prepared by spin-coating and dip-coating. Surface cracking and non-uniformity of the layers were evident; therefore, spray-coating was selected as the reference method.

As previously mentioned, Aerosil R504 was used to test the possibility of having a covalent bond between the amino groups on the surface of the SNPs and the underlying adhesive to confer abrasion resistance to the coating. R504 and R202 SNPs were dissolved in various solvents (THF, DCM, DMAC, $CHCl_3$, n-hexane, and cyclohexane), then sprayed on PC/ABS samples with and without the adhesive layer. The solvents were selected for their characteristics of organic solvents, capable of dissolving hydrophobic SNPs. Cyclohexane and n-hexane SNPs suspensions resulted in uniform and superhydrophobic coatings, while other solvents showed surface cracking and non-uniform distribution on the surface; n-hexane was selected as silica solvent for all the tests (interchangeable with cyclohexane).

Epoxy resin curing was performed in a drying oven at 70°C using Jeffamine D400 as the hardener. The deposition of the resin layer was difficult due to the absence of solvents. To summarize, approximately eighty samples were prepared to test the following mixtures:

- R202 or R504 in THF, DCM, DMAC, $CHCl_3$, n-hexane, or cyclohexane (2.5% wt)
- R202 or R504 in THF, DCM, DMAC, $CHCl_3$, n-hexane, or cyclohexane (2.5% wt)

- GY2600 + Jeffamine D400

The samples did not have superhydrophobic properties, with CAs ranging from 62° to 96°. Several problems have been observed, including non-uniform curing of the adhesive layer and a recurring coating surface cracking phenomenon, mainly attributed to the slow curing of the resin (Figure 36).

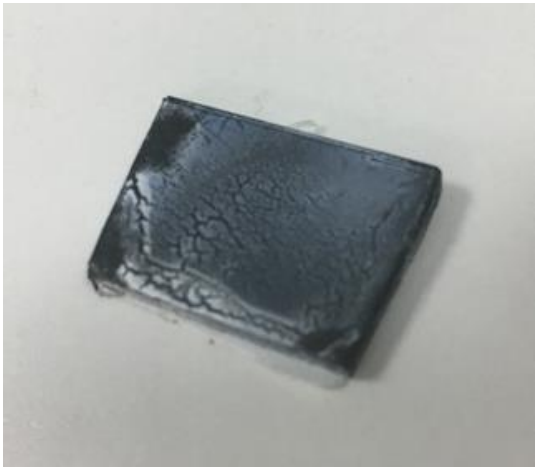

*Figure 36: Evident surface cracking on a sample prepared according to procedure A. The first layer is GY2600+D400; the second layer is R202 in n-hexane.*

In the second batch of tests, several GY2600 crosslinking agents were evaluated (Jeffamine D230 and D400, Jeffamine EDR148, Accelerator 400). Dissolution and spray coating tests were then carried out on GY2600 mixed with cross-linking agents to facilitate spray-coating deposition. DCM showed relatively fast evaporation in drying oven without surface cracking; this problem was still evident, if not exacerbated when using other solvents. EDR148 showed the most uniform curing and the shortest curing times among the tested agents, fully curing epoxy resin in 20 minutes in drying oven at 70°C, as mentioned in 3.2.2.2 Cross-linking agents. According to Procedure A, approximately eighty more samples were prepared, testing the following mixtures:

- R202 or R504 in cyclohexane (2.5% wt)
- R202 or R504 in n-hexane (2.5% wt)
- GY2600 (5% wt) + D230 (1:1) in THF, DCM, DMAC or $CHCl_3$
- GY2600 (5% wt) + EDR148 (1:1) in THF, DCM, DMAC or $CHCl_3$
- GY2600 (5% wt) + hexamethylenediamine (1:1) in THF, DCM or DMAC
- GY2600 (5% wt) + D230 + Accelerator 400 in DCM
- GY2600 (5% wt) + EDR148 + Accelerator 400 in DCM

PC/ABS was used as a substrate; CAs ranged between 61° and 140° (nearly SH). The highest CAs were observed on samples prepared by deposing an adhesive layer of

GY2600+EDR148, followed by a layer of R202/R504 in n-hexane. Epoxy resin was partially cured for 15 minutes at 70°C; partial curing was necessary to allow the SNPs layer to sink into the underlying layer, to improve coating resistance. Resistance, however, was mediocre and still needed improvement.

Procedure B was then designed to improve on Procedure A, according to the following scheme: 1) silica layer; 2) epoxy resin layer; 3) silica layer; 4) curing time t; 5) silica layer; 6) curing time t'. The composition of the layers is reported in Table 6. The curing temperature is 70°C.

| | |
|---|---|
| **Substrate** | PC/ABS; dimensions: 20x30x4mm |
| **Adhesive layer** | GY2600 (5% wt) + EDR148 (1:1) in DCM |
| **Curing time t, t'** | 5, 10, 15, or 20 minutes |
| **Silica layer** | n-hexane + Aerosil R504 or R202 (2.5% wt) |

*Table 6: Layer compositions and curing times for the coatings prepared according to Procedure B.*

Sixty samples were prepared according to Procedure B. CAs and resistance were measured. The coatings with curing time t = 15 minutes and t' = 10 minutes gave the best results. The difference in CAs between the R202 and R504 was minor and favored the former type of silica. Table 7 shows the CAs of two samples, S0189, and S0207, prepared according to Procedure B and curing times t = 15 min, t' = 10 min. S0189 was prepared with R202 silica, while S0207 was prepared with R504 silica. The coatings are resistant to finger scratching, with no variation in CA after applying the procedure. CAs were measured before and after 1, 2, 3, and 5 cycles of tape peeling. The amino group of R504 seems to have little to no influence on resistance; resistance is attributed to silica sinking into the epoxy layer. Silica excess allows keeping exposed nanoparticles, avoiding epoxy resin to completely cover the surface, thus depriving it of SH properties while maintaining a reasonable resistance level. As previously mentioned, a curing time of 15 minutes at 70°C allows only for partial curing (almost complete) of the epoxy layer. Non-complete curing ensures that the SNPs layer can partially sink into the underlying epoxy layer, improving coating resistance while maintaining sufficient SNPs exposure. The coating shows a significant increase in CA compared to the PC/ABS substrate alone (CA = 62°) and epoxy resin coating (CA = 96°) and shows mechanical strength compared to a layer of SNPs only deposited directly on the sample.

| | ***S0189 (R202)*** | ***S0207 (R504)*** |
|---|---|---|
| ***CA*** | 157° | 151° |
| ***TP x1 CA*** | 157° | 147° |
| ***TP x2 CA*** | 152° | 146° |
| ***TP x3 CA*** | 151° | 145° |
| ***TP x5 CA*** | 148° | 141° |

*Table 7: Contact angle before and after tape peeling (TP) cycles for samples S0189 (R202) and S0207 (R504).*

Additional procedures were designed in order to include more data in the ANN dataset. Several samples were prepared using a fast-curing commercial PDMS (Sylgard 184) as adhesive. PDMS has been previously used to prepare SH coatings, thanks to its hydrophobic and adhesive properties, mechanical flexibility, biocompatibility, and thermal/chemical stability[16,18,35,163,164]. Samples were spray-coated according to Procedure C: 1) R202 layer; 2) PDMS layer; 3) R202 layer; 4) curing 15 min; 5) R202 layer; 6) curing 10min. The scheme was designed starting from Procedure B by replacing the epoxy adhesive layer with PDMS. R202 (2.5% wt) was suspended in n-hexane. Sylgard 184, composed of part A (PDMS) and part B (hardener), was tested with THF, DCM, DMAC and $CHCl_3$ using several concentrations (0.25%, 0.5%, 2.5%, 5.0%, 10.0% wt). The coatings prepared according to Procedure C were superhydrophobic but not resistant. The procedure was replicated with R504, giving similar results. CAs ranged from 147° to 152° for each type of SNPs. As an additional test, a thin protective layer of PDMS (5% wt) in DCM was deposed on R202 and R504 samples to improve resistance. Such layer, however, leads to a loss of superhydrophobicity without appreciably modifying resistance.

Procedure D was designed to expand the dataset and was based on Procedure A. Samples were spray-coated according to the scheme: 1) PDMS 5% wt or 20% wt layer; 2) curing time t = 15 min; 3) silica 2.5%wt layer. PDMS was mixed in DCM, and R202/R504 were suspended in n-hexane. The samples did not show SH properties (CAs < 130°) and had mediocre abrasion resistance once wholly cured.

Finally, Procedure E was designed to test the effect of multiple PDMS layers. Several samples were prepared according to the scheme: 1) 1-4 layers of PDMS 5% wt or 10% wt; 2) curing time t = 15 min; 3) silica 5% wt layer; 4) curing time t’ = 10 min. The samples were prepared using spray- and dip-coating techniques. Samples showed high CAs (148°-152°) and SH properties but did not show an acceptable abrasion resistance degree. The lack of mechanical resistance was attributed to SNPs preventing PDMS proper curing by sinking in the adhesive layer.

### 3.3.1 Analysis and characterization of the obtained coating

Throughout the project, more than 550 samples were prepared using the described procedures. Many samples were not used in the dataset construction, particularly those prepared on substrates other than PC/ABS, as they did not provide useful information for ANN training purposes, reducing the number of samples in the dataset to 450. Analyzing the results obtained using the different procedures described, it can be observed that Procedure B provides the best results in terms of superhydrophobic properties, CA, and strength. More specifically, the samples yielding the best results were prepared via spray-coating on PC/ABS substrate according to the following scheme: 1) n-hexane + Aerosil R202 (2.5% wt) layer; 2) GY2600 (5% wt) + EDR148 (1:1) in DCM layer; 3) n-hexane + Aerosil R202 (2.5% wt) layer; 4) curing time t = 15 min; 5) n-hexane + Aerosil R202 (2.5% wt) layer; 6) curing time t' = 10 min. The curing temperature is 70°C. The coating is composed of four layers in total.

The procedure was initially replicated on five samples, all of which yielded remarkably similar results, with a variation in CA of ±1°. As already discussed, the coatings were resistant to finger scratching, with no variation in CA after applying the procedure. Moreover, the coating showed an adequate level of abrasion resistance, as shown in Table 7 for the sample S0189, with a relatively small CA degradation before and after 1, 2, 3, and 5 cycles of tape peeling. CAs were measured using an optical tensiometer on a sessile drop. Figure 37A shows the snapshot for sample S0189 before tape peeling, while Figure 37B shows a snapshot captured after five tape peeling cycles. It can be observed that the water droplet maintains a spherical profile, typical behavior in SH surfaces.

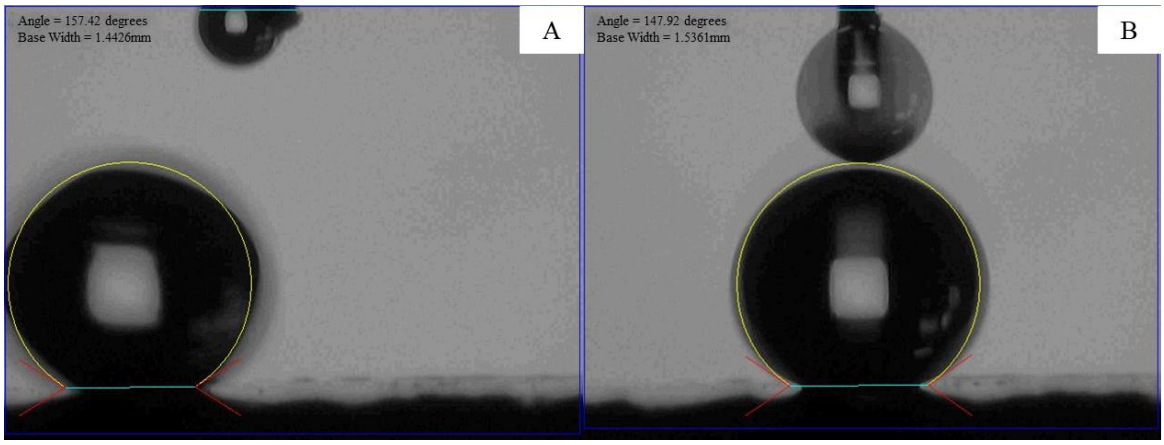


*Figure 37: Snapshot captured with an optical tensiometer for sample S0189 before (A) and after (B) five tape peeling cycles.*

SEM analysis for sample S0189 showed microscale spherical structures, which confirmed the presence of exposed silica nanoparticles and hierarchical roughness. SEM images show how the surface appears irregular, with a uniformly distributed roughness, a fundamental element in obtaining SH surfaces. Figure 38 and Figure 39 show magnifications at 2µm and 1µm, respectively. By observing SEM micrographs, the surfaces show a hierarchically distributed roughness at the micro- and nanoscale, which is more homogeneous and dense than the roughness displayed by lotus leaves SEM images that inspired SH surfaces (Figure 1).

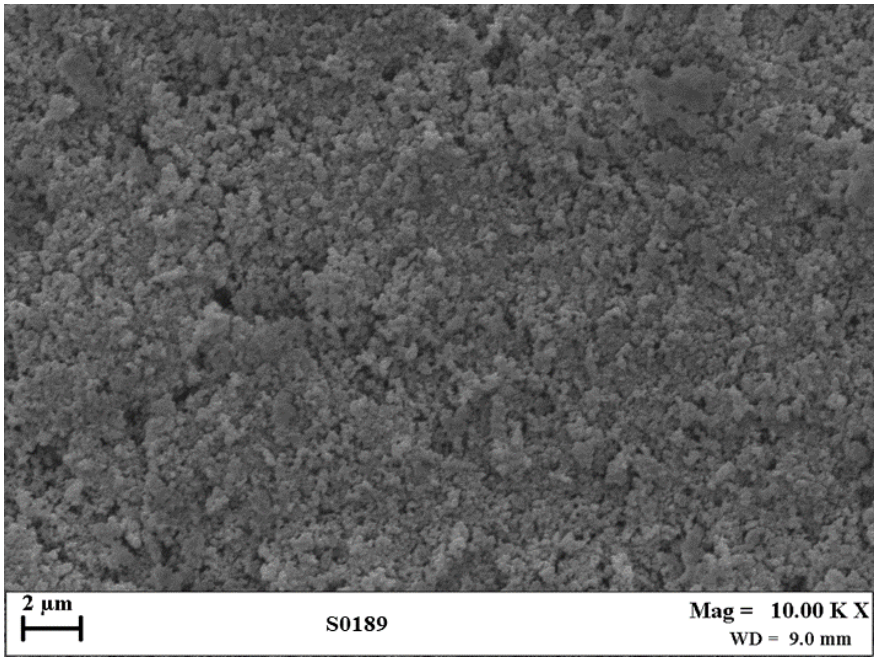


*Figure 38: SEM image at 2µm magnification for sample S0189.*

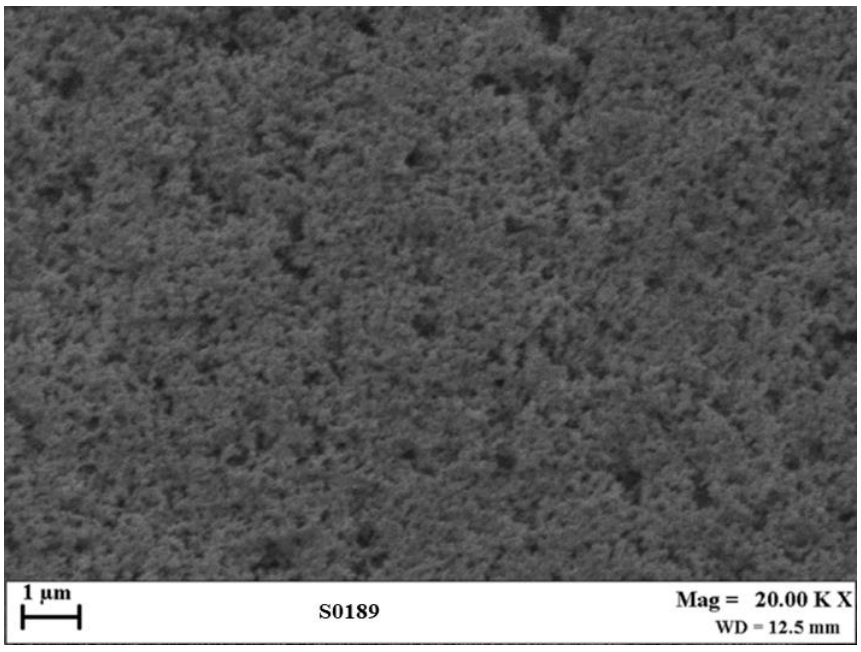


*Figure 39: SEM image at 1µm magnification for sample S0189.*

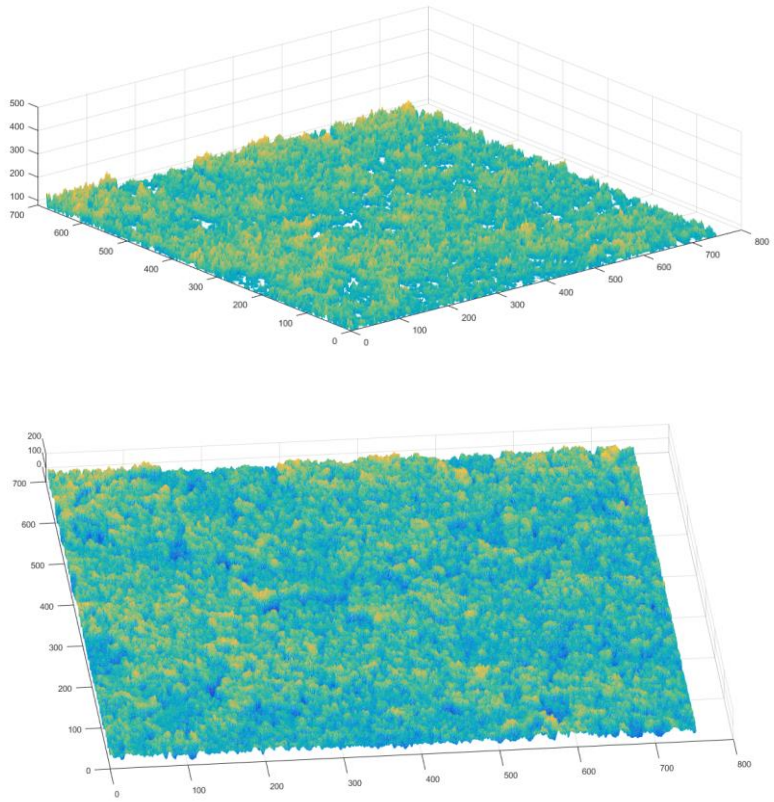

*Figure 40: digital surface reconstruction of S0189 sample.*

Figure 40 shows the 3D digital reconstruction of the S0189 surface in MATLAB. The surface roughness is homogeneously distributed on the surface of the sample, granting SH properties to the coating. Digital reconstruction of the surface at 200nm highlights the distribution of SNPs. The nanoscale size of the SNPs, and the presence of microscale aggregates, effectively reproduces the hierarchical roughness required to achieve a superhydrophobic surface.

Figure 41 shows the behavior of a water drop on the surface of sample S0189, obtained by capturing frame-by-frame the drop movement using a digital camera. It can be observed how the drop is immediately repulsed from the surface and does not leave any trace of water on it.

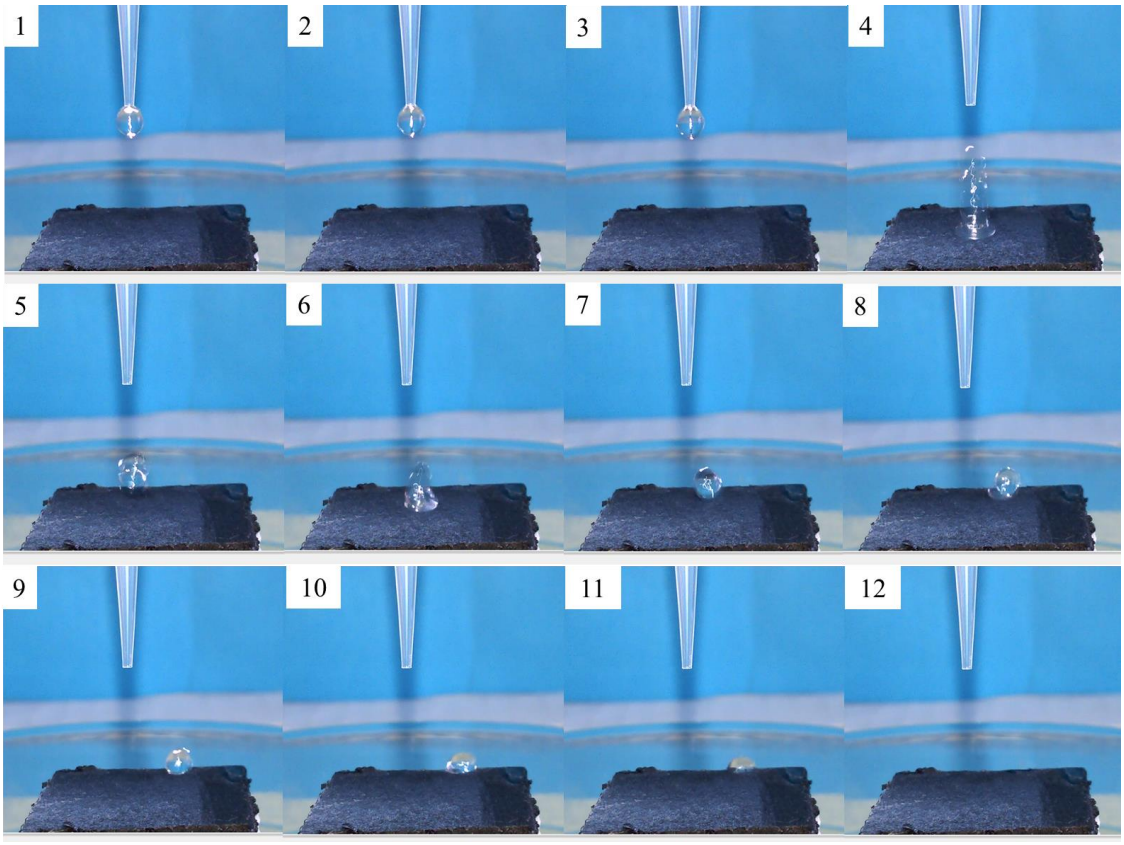


*Figure 41: Frame-by-frame capture of a water drop impacting on S0189 sample surface.*

To summarize, using Procedure B and R202 silica, it was possible to obtain a coating with excellent SH properties and a fair degree of mechanical resistance to abrasion. The coating shows promising features, which allow it to be applied in various settings. However, the limited degree of resistance means that the coating has to be further optimized.

The coating and the preparation process were further improved using the algorithms described in 4.1 Artificial Neural Network training and superhydrophobic coating prediction algorithm, focusing on enhancing coating resistance to mechanical solicitations. A new coating scheme was prepared, and a modified multistep method was devised using the trained algorithms. The new coating shows excellent SH and self-cleaning properties, with a CA > 160° and no degradation in the CA after 8+ cycles of tape peeling. CA measurements and SEM analysis results of the optimized coating are very similar to the results showed for S0189; the main difference is the increased tape peeling/abrasion resistance. Table 8 shows the average CA of five samples prepared according to the optimized scheme (OPT1-039).

| | ***OPT1-039*** |
|---|---|
| ***CA*** | 163°±2° |
| ***TP x1 CA*** | 163°±2° |
| ***TP x2 CA*** | 163°±2° |
| ***TP x3 CA*** | 163°±2° |
| ***TP x5 CA*** | 163°±2° |
| ***TP x8 CA*** | 162°±2° |
| ***TP x10 CA*** | 158°±1° |

*Table 8: Contact angle before and after tape peeling (TP) cycles for OPT1-039 procedure.*

The coating and the preparation process are being evaluated for possible patentability, and no further data can be disclosed at the time of writing. Obtaining a surface with outstanding SH characteristics and a high level of abrasion resistance and designing a deposition method that is easy to apply and cost-effective mark the achievement of the main objectives of the project. Future perspectives involve the scaling up and design of aseptic surfaces in a large-scale industrial setting.

### 3.3.2 Potential market and application of the developed coatings

In 2015, the hydrophobic coating market global size was EUR 1.10 billion and was projected to see substantial growth due to its rising area of use in the automotive, aerospace, biomedical, and construction industries[165]. Besides, the advancements of technology for applying nanoparticles in superhydrophobic coatings were expected to open new avenues for the industry growth. SH surfaces have potential application in the fields of anti-corrosion[14-18], anti-icing[10,19-23], anti-fogging[7,10,24-28], self-cleaning[7-13], anti-fouling[11,22,29-32], and other sectors[30,33-36], with a noticeable forecast increase in the market volume request for the anti-corrosion and antimicrobial sectors[165] (Figure 42).

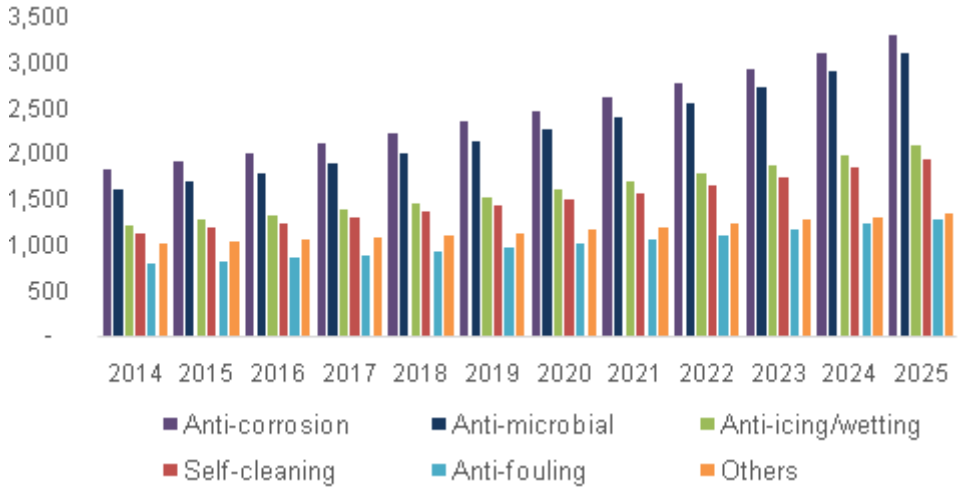


*Figure 42: Market report for SH coatings, updated to 2016 and projected to 2025*[165].

This project was developed to obtain a surface with strong superhydrophobic properties and an easy, cost-effective, and scalable preparation process for application in antimicrobial surfaces and biomedical devices. The demand for durable, effective anti-microbial coatings is high, and it is expected to grow even more with the outbreak of the COVID-19 pandemic[39,40,166,167]. SH surfaces could even find potential application in preventing the spread of COVID-19 thanks to the self-cleaning properties[37,38]. As already discussed, SH surfaces can prevent the growth of microbial substrates and can find wide application in the production of aseptic surfaces, nonwovens such as gowns & gloves, surgical tools, coronary stents, and catheters, or orthopedic implants. The rising demand for antimicrobial coatings in catheters, implantable, and surgical instruments as they are biocompatible, non-toxic, and biostable will promote industrial development in the next years[167]. Thanks to the excellent SH properties, the coatings developed in this project framework can be applied to develop antibacterial surfaces. The few limitations of the coatings do not allow their use in internal medical devices or surgical instruments. An interesting use could be the application of the coating to the surfaces of operating rooms, thus including all the necessary instrumentation and furniture in an instrument where sterility is a fundamental requirement (operatory tables, trays, faucets, sinks, etc.). The coatings could be applied to everyday/public-use surfaces, which act as potential carriers of pathogenic bacteria, for example in a hospital environment. The developed coatings could, for example, be applied to bedrails, handrails, over-bed tables, sinks, faucets, doorknobs, or toilet hardware in hospitals; could find application in elevators, shopping cart handles, kitchen surfaces in public facilities, or even in handrails, grab bars, or seats in mass transportation.

# CHAPTER 4
# Application of Artificial Neural Networks

## 4.1 Artificial Neural Network training and superhydrophobic coating prediction algorithm

Coating and process optimization has many parameters to consider. It is an example of multivariate analysis, not treatable with conventional methods. For this reason, the use of advanced computational tools such as ANN and DL methods[24] proved to be essential. Using ANNs, indeed, it is possible to tackle problems that are generally impossible or difficult to solve by human or statistical standards. Moreover, ANNs have self-learning capabilities that allow them to deliver better outcomes as more data becomes available.

Using data collected from the SH coatings preparation, an extensive dataset was collected, containing information about the materials used, the operating parameters, and the developed coatings main features (SH and non-SH). This dataset was used to train an ANN, obtaining two algorithms that, combined, predict the CA and abrasion resistance degree of a coating. The algorithms were used to design a durable, highly SH coating and to optimize the preparation method. The design of the computational experiments, the Artificial Neural Networks training, and the development of the algorithms and methods were conducted in collaboration with SmartVASE Srl, a spin-off of the University of Salerno active on biomaterials and superhydrophobic coatings[168].

### 4.1.1 Dataset preparation

Data collected from the prepared samples (e.g., reagents, concentrations, number of layers, curing time, resistance) have been used to build an extensive dataset structured as a matrix. The matrix was used to train an ANN, aimed at optimizing the coating itself. The matrix was prepared to make it readable by the ANN. For the proper training of a neural network, it is necessary that data are formatted and labeled appropriately. The used algorithm is based on supervised learning, i.e., learning that provides the network with a set of labeled inputs to which correspond known outputs[169]. Labeled data implies that inputs and outputs have known values. Using ANNs, it is possible to find the relationship between inputs and outputs, obtaining a mathematical model or algorithm. The objective is to predict the output given a new input once the model has been trained. On the contrary, unsupervised learning is used when data are not labeled and outputs are unknown.

The dataset was prepared in successive steps, editing and optimizing the labeling and organization following several ANN training iterations. The final dataset structure is based on Procedure B and involves four possible layers in the preparation process, including data

from Procedures A-E. Each row of the dataset contains the data of a sample. Columns contain the following data:

1) Sample ID
2) Composition of layer 1
3) Composition of layer 2
4) Composition of layer 3
5) Composition of layer 4
6) Contact angle
7) Resistance level

The complete structure of the dataset is outlined later in this subsection. Each layer composition is divided into several columns, one for each used material, e.g., a column for the epoxy resin, one for hardener D400, one for EDR148, one for R202 silica, etc.

Moreover, for each layer composition, a column for the curing time and another for the number of repeated layers are reported. Each layer, therefore, includes every used material. The value is generally set at their wt% for the given layer. The value for a material not used in a specific layer is set to 0. Solvents are set to 1 if present in the given layer or 0 if not present.

Contact angle and resistance columns were set as the output for the training of the ANN. The training, however, requires numerical data only since ANNs cannot process structured language per se, e.g., the network could not process the resistance feature if it were set to "yes" or "no". For this reason, while CAs were reported in degrees, a workaround was applied to resistance values. Expressly, inspired by binary programming, for abrasion-resistant samples, the resistance value was set to 1, while for non-resistant samples, it was set to 0. Adapting the values to the need, for the samples that showed intermediate resistance but not enough for coating development, the value was set to 0.5.

The final dataset was stored in comma-separated values format (CSV). It is composed of 83 columns and 450 rows plus headers. The dataset headers, which reflect the dataset structure, are the following (in CSV):

```
Sample; epoxy_1; D320_1; D400_1; accelerator400_1; EDR148_1; PDMS_1;
THF_1; DCM_1; DMAC_1; CHCl3_1; C-silica_1; N-silica_1; nHEX_1; cHEX_1;
THF_1; DCM_1; DMAC_1; CHCl3_1; layers_1; curing_1; epoxy_2; D320_2; D400_2;
accelerator400_2; EDR148_2; PDMS_2; THF_2; DCM_2; DMAC_2; CHCl3_2; C-
silica_2; N-silica_2; nHEX_2; cHEX_2; THF_2; DCM_2; DMAC_2; CHCl3_2;
layers_2; curing_2; epoxy_3; D320_3; D400_3; accelerator400_3; EDR148_3;
PDMS_3; THF_3; DCM_3; DMAC_3; CHCl3_3; C-silica_3; N-silica_3; nHEX_3;
cHEX_3; THF_3; DCM_3; DMAC_3; CHCl3_3; layers_3; curing_3; epoxy_4; D320_4;
D400_4; accelerator400_4; EDR148_4; PDMS_4; THF_4; DCM_4; DMAC_4; CHCl3_4;
```

`C-silica_4; N-silica_4; nHEX_4; cHEX_4; THF_4; DCM_4; DMAC_4; CHCl3_4; layers_4; curing_4; CA; resistance.`

A number represents each layer of a given coating. The first layer materials will have a "_1" in the headers. For the second layer, the headers will have the material denomination followed by "_2" and so forth for the third and fourth layers. Table 9 shows an excerpt of the dataset structure. For example, S0189 sample first layer is composed of R202 2.5% wt in n-hexane. Therefore, the value of R202_1 is set at 2.5 in the table, while n-hexane is set as 1 (similar to "yes" for binary language). A single layer of R202 is deposited, and layers_1 value is set at 1, while curing is set at 0 (minutes) since the first layer does not involve curing. All the other values are set at 0.

| | STEP_1 | | | | | | | | | STEP_2-4 | OUTPUT | |
|---|---|---|---|---|---|---|---|---|---|---|---|---|
| **Sample** | **epoxy_1** | **EDR148_1** | **PDMS_1** | **DCM_1** | **R202_1** | **R504_1** | **nHEX_1** | **layers_1** | **curing_1** | **(…)** | **CA** | **Res** |
| S0175 | 1.0 | 0.0 | 0.0 | 1.0 | 0.0 | 0.0 | 0.0 | 1.0 | 10.0 | (…) | 126 | 0 |
| S0176 | 12.5 | 0.0 | 0.0 | 1.0 | 0.0 | 3.5 | 0.0 | 0.0 | 6.0 | (…) | 80 | 1 |
| S0177 | 12.5 | 0.0 | 0.0 | 1.0 | 0.0 | 3.5 | 0.0 | 0.0 | 8.0 | (…) | 84 | 1 |
| S0178 | 12.5 | 0.0 | 0.0 | 1.0 | 0.0 | 3.5 | 0.0 | 0.0 | 10.0 | (…) | 100 | 1 |
| S0179 | 12.5 | 0.0 | 0.0 | 1.0 | 3.5 | 0.0 | 0.0 | 0.0 | 6.0 | (…) | 88 | 1 |
| S0180 | 12.5 | 0.0 | 0.0 | 1.0 | 3.5 | 0.0 | 0.0 | 0.0 | 8.0 | (…) | 84 | 1 |
| S0181 | 12.5 | 0.0 | 0.0 | 1.0 | 3.5 | 0.0 | 0.0 | 0.0 | 10.0 | (…) | 121 | 1 |
| S0182 | 12.5 | 3.5 | 0.0 | 1.0 | 3.5 | 0.0 | 0.0 | 5.0 | 20.0 | (…) | 90 | 1 |
| S0183 | 12.5 | 3.5 | 0.0 | 1.0 | 3.5 | 0.0 | 0.0 | 4.0 | 20.0 | (…) | 90 | 1 |
| S0184 | 12.5 | 3.5 | 0.0 | 1.0 | 3.5 | 0.0 | 0.0 | 2.0 | 20.0 | (…) | 79 | 1 |
| S0185 | 12.5 | 3.5 | 0.0 | 1.0 | 3.5 | 0.0 | 0.0 | 2.0 | 20.0 | (…) | 76 | 1 |
| S0186 | 12.5 | 3.5 | 0.0 | 1.0 | 3.5 | 0.0 | 0.0 | 5.0 | 0.0 | (…) | 102 | 1 |
| S0187 | 12.5 | 3.5 | 0.0 | 1.0 | 3.5 | 0.0 | 0.0 | 2.0 | 0.0 | (…) | 78 | 1 |
| S0188 | 1.0 | 1.0 | 0.0 | 1.0 | 0.0 | 0.0 | 0.0 | 2.0 | 0.0 | (…) | 102 | 1 |
| S0189 | 0.0 | 0.0 | 0.0 | 0.0 | 2.5 | 0.0 | 1.0 | 1.0 | 0.0 | (…) | 157 | 1 |
| S0190 | 0.0 | 0.0 | 0.0 | 0.0 | 2.5 | 0.0 | 1.0 | 1.0 | 0.0 | (…) | 148 | 1 |
| S0191 | 1.0 | 1.0 | 0.0 | 1.0 | 0.0 | 0.0 | 0.0 | 1.0 | 0.0 | (…) | 128 | 1 |
| S0192 | 1.0 | 1.0 | 0.0 | 1.0 | 0.0 | 0.0 | 0.0 | 1.0 | 0.0 | (…) | 133 | 1 |
| S0193 | 0.0 | 0.0 | 0.0 | 0.0 | 2.5 | 0.0 | 1.0 | 1.0 | 0.0 | (…) | 148 | 0.5 |
| S0194 | 0.0 | 0.0 | 0.0 | 0.0 | 2.5 | 0.0 | 1.0 | 1.0 | 0.0 | (…) | 146 | 0.5 |

*Table 9: Superhydrophobic coatings dataset excerpt. The reported excerpt is only representative of the final dataset, as it can be seen from the missing data and the hidden columns; it was reported with the sole purpose of exemplifying the structure of the dataset. Step 1 is missing several columns containing different materials, while steps 2, 3, and 4 are hidden. Only 20 of 450 rows are reported.*

### 4.1.2 Artificial Neural Network training and prediction algorithms

As discussed in CHAPTER 2

Artificial Neural Networks, ANNs are calculation systems that learn to execute commands without being programmed. An ANN is based on a set of connected artificial neurons. Each

connection can transmit a signal to other neurons. An artificial neuron that receives a signal processes it and can send it to the connected neurons. In the present work, the initial inputs are the operating parameters (STEP1 to STEP4 of the dataset), the targets are the contact angle and resistance, and the final output is equations for the optimization of the used parameters, which provide the best composition to prepare a coating that is both resistant and superhydrophobic.

The used algorithm is based on supervised learning[169]. By analyzing the data provided, the network predicts the possible link between data points and, in this way, learns to calculate correct associations between the input data provided. As the network processes data, it applies corrections to improve the outputs, increasing the weight of the parameters that determine the correct outputs and decreasing those that generate invalid values. The supervised learning mechanism, therefore, employs error backpropagation[170].

The network training has been carried out considering all the operational parameters involved in preparing the samples. The matrix initially used was composed of 250 samples, of which 80% was selected randomly as the training set, while the remaining 20% was used as the validation set. The training set is used for the actual learning phase of the ANN, while the validation set is necessary to ensure that the algorithm is capable of performing the correct predictions. As previously discussed, the output parameters on which attention has been focused are two: contact angle and coating resistance. The first attempts to train the network were poorly precise due to the gaps in the initial dataset. Therefore, it was necessary to fill in missing data by preparing new samples to obtain a complete matrix. Several iterative training steps of the ANN were performed, using the feedback to evaluate the new samples needed to optimize the dataset. It was a long and time-consuming process since the preparation of the sample was performed manually on a small scale; automation of the preparation process could significantly improve the efficiency of the workflow.

The final dataset, which was used to train the working algorithms, comprises 450 samples and is described in the previous subsection. For the training, the dataset was split into 80% training set and 20% validation set. The software used for training automatically generates *n* models for each target. The models are ranked according to their performance, and the most accurate model is selected. Two different predictive algorithms were obtained, one to predict the contact angle of compositions, the other to evaluate its resistance.

Table 10 summarizes the principal values of the network accuracy with CA as the target, while Table 11 summarizes the data for resistance as the target. The values reported in the *Model Fit* column are relative to the training set, while the *Predictions* column refers to the

validation set. The *Number of observations* row shows the number of elements on which the analysis is performed. As already discussed, the dataset consists of 450 samples; 360 represents the number of samples used in training (80%), while 90 observations correspond to 20% of the total dataset, used as the validation set.

| ***Contact Angle*** | ***Model Fit*** | ***Predictions*** |
|---|---|---|
| ***Number of observations*** | 360 | 90 |
| ***Mean absolute error (MAE)*** | 9.63 | 8.13 |
| ***Coefficient of determination ($R^2$)*** | 0.80 | 0.83 |
| ***Correlation (Pearson)*** | 0.89 | 0.92 |

*Table 10: Prediction accuracy of the trained ANN with Contact Angle as the target.*

| ***Resistance*** | ***Model Fit*** | ***Predictions*** |
|---|---|---|
| ***Number of observations*** | 360 | 90 |
| ***Mean absolute error*** | 0.032 | 0.053 |
| ***Coefficient of determination ($R^2$)*** | 0.88 | 0.75 |
| ***Correlation (Pearson)*** | 0.94 | 0.87 |

*Table 11: Prediction accuracy of the trained ANN with Resistance as the target.*

*Mean absolute error*, *Coefficient of determination*, and *Correlation* are accuracy measures used to evaluate the trained ANN performance. Mean absolute error (MAE) is a good measure of errors between paired observations[171]. MAE uses the same scale as the data being measured; therefore, MAE cannot compare series using different scales. It can be observed that MAE has different values for the two obtained algorithms; this is due to the different scales used for the two target parameters (CA and resistance). For CA, which ranges from 62° to 157°, the MAE is ~9% of the total, resulting in a sufficiently low error, indicating good accuracy of the algorithm. The trained algorithm for resistance shows an even lower MAE, approximately 4% of the total since resistance values range from 0.0 to 1.0. The coefficient of determination ($R^2$) is a widely used accuracy measure, representing the variance in the dependent variable that is predictable from the independent variable(s). $R^2$ provides a measure of how well observed outcomes are replicated by the model, based on the proportion of total variation of outcomes explained by the model[172,173], and is a statistical measure of how well the predictions approximate the real data points. $R^2$ values range between 0 and 1, and an $R^2$ of 1 means that the predictions perfectly fit data. Both trained algorithms show relatively high (>0.75) $R^2$ values, confirming the models excellent accuracy level. The correlation coefficient represents the statistical relationship between real and

predicted values, with 1 being the most robust possible agreement between the values; Pearson correlation is reported for the trained algorithms. Pearson correlation measures the strength and direction of linear relationships between pairs of continuous variables and evaluates whether there is statistical evidence for a linear relationship among the same pairs of variables in the population[174]. The correlation values obtained for the algorithms at issue are indicative of an adequate level of accuracy.

The predictive models are complex equations consisting of several sub-equations that correlate the parameters of the dataset. The algorithms can predict the CA and resistance level of a coating by analyzing input data, i.e., user-defined material quantities and operating parameters. Equation 4 and Equation 5 describe the predictive models for CA and resistance forecasting, respectively. Only the main equation is reported, but not all of the sub-equations, for copyright reasons. Each *N* in the equations represents a sub-equation, which in turn is composed of several sub-equations.

```
Y1 = -27.4944 + N784*0.892439 - N784*N18*0.00957053 +
N18*0.674638 + N18^2*0.00655458
```

*Equation 4: Predictive model for contact angle forecast.*

```
Y2 = 0.00223978 - N821*4.49856 - N821*N24*5.57253 +
N821^2*5.564 + N24*5.42902 + N24^2*0.0757837
```

*Equation 5: Predictive model for resistance forecast.*

The algorithms were successfully applied for the design of an optimized coating. After several tests, a coating with a CA > 160° with excellent self-cleaning properties was prepared, based on an optimized coating predicted by the algorithms. The preparation required a slightly modified multistep deposition scheme suggested by the prediction. The resulting coating also showed a high degree of abrasion resistance, with no CA degradation after 8+ cycles of tape peeling. The new preparation scheme, the modified multistep deposition method, and the coating composition are under patent evaluation at the time of writing, and no further data can be disclosed.

### 4.2 Computational methods

The Artificial Neural Network was trained using the GMDH Shell DS 3.8.9[175] software application, selecting a regression forecasting model. The used core learning algorithm was the GMDH-type Neural Network (Group Method of Data Handling)[176,177]. GMDH Neural Networks, also known as polynomial Neural Networks, are Feedforward Multilayer

Perceptron networks that use the combinatorial algorithm to improve neuronal connection[178]. The selected internal function for neurons was the quadratic polynomial function, and the upper limit for the number of network layers created by the algorithm was set at 33. GMDH-type networks generate many layers, and an upper limit of 33 layers was set to reduce the quickly growing computer memory and time consumption while maintaining good predictive accuracy. The reordering of rows, used to achieve uniform statistical characteristics of training and testing samples and to make them equally informative, was performed with the *odd/even* method, which places all even instances after odd instances. The selected validation strategy was the *k-fold validation* (2 folds): the dataset is split k parts, and then a model is trained for k times, using k-1 parts. The performance of the model was measured at each training using a new remaining part. The selected validation criterion for both the core algorithm and variables ranking was the RMSE (Root-Mean-Squared Error). The variables were ranked by correlation, and only the 20 top-ranked variables were considered for model evaluation; the reduction of variables was necessary for quicker processing of the high-dimensional dataset. GMDH-type networks have been successfully used for numerous applications in the past[176-183]. GMDH Shell DS 3.8.9 software application was selected for its relative ease of use. It does not require extensive knowledge of programming languages and can train ANNs quickly and effectively, without losing quality compared to other software applications and ANN frameworks.

### 4.3 Other applications of ANNs in parallel to the thesis project

Artificial Neural Network techniques have a vast range of applications. Since the project main objectives were achieved ahead of schedule, and because of the delays and the shift in research caused by the COVID-19 pandemic outbreak, new computational projects were carried out in parallel with the development of SH surfaces and optimization algorithms.

The acquired techniques were used to develop an ANN-based tool for the identification, activity prediction, and optimization of antimicrobial peptides (AMPs), currently a working prototype. Two AMPs were predicted using the tool and synthesized, showing antibacterial activity against *Staphylococcus aureus* from preliminary tests.

In collaboration with the research group of Professor Amedeo Caflisch, Biochemistry Department of the University of Zurich, a project for the development of an ANN-based software application for anticancer drug design has been started. This project is still in the pre-prototype phase but has shown promising potential. One of the project aims is to

interface classical computational docking techniques to ANN methods, to develop a fast and efficient *in silico* drug discovery tool.

### 4.3.1 NN-AMP: a tool for the design of new Antimicrobial Peptides

During the Ph.D. program, in parallel with the work on SH surfaces, an ANN-based prototype software application to predict and optimize antimicrobial peptides was developed in collaboration with SoftMining Srl[184], specialized in the application of Artificial Intelligence methods to drug discovery and life sciences.

Antimicrobial resistance is an ever-growing concern and poses a severe threat to global public health. Resistant pathogens are on the rise, and the geographic areas affected are expanding. Pathogens that were under drug control have become resistant to treatments, and this has begun to occur, especially in hospitals where antibiotic use was initially widespread[73,74]. Antimicrobial peptides (AMPs) are oligopeptides with a variable number of amino acids (from 5 to 100) whose targets are microorganisms, from viruses to parasites. AMPs are biosynthesized by microbes, plants, and animals from diverse taxonomical hierarchy. These are the first line of host defense peptides, present across all kingdoms. Antimicrobial peptides are particularly interesting because they are less prone to generate microbial resistance, offering a potential solution to the long-standing antibiotics resistance problem[185-188].

Currently a working prototype, NN-AMP is a software application for predicting antimicrobial peptides activity and new antimicrobial sequences. The tool can discover entirely new sequences, obtain new, more active sequences starting from known AMPs, and evaluate the obtained sequences patentability. The tool can help discover new drugs to fight multi-drug resistant bacterial strains while shortening the discovery and development process. The tool is oriented to the generation of highly specific peptides, thus aiming at selectivity rather than potency.

The training dataset is a curated set of AMPs data, mainly based on YADAMP, a database of antimicrobial sequences developed by Piotto et al.[189]. Decoy sequences, i.e., inactive sequences structurally similar to active AMPs, were also included. The activity prediction models were generated by training a neural network. The tool focuses on linear sequences because they have a lower computational cost, allowing faster software response times compared, for example, to circular AMPs, which require more complex and resource-intensive tools.

The initial training was carried out on a small number of active sequences, to which a small number of inactive sequences was added. The initial activity targets were *E. coli*, *P. aeruginosa,* and *S. aureus*. These three bacterial strains are among the most common causes of antibiotic-resistant infection and are the most represented strains in the dataset (the strains on which more data were present). The network underwent progressive training, increasing the number of sequences used and exploiting different datasets.

Nine predictive algorithms have been obtained so far, targeting the three different pathogens. Each algorithm is selective for a given pathogen. The nine models show consensus in predicting the activity and selectivity of a given sequence. The prediction of selectivity is the main target of the algorithms, with the ultimate goal of generating highly specific sequences for a given bacterial strain.

The algorithms have been packaged in a software tool for the activity prediction of an input sequence. GMDH-type methods have been used for the training of the ANNs. For the training of Neural Networks, numerous parameters have been considered for each sequence of the dataset, setting as target the experimental activity data reported in the scientific literature. Several physicochemical properties, such as charge, helicity, flexibility, isoelectric point, Boman index, and instability index, were calculated *in silico*. Attention has been focused in particular on helicity. The term helicity refers to the tendency of a protein to form the α-helix. It plays a crucial role in the specificity and toxicity of antimicrobial peptides, and it has been observed that peptides with a high helicity value manifest strong antimicrobial activity[190]. Antimicrobial activity data is reported as Minimal inhibitory concentration[191] (MIC), defined as the lowest concentration of an antimicrobial substance capable of inhibiting a bacterium growth. The training of ANNs has been a very long iterative process, with the gradual expansion and adaptation of the dataset. At the time of writing, it has not yet been possible to obtain a general-purpose algorithm. However, specialized algorithms are particularly advantageous since it is possible to design and optimize highly specific peptides active on a specific pathogen strain.

The tool can also generate new and more active sequences by modifying an initial sequence or predicting new sequences. The tool generates all the possible amino acid (aa) substitutions (pool of 20 aa) for a random position of an input sequence; addition and deletion are also considered. The software application then applies the algorithms obtained through ANN to calculate the MIC of the sequence and the reliability of the models (through a scoring function). For each generation, the sequence with the best scoring value is selected and forwarded to become the next cycle input sequence. The software application is the

combination of four different tools, each with a different role. An overview of the application workflow is shown in Figure 43. The platform is divided into the following tools:

- pep1: prediction of antimicrobial activity and selectivity of a known sequence. It processes user-defined sequences.
- pep2: generation of new active sequences from known sequences (improvement of existing sequences). It generates analogue sequences by random substitutions.
- pep3: generation of potentially active random sequences of user-defined length.
- pep_patent: preliminary patent evaluation tool. The pep_patent tool searches for the selected peptide in the four most important patent databases, i.e., Korean, American, Japanese, and European Patent Offices. This tool searches the selected sequence or 8aa-long fragments in the databases to exclude patent-protected sequences as a preliminary patentability assessment.

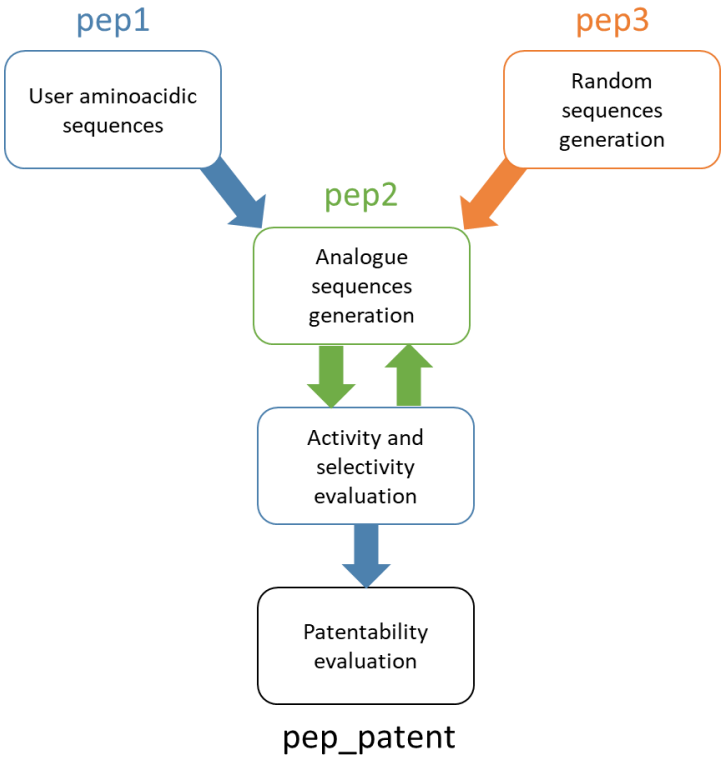


*Figure 43: NN-AMP general workflow.*

#### 4.3.1.1 Sequence generation and activity evaluation

The tool pep1 applies the models obtained from ANN to a list of sequences, thus obtaining a MIC value for each model. The first step involves the calculation of over 530 parameters using the YADAMP_descriptor tool. These descriptors are the parameters used by the mathematical models obtained through Neural Networks. The next step is the MIC

calculation. For each sequence, an alignment and a calculation of each model distance from the datasets are performed. The alignment (*pairwise*) uses a *BLOSUM50* matrix, while the distance is calculated through the *alignment score* method (see below). The models are calibrated on selectivity accuracy more than potency accuracy. This calibration is essential to obtain highly selective peptides, leading to the development of targeted AMPs.

The tool pep2 generates new sequences from a single initial sequence. A random position is selected, and twenty changes are performed, i.e., twenty new sequences are generated, performing a swap for each amino acid in the initial pool. The positions can also be subject to the addition or deletion of amino acids. Once the sequences are generated, descriptors, MICs, and distances are calculated by pep1. The sequence with the best scoring value will be selected at each cycle, and a new cycle will be performed. The output file will show the list of modified sequences, their MICs, distances, scoring values, and the geometric mean of the MICs for each sequence and each generation. Example:

| | |
|---|---|
| starting sequence: | EPFKISIHL |
| I generation selected sequence: | EPFKISICL |
| II generation selected sequence: | EPFKISICR |
| III generation selected sequence: | CPFKISICR |
| *n* generation selected sequence: | CMFRQSIG_ |

The tool can process a single sequence or a list of sequences. It also allows selecting which model to test the peptides (*E. coli*, *P. aeruginosa*, *S. aureus*, or all three).

The pep3 tool generates completely random sequences of user-defined length; pep1 is then applied to these random peptides for MIC calculation.

#### 4.3.1.2 Scoring function

The scoring function used to evaluate the generated sequences is the following:

$$\textbf{score} = harmonic\ mean(\sum_1^i (MIC_i * d_i * 100) + 5)$$

Where $MIC_i$ is the MIC calculated from model $i$ and $d_i$ is the distance from model $i$. The scoring function is the harmonic average of the sum of MIC products and distances. The +5 is necessary to exclude values equal to 0, which would lead to an error in calculating the harmonic mean. The 0 appears if the tested or produced sequence is equal to a sequence already present in the initial dataset. The harmonic averaging has been chosen because it gives more weight to lower values, giving less importance to higher values; thus, lower MICs

are favored. In general, the scoring function is necessary to assess which peptides to accept and which to reject.

#### 4.3.1.3 Alignment score method

The distance (*d*) between two sequences (1, 2) is computed from the pairwise alignment score between the two sequences ($score_{12}$), and the pairwise alignment score between each sequence and itself ($score_{11}$, $score_{22}$) as follows:

$$d = (1-score_{12}/score_{11}) * (1-score_{12}/score_{22})$$

Two identical sequences will have $d = 0$. As *d* increases, the difference between the two sequences increases.

#### 4.3.1.4 Patentability evaluation

The databases containing every protein sequence published in patents have been obtained from a public repository[192] (*fasta* format). The databases come from the European, Korean, Japanese, and US patent offices. A script has been created to sequentially generate eight aa-long fragments, starting from the first amino acid of the input sequence (e.g., `ABCDEFGHIJKLMNO`; sequence 1: `ABCDEFGH`; sequence 2: `BCDEFGHI`). The tool automatically searches the entire sequence and the fragments in the databases. The output provides the input string its presence or absence within the databases reported as *true* or *false*.

#### 4.3.1.5 Applications and future perspectives

Using NN-AMP, a set of 20 new sequences were generated. The solubility of the peptides was calculated, and six water-soluble sequences between 12 and 27 amino acids were selected (SM1-SM6). These sequences underwent preliminary antimicrobial tests. SM1 and SM3, respectively 12-aa and 14-aa long and which were trained for selectivity on *S. aureus*, actually showed inhibition against *S. aureus* (ATCC 6538) but did not inhibit the growth of *P. aeruginosa* (ATCC 9027) or *E.coli* (ATCC 8739). The potency of the peptides is low, but the results of the preliminary tests show selectivity towards *S. aureus*, in accord with the predicted selectivity. These sequences are currently under patent evaluation and will be used as lead compounds to generate new, more active sequences, potentially active on *S. aureus* and Gram+ pathogens. Future perspectives for the tool are expanding the dataset to include a wider range of pathogenic strains, focusing on the most widespread superbugs (i.e.,

bacteria resistant to most antibiotics[188]), and optimizing the algorithms to obtain potent and selective AMPs. Figure 44 schematizes the optimization process that will be applied.

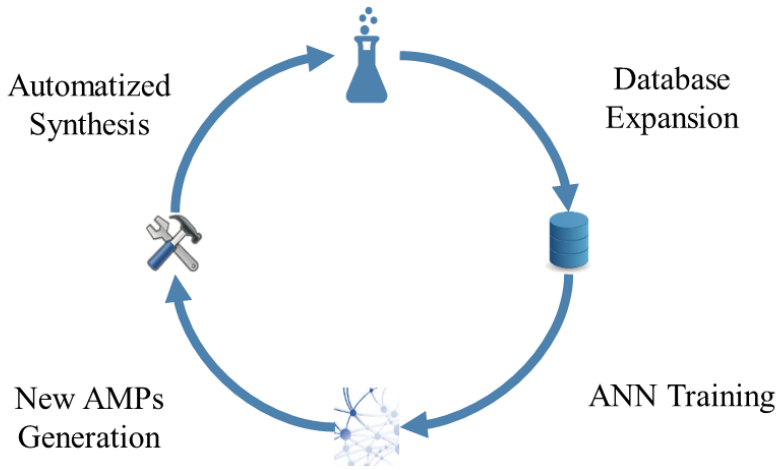


*Figure 44: NN-AMP recursive training scheme.*

A process for the automated rapid synthesis of small amounts of peptides is currently under development at SoftMining Srl at the time of writing. This process could be used to apply an iterative ANN training protocol. The protocol would involve the synthesis of NN-AMP-generated sequences and testing for antimicrobial activity. The resulting data would be used to improve the accuracy of current predictive algorithms.

Finally, a very interesting approach, currently in an initiation-stage project, could be the development of dual-function antibacterial surfaces[72], combining optimized SH surfaces and generated AMPs. Surfaces with bacteria-resisting and bacteria-killing features could prove particularly useful in the biomedical field to develop surgical tools and implantable devices with high antibacterial efficiency.

### 4.3.2 Development of an ANN-based tool for anti-cancer drug discovery and repurposing

ANNs are a potent tool. Their multiple advantages have led to their use in a variety of biomedical fields, including drug discovery. ANNs have found wide application in this field, entering the initial phase of research and development, with the potential to drastically cut costs and time needed in the initial phases of drug discovery[110,111,113,193-195]. Computational activity prediction of molecules is a time-consuming and resource-heavy process that uses tools and methods as Molecular Docking, Molecular Dynamics, DFT calculations, QSARs prediction, etc. Artificial Neural Networks (ANN) are widely used in various biomedical fields like bioinformatics, cheminformatics, QSARs, medical imaging, and disease prediction. One of the main advantages of using ANN over the classical methods is that they

require less computational time and fewer resources, giving the same or higher accuracy than the other computational methods. ANNs are widely used with large datasets and multivariate problems that cannot be solved using classical methods and linear functions. Another significant advantage of ANNs is learning and self-correcting in nonlinear, complex, and noisy environments. ANNs can reduce the required times and resource use while also dealing with large datasets and nonlinear problems. ANNs have also been applied for the development of improved and more efficient computational docking methods[193,195,196].

During the Ph.D. program years, a secondary project for developing an ANN-based software application for anticancer drug design has been initiated. In the first part of the project, a neural network-based tool for small molecule activity prediction was started. A relatively small dataset of molecules active on Carbonic Anhydrase, a target for anticancer drug development, was initially selected[197]. Various descriptors have been calculated, such as structural, biochemical, biophysical, and electronic properties. The descriptors were integrated with docking data to build an extensive dataset, and an ANN was trained to predict compounds activity. This approach is interesting because it could be extended to any target by training new ANNs. However, the algorithms obtained so far are not accurate, and the system still needs to be improved. The project was developed in collaboration with Prof. Caflisch's research group at the University of Zurich to implement AI methods to classical bioinformatics methods. During the collaboration, the knowledge and methods acquired were applied to the development and improvement of the described tool, which still needs further improvement. The final goal is to obtain an extensive ANN algorithm for the fast and accurate prediction of small molecule activity for hit discovery and drug repurposing.

# CONCLUSIONS

## Conclusions

Superhydrophobic surfaces show excellent self-cleaning, anti-biofilm, and anti-fouling properties, with a high potential for application in many industrial fields and biomedical devices, especially in developing antimicrobial surfaces for biomedical use. However, these surfaces suffer from low mechanical resistance, and the preparation processes are often costly and not applicable on a large scale.

The research work carried out in the frame of the three years Ph.D. in Drug Discovery and Development has been focused on the design and development of a resistant superhydrophobic surface, using a simple and scalable method, and on the application of Artificial Neural Networks to optimize both the coating and the process. In the first part of the work, the general process for coating design was outlined. Several preparation methods were discussed, finally selecting spray-coating deposition and a multi-step layer-by-layer process. This method is the most effective in coating preparation and potentially applicable on a large scale. The iterative coating preparation process was then discussed, using five different procedures (Procedures A-E), each with a different layer pattern, and using a wide range of materials, solvents, and operating parameters. A coating based on silica nanoparticles was prepared, with strong superhydrophobic characteristics (contact angle = 157°) and a reasonable degree of resistance to abrasion. The coating consisted of four different layers and was prepared according to the scheme:

| | |
|---|---|
| layer 1 | Aerosil R202 silica nanoparticles (2.5% wt) in n-hexane |
| layer 2 | GY2600 epoxy resin (5% wt) + EDR148 hardener (1:1) in DCM |
| layer 3 | Aerosil R202 silica nanoparticles (2.5% wt) in n-hexane |
| | curing time 15 minutes |
| layer 4 | Aerosil R202 silica nanoparticles (2.5% wt) in n-hexane |
| | curing time 10 minutes |

All data regarding the applied schemes, the materials used, and the operational parameters were collected to prepare a dataset. This dataset was used for the training of an Artificial Neural Network. The structure of the dataset and the training process of the network was described. Two accurate algorithms for predicting the contact angle and the degree of resistance of silica-based coatings have been obtained. These algorithms have been successfully used for the preparation of an optimized superhydrophobic, abrasion-resistant, self-cleaning coating. Currently under patent evaluation, the coating shows a CA > 160° and no degradation in the CA after 8+ cycles of tape peeling. It has excellent potential for both

biomedical and general applications. The materials and preparation process cannot be disclosed at the time of writing. The main objective of this work was to obtain an abrasion-resistant superhydrophobic coating for biomedical and antibacterial applications. Using Artificial Neural Networks, it was possible to achieve this. Despite the excellent properties, the coatings cannot be used to develop biomedical devices yet, but show promising results for the development of external antibacterial surfaces. At the time of writing, there are no commercially available superhydrophobic surfaces used in hospital or biomedical settings to the author's knowledge. The developed coatings may pave the way for market entry of an antibacterial coating or material suitably modified for preparation in an industrial setting. Future perspectives are the industrial scaling of the preparation process and the application of the coating to fabricate antimicrobial surfaces.

Finally, two applications of Artificial Neural Networks carried out in parallel to the main project were discussed. In particular, promising results have been obtained from the NN-AMP software to design new antimicrobial peptides. The tool has been used to predict two selective sequences with antimicrobial activity against *Staphylococcus aureus*, currently under patent evaluation. The software selectivity prediction was in accord with the preliminary tests. The two peptides show low potency, but the showed selectivity is promising and prompts further improvements of the software application. The sequences will be used as potential lead compounds to develop new peptide antibiotics.

## References


1 Xu, Q., Zhang, W., Dong, C., Sreeprasad Theruvakkattil, S. & Xia, Z. Biomimetic self-cleaning surfaces: synthesis, mechanism and applications. *Journal of The Royal Society Interface* **13**, 20160300, doi:10.1098/rsif.2016.0300 (2016).

2 Barthlott, W. & Neinhuis, C. Purity of the sacred lotus, or escape from contamination in biological surfaces. *Planta* **202**, 1-8, doi:10.1007/s004250050096 (1997).

3 Nosonovsky, M. & Bhushan, B. Biologically Inspired Surfaces: Broadening the Scope of Roughness**. *Advanced Functional Materials* **18**, 843-855, doi:10.1002/adfm.200701195 (2008).

4 Guo, Z., Liu, W. & Su, B.-L. Superhydrophobic surfaces: From natural to biomimetic to functional. *Journal of Colloid and Interface Science* **353**, 335-355, doi:https://doi.org/10.1016/j.jcis.2010.08.047 (2011).

5 Bhushan, B., Jung, C. J. & Nosonovsky, M. in *Lotus Effect: Surfaces with Roughness-Induced Superhydrophobicity, Self-Cleaning, and Low Adhesion* (ed B. Bhushan) 1437-1524 (Springer, 2010).

6 Nuraje, N., Khan, W. S., Lei, Y., Ceylan, M. & Asmatulu, R. Superhydrophobic electrospun nanofibers. *Journal of Materials Chemistry A* **1**, 1929-1946, doi:10.1039/C2TA00189F (2013).

7 Howarter, J. A. & Youngblood, J. P. Self-Cleaning and Anti-Fog Surfaces via Stimuli-Responsive Polymer Brushes. *Advanced Materials* **19**, 3838-3843, doi:https://doi.org/10.1002/adma.200700156 (2007).

8 Ganesh, V. A., Raut, H. K., Nair, A. S. & Ramakrishna, S. A review on self-cleaning coatings. *Journal of Materials Chemistry* **21**, 16304-16322, doi:10.1039/C1JM12523K (2011).

9 Latthe, S. S., Terashima, C., Nakata, K., Sakai, M. & Fujishima, A. Development of sol–gel processed semi-transparent and self-cleaning superhydrophobic coatings. *Journal of Materials Chemistry A* **2**, 5548-5553, doi:10.1039/C3TA15017H (2014).

10 Ellinas, K., Tserepi, A. & Gogolides, E. Durable superhydrophobic and superamphiphobic polymeric surfaces and their applications: A review. *Advances in Colloid and Interface Science* **250**, 132-157, doi:https://doi.org/10.1016/j.cis.2017.09.003 (2017).

11 Li, Y., Zhang, Z., Wang, M., Men, X. & Xue, Q. Environmentally safe, substrate-independent and repairable nanoporous coatings: large-scale preparation, high transparency and antifouling properties. *Journal of Materials Chemistry A* **5**, 20277-20288, doi:10.1039/C7TA05112C (2017).

12 Pakdel, E., Wang, J., Kashi, S., Sun, L. & Wang, X. Advances in photocatalytic self-cleaning, superhydrophobic and electromagnetic interference shielding textile treatments. *Advances in Colloid and Interface Science* **277**, 102116, doi:https://doi.org/10.1016/j.cis.2020.102116 (2020).

13 Bhushan, B. & Jung, Y. C. Natural and biomimetic artificial surfaces for superhydrophobicity, self-cleaning, low adhesion, and drag reduction. *Progress in Materials Science* **56**, 1-108, doi:https://doi.org/10.1016/j.pmatsci.2010.04.003 (2011).

14 Chen, Y. *et al.* Fabrication and anti-corrosion property of superhydrophobic hybrid film on copper surface and its formation mechanism. *Surface and Interface Analysis* **41**, 872-877, doi:https://doi.org/10.1002/sia.3102 (2009).

15 Isimjan, T. T., Wang, T. & Rohani, S. M. F. A novel method to prepare superhydrophobic, UV resistance and anti-corrosion steel surface. *Chemical Engineering Journal*, doi:10.1016/j.cej.2012.08.090 (2012).

16 Wang, Y., Huang, Z., Gurney, R. S. & Liu, D. Superhydrophobic and photocatalytic PDMS/TiO2 coatings with environmental stability and multifunctionality. *Colloids and Surfaces A: Physicochemical and Engineering Aspects* **561**, 101-108, doi:https://doi.org/10.1016/j.colsurfa.2018.10.054 (2019).

17 Wei, Y., Hongtao, L. & Wei, Z. Preparation of anti-corrosion superhydrophobic coatings by an Fe-based micro/nano composite electro-brush plating and blackening process. *RSC Advances* **5**, 103000-103012, doi:10.1039/C5RA15640H (2015).

18 Zhang, B., Duan, J., Huang, Y. & Hou, B. Double layered superhydrophobic PDMS-Candle soot coating with durable corrosion resistance and thermal-mechanical robustness. *Journal of Materials Science & Technology* **71**, 1-11, doi:https://doi.org/10.1016/j.jmst.2020.09.011 (2021).

19 Boinovich, L. & Emelyanenko, A. Anti-icing Potential of Superhydrophobic Coatings. *Mendeleev Communications* **23**, 3–10, doi:10.1016/j.mencom.2013.01.002 (2013).

20 Latthe, S. S. *et al.* Recent developments in air-trapped superhydrophobic and liquid-infused slippery surfaces for anti-icing application. *Progress in Organic Coatings* **137**, 105373, doi:https://doi.org/10.1016/j.porgcoat.2019.105373 (2019).

21 Li, W., Zhan, Y. & Yu, S. Applications of superhydrophobic coatings in anti-icing: Theory, mechanisms, impact factors, challenges and perspectives. *Progress in Organic Coatings* **152**, 106117, doi:https://doi.org/10.1016/j.porgcoat.2020.106117 (2021).

22 Nguyen-Tri, P. *et al.* Recent progress in the preparation, properties and applications of superhydrophobic nano-based coatings and surfaces: A review. *Progress in Organic Coatings* **132**, 235-256, doi:https://doi.org/10.1016/j.porgcoat.2019.03.042 (2019).

23 Qu, B. *et al.* Preparation and Anti-Icing of Hydrophobic Polypyrrole Coatings on Wind Turbine Blade. *International Journal of Rotating Machinery* **2020**, 8626457, doi:10.1155/2020/8626457 (2020).

24 Chen, Y.-Y., Lin, Y.-H., Kung, C.-C., Chung, M.-H. & Yen, I. H. Design and Implementation of Cloud Analytics-Assisted Smart Power Meters Considering Advanced Artificial Intelligence as Edge Analytics in Demand-Side Management for Smart Homes. *Sensors (Basel)* **19**, 2047, doi:10.3390/s19092047 (2019).

25 Durán, I. R. & Laroche, G. Water drop-surface interactions as the basis for the design of anti-fogging surfaces: Theory, practice, and applications trends. *Advances in Colloid and Interface Science* **263**, 68-94, doi:https://doi.org/10.1016/j.cis.2018.11.005 (2019).

26 England, M. W., Urata, C., Dunderdale, G. J. & Hozumi, A. Anti-Fogging/Self-Healing Properties of Clay-Containing Transparent Nanocomposite Thin Films. *ACS Applied Materials & Interfaces* **8**, 4318-4322, doi:10.1021/acsami.5b11961 (2016).

27 Gan, W. Y. *et al.* Novel TiO2 thin film with non-UV activated superwetting and antifogging behaviours. *Journal of Materials Chemistry* **17**, 952-954, doi:10.1039/B618280A (2007).

28 Manakasettharn, S. *et al.* Transparent and superhydrophobic Ta2O5 nanostructured thin films. *Opt. Mater. Express* **2**, 214-221, doi:10.1364/OME.2.000214 (2012).

29 Banerjee, I., Pangule, R. C. & Kane, R. S. Antifouling coatings: recent developments in the design of surfaces that prevent fouling by proteins, bacteria, and marine organisms. *Adv Mater* **23**, 690-718, doi:10.1002/adma.201001215 (2011).

30 Ijaola, A. O., Farayibi, P. K. & Asmatulu, E. Superhydrophobic coatings for steel pipeline protection in oil and gas industries: A comprehensive review. *Journal of Natural Gas Science and Engineering* **83**, 103544, doi:https://doi.org/10.1016/j.jngse.2020.103544 (2020).

31 Liu, L. *et al.* Understanding the fouling/scaling resistance of superhydrophobic/omniphobic membranes in membrane distillation. *Desalination* **499**, 114864, doi:https://doi.org/10.1016/j.desal.2020.114864 (2021).

32 Chen, L. *et al.* Biomimetic surface coatings for marine antifouling: Natural antifoulants, synthetic polymers and surface microtopography. *Science of The Total Environment* **766**, 144469, doi:https://doi.org/10.1016/j.scitotenv.2020.144469 (2021).

33 Dalawai, S. P. *et al.* Recent Advances in durability of superhydrophobic self-cleaning technology: A critical review. *Progress in Organic Coatings* **138**, 105381, doi:https://doi.org/10.1016/j.porgcoat.2019.105381 (2020).

34 Das, S., Kumar, S., Samal, S. K., Mohanty, S. & Nayak, S. K. A Review on Superhydrophobic Polymer Nanocoatings: Recent Development and Applications. *Industrial & Engineering Chemistry Research* **57**, 2727-2745, doi:10.1021/acs.iecr.7b04887 (2018).

35 Chen, H., Shen, Y., He, Z., Wu, Z. & Xie, X. Facilely fabricating superhydrophobic coated-mesh materials for effective oil-water separation: Effect of mesh size towards various organic liquids. *Journal of Materials Science & Technology* **51**, 151-160, doi:https://doi.org/10.1016/j.jmst.2020.03.021 (2020).

36 Xue, Z., Cao, Y., Liu, N., Feng, L. & Jiang, L. Special wettable materials for oil/water separation. *Journal of Materials Chemistry A* **2**, 2445-2460, doi:10.1039/C3TA13397D (2014).

37 Meguid, S. A. & Elzaabalawy, A. Potential of combating transmission of COVID-19 using novel self-cleaning superhydrophobic surfaces: part I—protection strategies against fomites. *International Journal of Mechanics and Materials in Design* **16**, 423-431, doi:10.1007/s10999-020-09513-x (2020).

38 Elzaabalawy, A. & Meguid, S. A. Potential of combating transmission of COVID-19 using novel self-cleaning superhydrophobic surfaces: part II—thermal, chemical, and mechanical durability. *International Journal of Mechanics and Materials in Design* **16**, 433-441, doi:10.1007/s10999-020-09512-y (2020).

39 Balasubramaniam, B. *et al.* Antibacterial and Antiviral Functional Materials: Chemistry and Biological Activity toward Tackling COVID-19-like Pandemics. *ACS Pharmacology & Translational Science* **4**, 8-54, doi:10.1021/acsptsci.0c00174 (2021).

40 Hasan, J., Crawford, R. J. & Ivanova, E. P. Antibacterial surfaces: the quest for a new generation of biomaterials. *Trends in Biotechnology* **31**, 295-304, doi:https://doi.org/10.1016/j.tibtech.2013.01.017 (2013).

41 Dettre, R. H. & Johnson, R. E. in *Contact Angle, Wettability, and Adhesion* Vol. 43 *Advances in Chemistry* Ch. 8, 136-144 (AMERICAN CHEMICAL SOCIETY, 1964).

42 Moldoveanu, S. C. & David, V. in *Selection of the HPLC Method in Chemical Analysis* (eds Serban C. Moldoveanu & Victor David) 279-328 (Elsevier, 2017).

43 Yan, Y. Y., Gao, N. & Barthlott, W. Mimicking natural superhydrophobic surfaces and grasping the wetting process: A review on recent progress in preparing superhydrophobic surfaces. *Advances in Colloid and Interface Science* **169**, 80-105, doi:https://doi.org/10.1016/j.cis.2011.08.005 (2011).

44 Zhang, X., Wang, L. & Levanen, E. Superhydrophobic surfaces for the reduction of bacterial adhesion. *RSC Advances* **3**, 12003-12020, doi:10.1039/C3RA40497H (2013).

45 Lima, A. C. & Mano, J. F. Micro-/nano-structured superhydrophobic surfaces in the biomedical field: part I: basic concepts and biomimetic approaches. *Nanomedicine* **10**, 103-119, doi:10.2217/nnm.14.174 (2015).

46 Dash, S., Kumari, N. & Garimella, S. Characterization of ultrahydrophobic hierarchical surfaces fabricated using a single-step fabrication methodology. *Journal of Micromechanics and Microengineering* **21**, 105012, doi:10.1088/0960-1317/21/10/105012 (2011).

47 Long, C. J., Schumacher, J. F. & Brennan, A. B. Potential for Tunable Static and Dynamic Contact Angle Anisotropy on Gradient Microscale Patterned Topographies. *Langmuir* **25**, 12982-12989, doi:10.1021/la901836w (2009).

48 Good, R. J. A Thermodynamic Derivation of Wenzel's Modification of Young's Equation for Contact Angles; Together with a Theory of Hysteresis1. *Journal of the American Chemical Society* **74**, 5041-5042, doi:10.1021/ja01140a014 (1952).

49 Simpson, J., Hunter, S. & Aytug, T. Superhydrophobic materials and coatings: A review. *Reports on progress in physics. Physical Society (Great Britain)* **78**, 086501, doi:10.1088/0034-4885/78/8/086501 (2015).

50 Rioboo, R., Delattre, B., Duvivier, D., Vaillant, A. & De Coninck, J. Superhydrophobicity and liquid repellency of solutions on polypropylene. *Advances in Colloid and Interface Science* **175**, 1-10, doi:https://doi.org/10.1016/j.cis.2012.03.003 (2012).

51 Young, T. III. An essay on the cohesion of fluids. *Philosophical Transactions of the Royal Society of London* **95**, 65-87, doi:doi:10.1098/rstl.1805.0005 (1805).

52 Falde, E. J., Yohe, S. T., Colson, Y. L. & Grinstaff, M. W. Superhydrophobic materials for biomedical applications. *Biomaterials* **104**, 87-103, doi:https://doi.org/10.1016/j.biomaterials.2016.06.050 (2016).

53 Marmur, A. Wetting on Hydrophobic Rough Surfaces: To Be Heterogeneous or Not To Be? *Langmuir* **19**, 8343-8348, doi:10.1021/la0344682 (2003).

54 Bormashenko, E. Progress in understanding wetting transitions on rough surfaces. *Advances in Colloid and Interface Science* **222**, 92-103, doi:https://doi.org/10.1016/j.cis.2014.02.009 (2015).

55 Murakami, D., Jinnai, H. & Takahara, A. Wetting Transition from the Cassie–Baxter State to the Wenzel State on Textured Polymer Surfaces. *Langmuir* **30**, 2061-2067, doi:10.1021/la4049067 (2014).

56 Moulinet, S. & Bartolo, D. Life and death of a fakir droplet: Impalement transitions on superhydrophobic surfaces. *The European Physical Journal E* **24**, 251-260, doi:10.1140/epje/i2007-10235-y (2007).

57 Ciasca, G. *et al.* Recent advances in superhydrophobic surfaces and their relevance to biology and medicine. *Bioinspir Biomim* **11**, 011001, doi:10.1088/1748-3190/11/1/011001 (2016).

58 Zhang, Z.-h. *et al.* One-step fabrication of robust superhydrophobic and superoleophilic surfaces with self-cleaning and oil/water separation function. *Scientific Reports* **8**, 3869, doi:10.1038/s41598-018-22241-9 (2018).

59 Scarratt, L. R. J., Steiner, U. & Neto, C. A review on the mechanical and thermodynamic robustness of superhydrophobic surfaces. *Advances in Colloid and Interface Science* **246**, 133-152, doi:https://doi.org/10.1016/j.cis.2017.05.018 (2017).

60 Celia, E., Darmanin, T., Taffin de Givenchy, E., Amigoni, S. & Guittard, F. Recent advances in designing superhydrophobic surfaces. *Journal of Colloid and Interface Science* **402**, 1-18, doi:https://doi.org/10.1016/j.jcis.2013.03.041 (2013).

61 Biswas, A. *et al.* Advances in top–down and bottom–up surface nanofabrication: Techniques, applications & future prospects. *Advances in Colloid and Interface Science* **170**, 2-27, doi:https://doi.org/10.1016/j.cis.2011.11.001 (2012).

62 Kobina Sam, E. *et al.* Recent development in the fabrication of self-healing superhydrophobic surfaces. *Chemical Engineering Journal* **373**, 531-546, doi:https://doi.org/10.1016/j.cej.2019.05.077 (2019).

63 Zhang, X., Shi, F., Niu, J., Jiang, Y. & Wang, Z. Superhydrophobic surfaces: from structural control to functional application. *Journal of Materials Chemistry* **18**, 621-633, doi:10.1039/B711226B (2008).

64 Yilgor, I., Bilgin, S., Isik, M. & Yilgor, E. Facile preparation of superhydrophobic polymer surfaces. *Polymer* **53**, 1180-1188, doi:https://doi.org/10.1016/j.polymer.2012.01.053 (2012).

65 Gogolides, E., Ellinas, K. & Tserepi, A. Hierarchical micro and nano structured, hydrophilic, superhydrophobic and superoleophobic surfaces incorporated in microfluidics, microarrays and lab on chip microsystems. *Microelectronic Engineering* **132**, 135-155, doi:https://doi.org/10.1016/j.mee.2014.10.002 (2015).

66 Lima, A. C. & Mano, J. F. Micro/nano-structured superhydrophobic surfaces in the biomedical field: part II: applications overview. *Nanomedicine* **10**, 271-297, doi:10.2217/nnm.14.175 (2015).

67 Lichter, J. A., Van Vliet, K. J. & Rubner, M. F. Design of Antibacterial Surfaces and Interfaces: Polyelectrolyte Multilayers as a Multifunctional Platform. *Macromolecules* **42**, 8573-8586, doi:10.1021/ma901356s (2009).

68 Zhang, X.-F., Zhao, J.-P. & Hu, J.-M. Abrasion-Resistant, Hot Water-Repellent and Self-Cleaning Superhydrophobic Surfaces Fabricated by Electrophoresis of Nanoparticles in Electrodeposited Sol–Gel Films. *Advanced Materials Interfaces* **4**, 1700177, doi:10.1002/admi.201700177 (2017).

69 Genzer, J. & Efimenko, K. Recent developments in superhydrophobic surfaces and their relevance to marine fouling: a review. *Biofouling* **22**, 339-360, doi:10.1080/08927010600980223 (2006).

70 Crick, C. R., Ismail, S., Pratten, J. & Parkin, I. P. An investigation into bacterial attachment to an elastomeric superhydrophobic surface prepared via aerosol assisted deposition. *Thin Solid Films* **519**, 3722-3727, doi:https://doi.org/10.1016/j.tsf.2011.01.282 (2011).

71 Privett, B. J. *et al.* Antibacterial Fluorinated Silica Colloid Superhydrophobic Surfaces. *Langmuir : the ACS journal of surfaces and colloids* **27**, 9597-9601, doi:10.1021/la201801e (2011).

72 Zou, Y., Zhang, Y., Yu, Q. & Chen, H. Dual-function antibacterial surfaces to resist and kill bacteria: Painting a picture with two brushes simultaneously. *Journal of Materials Science & Technology* **70**, 24-38, doi:https://doi.org/10.1016/j.jmst.2020.07.028 (2021).

73 Chu, D. T. W. in *Annual Reports in Medicinal Chemistry* Vol. 33 (ed James A. Bristol) 141-150 (Academic Press, 1998).

74 Levy, S. B. & Marshall, B. Antibacterial resistance worldwide: causes, challenges and responses. *Nature Medicine* **10**, S122-S129, doi:10.1038/nm1145 (2004).

75 Piotto, S. *et al.* Novel antimicrobial polymer films active against bacteria and fungi. *Polym Compos* **34**, 1489-1492, doi:10.1002/pc.22410 (2013).

76 Piotto, S. *et al.* Synthesis and antimicrobial studies of new antibacterial azo-compounds active against staphylococcus aureus and listeria monocytogenes. *Molecules* **22**, doi:10.3390/molecules22081372 (2017).

77 Piotto, S., Di Biasi, L., Sessa, L. & Concilio, S. Transmembrane peptides as sensors of the membrane physical state. *Frontiers in Physics* **6**, 48, doi:https://doi.org/10.3389/fphy.2018.00048 (2018).

78 Concilio, S. *et al.* Structure modification of an active azo-compound as a route to new antimicrobial compounds. *Molecules* **22**, doi:10.3390/molecules22060875 (2017).
79 Concilio, S. *et al.* Biodegradable antimicrobial films based on poly(lactic acid) matrices and active azo compounds. *Journal of Applied Polymer Science* **132**, doi:10.1002/app.42357 (2015).
80 Clauss-Lendzian, E. *et al.* Stress response of a clinical Enterococcus faecalis isolate subjected to a novel antimicrobial surface coating. *Microbiological research* **207**, 53-64 (2018).
81 Gwisai, T. *et al.* Repurposing niclosamide as a versatile antimicrobial surface coating against device-associated, hospital-acquired bacterial infections. *Biomedical Materials* **12**, 045010 (2017).
82 Ren, T., Yang, M., Wang, K., Zhang, Y. & He, J. CuO Nanoparticles-Containing Highly Transparent and Superhydrophobic Coatings with Extremely Low Bacterial Adhesion and Excellent Bactericidal Property. *ACS Applied Materials and Interfaces* **10**, 25717-25725, doi:10.1021/acsami.8b09945 (2018).
83 Zhao, Q., Wang, S. & Müller-Steinhagen, H. Tailored surface free energy of membrane diffusers to minimize microbial adhesion. *Applied Surface Science* **230**, 371, doi:10.1016/j.apsusc.2004.02.052 (2004).
84 Callow, M. E. & Fletcher, R. L. The influence of low surface energy materials on bioadhesion — a review. *International Biodeterioration & Biodegradation* **34**, 333-348, doi:https://doi.org/10.1016/0964-8305(94)90092-2 (1994).
85 Pereni, C. I., Zhao, Q., Liu, Y. & Abel, E. Surface free energy effect on bacterial retention. *Colloids Surf B Biointerfaces* **48**, 143-147, doi:10.1016/j.colsurfb.2006.02.004 (2006).
86 Okada, A. *et al.* Inhibition of biofilm formation using newly developed coating materials with self-cleaning properties. *Dent Mater J* **27**, 565-572, doi:10.4012/dmj.27.565 (2008).
87 Raulio, M. *et al.* Microbe repelling coated stainless steel analysed by field emission scanning electron microscopy and physicochemical methods. *Journal of Industrial Microbiology & Biotechnology* **35**, 751-760, doi:10.1007/s10295-008-0343-8 (2008).
88 Ji, J. & Zhang, W. Bacterial behaviors on polymer surfaces with organic and inorganic antimicrobial compounds. *J Biomed Mater Res A* **88**, 448-453, doi:10.1002/jbm.a.31759 (2009).
89 Lee, J. H., Khang, G., Lee, J. W. & Lee, H. B. Interaction of Different Types of Cells on Polymer Surfaces with Wettability Gradient. *J Colloid Interface Sci* **205**, 323-330, doi:10.1006/jcis.1998.5688 (1998).
90 Arima, Y. & Iwata, H. Effect of wettability and surface functional groups on protein adsorption and cell adhesion using well-defined mixed self-assembled monolayers. *Biomaterials* **28**, 3074-3082, doi:10.1016/j.biomaterials.2007.03.013 (2007).
91 Stallard, C. P., McDonnell, K. A., Onayemi, O. D., O'Gara, J. P. & Dowling, D. P. Evaluation of protein adsorption on atmospheric plasma deposited coatings exhibiting superhydrophilic to superhydrophobic properties. *Biointerphases* **7**, 31, doi:10.1007/s13758-012-0031-0 (2012).
92 Koc, Y. *et al.* Nano-scale superhydrophobicity: suppression of protein adsorption and promotion of flow-induced detachment. *Lab on a Chip* **8**, 582-586, doi:10.1039/B716509A (2008).
93 Pernites, R. B. *et al.* Tunable Protein and Bacterial Cell Adsorption on Colloidally Templated Superhydrophobic Polythiophene Films. *Chemistry of Materials* **24**, 870-880, doi:10.1021/cm2007044 (2012).

94 Zhang, H., Lamb, R. & Lewis, J. Engineering nanoscale roughness on hydrophobic surface—preliminary assessment of fouling behaviour. *Science and Technology of Advanced Materials* **6**, 236-239, doi:10.1016/j.stam.2005.03.003 (2005).

95 Li, S. *et al.* Biomimetic superhydrophobic and antibacterial stainless-steel mesh via double-potentiostatic electrodeposition and modification. *Surface and Coatings Technology* **403**, 126355, doi:https://doi.org/10.1016/j.surfcoat.2020.126355 (2020).

96 Tang, M. *et al.* Inhibition of bacterial adhesion and biofilm formation by a textured fluorinated alkoxyphosphazene surface. *Bioactive Materials* **6**, 447-459, doi:https://doi.org/10.1016/j.bioactmat.2020.08.027 (2021).

97 Malavasi, I., Bernagozzi, I., Antonini, C. & Marengo, M. Assessing durability of superhydrophobic surfaces. *Surface Innovations* **3**, 49-60, doi:10.1680/si.14.00001 (2015).

98 Krogh, A. What are artificial neural networks? *Nature Biotechnology* **26**, 195-197, doi:10.1038/nbt1386 (2008).

99 Mitchell, T. M. *Machine Learning*. (McGraw-Hill, 1997).

100 Nilsson, N. J. *Learning machines*. (New York, 1965).

101 Alpaydin, E. *Introduction to Machine Learning (Fourth ed.)*. xix, 1–3, 13–18. (MIT, 2020).

102 Saba, T. Recent advancement in cancer detection using machine learning: Systematic survey of decades, comparisons and challenges. *Journal of Infection and Public Health* **13**, 1274-1289, doi:https://doi.org/10.1016/j.jiph.2020.06.033 (2020).

103 Noorbakhsh, J., Chandok, H., Karuturi, R. K. M. & George, J. Machine Learning in Biology and Medicine. *Advances in Molecular Pathology* **2**, 143-152, doi:https://doi.org/10.1016/j.yamp.2019.07.010 (2019).

104 van Assen, M., Lee, S. J. & De Cecco, C. N. Artificial intelligence from A to Z: From neural network to legal framework. *European Journal of Radiology* **129**, 109083, doi:https://doi.org/10.1016/j.ejrad.2020.109083 (2020).

105 Kim, E. *et al.* The Evolving Use of Electronic Health Records (EHR) for Research. *Seminars in Radiation Oncology* **29**, 354-361, doi:https://doi.org/10.1016/j.semradonc.2019.05.010 (2019).

106 Si, Y. *et al.* Deep representation learning of patient data from Electronic Health Records (EHR): A systematic review. *Journal of Biomedical Informatics*, 103671, doi:https://doi.org/10.1016/j.jbi.2020.103671 (2020).

107 Garcelon, N., Burgun, A., Salomon, R. & Neuraz, A. Electronic health records for the diagnosis of rare diseases. *Kidney International* **97**, 676-686, doi:https://doi.org/10.1016/j.kint.2019.11.037 (2020).

108 Chauhan, H., Bernick, J., Prasad, D. & Masand, V. in *Artificial Neural Network for Drug Design, Delivery and Disposition* (eds Munish Puri *et al.*) 15-27 (Academic Press, 2016).

109 Puri, M. *et al.* in *Artificial Neural Network for Drug Design, Delivery and Disposition* (eds Munish Puri *et al.*) 3-13 (Academic Press, 2016).

110 Zhang, L., Tan, J., Han, D. & Zhu, H. From machine learning to deep learning: progress in machine intelligence for rational drug discovery. *Drug Discov Today* **22**, 1680-1685, doi:10.1016/j.drudis.2017.08.010 (2017).

111 Lai, K., Twine, N., O'Brien, A., Guo, Y. & Bauer, D. in *Encyclopedia of Bioinformatics and Computational Biology* (eds Shoba Ranganathan, Michael Gribskov, Kenta Nakai, & Christian Schönbach) 272-286 (Academic Press, 2019).

112 Reker, D. Practical considerations for active machine learning in drug discovery. *Drug Discovery Today: Technologies* **32-33**, 73-79, doi:https://doi.org/10.1016/j.ddtec.2020.06.001 (2019).

113 Chan, H. C. S., Shan, H., Dahoun, T., Vogel, H. & Yuan, S. Advancing Drug Discovery via Artificial Intelligence. *Trends Pharmacol Sci* **40**, 592-604, doi:10.1016/j.tips.2019.06.004 (2019).

114 Yang, G. R. & Wang, X.-J. Artificial Neural Networks for Neuroscientists: A Primer. *Neuron* **107**, 1048-1070, doi:https://doi.org/10.1016/j.neuron.2020.09.005 (2020).

115 Muehlematter, U. J., Daniore, P. & Vokinger, K. N. Approval of artificial intelligence and machine learning-based medical devices in the USA and Europe (2015–20): a comparative analysis. *The Lancet Digital Health*, doi:https://doi.org/10.1016/S2589-7500(20)30292-2 (2021).

116 Goecks, J., Jalili, V., Heiser, L. M. & Gray, J. W. How Machine Learning Will Transform Biomedicine. *Cell* **181**, 92-101, doi:https://doi.org/10.1016/j.cell.2020.03.022 (2020).

117 Cholewinski, A., Trinidad, J., McDonald, B. & Zhao, B. Bio-inspired polydimethylsiloxane-functionalized silica particles - epoxy bilayer as a robust superhydrophobic surface coating. *Surface and Coatings Technology* **254**, 230-237, doi:https://doi.org/10.1016/j.surfcoat.2014.06.020 (2014).

118 Jamshidian, M., Tehrany, E. A., Imran, M., Jacquot, M. & Desobry, S. Poly-Lactic Acid: Production, Applications, Nanocomposites, and Release Studies. *Comprehensive Reviews in Food Science and Food Safety* **9**, 552-571, doi:10.1111/j.1541-4337.2010.00126.x (2010).

119 Miller, K., Hsu, J. E. & Soslowsky, L. J. in *Comprehensive Biomaterials* (ed Paul Ducheyne) 257-279 (Elsevier, 2011).

120 Luo, Y., Baldamus, J. & Hou, Z. Scandium Half-Metallocene-Catalyzed Syndiospecific Styrene Polymerization and Styrene−Ethylene Copolymerization: Unprecedented Incorporation of Syndiotactic Styrene−Styrene Sequences in Styrene−Ethylene Copolymers. *Journal of the American Chemical Society* **126**, 13910-13911, doi:10.1021/ja046063p (2004).

121 Matyjaszewski, K. in *Comprehensive Polymer Science and Supplements* (eds Geoffrey Allen & John C. Bevington) 639-671 (Pergamon, 1989).

122 Abenojar, J., Torregrosa-Coque, R., Martínez, M. A. & Martín-Martínez, J. M. Surface modifications of polycarbonate (PC) and acrylonitrile butadiene styrene (ABS) copolymer by treatment with atmospheric plasma. *Surface and Coatings Technology* **203**, 2173-2180, doi:https://doi.org/10.1016/j.surfcoat.2009.01.037 (2009).

123 Mukherjee, P., Rani, A. & Saravanan, P. in *3D Printing Technology in Nanomedicine* (eds Nabeel Ahmad, P. Gopinath, & Rajiv Dutta) 63-81 (Elsevier, 2019).

124 Landrock, A. H. in *Handbook of Plastic Foams* (ed Arthur H. Landrock) 221-245 (William Andrew Publishing, 1995).

125 Campo, E. A. in *Selection of Polymeric Materials* (ed E. Alfredo Campo) 1-39 (William Andrew Publishing, 2008).

126 Wehrmann, R. in *Encyclopedia of Materials: Science and Technology* (eds K. H. Jürgen Buschow *et al.*) 7149-7151 (Elsevier, 2001).

127 Pham, H. Q. M., Maurice J. . in *Ullmann's Encyclopedia of Industrial Chemistry* (2005).

128 May, C. *Epoxy Resins : Chemistry and Technology, Second Edition*. (Routledge, 2018).

129 Jolanki, R., Kanerva, L. & Estlander, T. in *Condensed Handbook of Occupational Dermatology* (eds Lasse Kanerva, Peter Elsner, Jan E. Wahlberg, & Howard I. Maibach) 347-363 (Springer Berlin Heidelberg, 2004).

130 Lopattananon, N., Payae, Y. & Seadan, M. Influence of fiber modification on interfacial adhesion and mechanical properties of pineapple leaf fiber-epoxy

composites. *Journal of Applied Polymer Science* **110**, 433-443, doi:10.1002/app.28496 (2008).

131 Wu, C.-C. & Lee, W.-J. Synthesis and properties of copolymer epoxy resins prepared from copolymerization of bisphenol A, epichlorohydrin, and liquefied Dendrocalamus latiflorus. *Journal of Applied Polymer Science* **116**, 2065-2073, doi:10.1002/app.31703 (2010).

132 Dorsey, J. G., Dorsey, G. F., Rutenberg, A. C. & Green, L. A. Determination of the epoxide equivalent weight of glycidyl ethers by proton magnetic resonance spectrometry. *Analytical Chemistry* **49**, 1144-1145, doi:10.1021/ac50016a020 (1977).

133 Pramanik, M., Mendon, S. K. & Rawlins, J. W. Determination of epoxy equivalent weight of glycidyl ether based epoxides via near infrared spectroscopy. *Polymer Testing* **31**, 716-721, doi:https://doi.org/10.1016/j.polymertesting.2012.04.004 (2012).

134 Shechter, L. & Wynstra, J. Glycidyl Ether Reactions with Alcohols, Phenols, Carboxylic Acids, and Acid Anhydrides. *Industrial & Engineering Chemistry* **48**, 86-93, doi:10.1021/ie50553a028 (1956).

135 Horie, K., Hiura, H., Sawada, M., Mita, I. & Kambe, H. Calorimetric investigation of polymerization reactions. III. Curing reaction of epoxides with amines. *Journal of Polymer Science Part A-1: Polymer Chemistry* **8**, 1357-1372, doi:10.1002/pol.1970.150080605 (1970).

136 Shechter, L., Wynstra, J. & Kurkjy, R. P. Glycidyl Ether Reactions with Amines. *Industrial & Engineering Chemistry* **48**, 94-97, doi:10.1021/ie50553a029 (1956).

137 Tang, L. & Cheng, J. Nonporous Silica Nanoparticles for Nanomedicine Application. *Nano today* **8**, 290-312, doi:10.1016/j.nantod.2013.04.007 (2013).

138 Huang, R. *et al.* Mesoporous silica nanoparticles: facile surface functionalization and versatile biomedical applications in oncology. *Acta Biomaterialia* **116**, 1-15, doi:https://doi.org/10.1016/j.actbio.2020.09.009 (2020).

139 Taleghani, A. S. *et al.* Mesoporous silica nanoparticles as a versatile nanocarrier for cancer treatment: A review. *Journal of Molecular Liquids* **328**, 115417, doi:https://doi.org/10.1016/j.molliq.2021.115417 (2021).

140 Abeer, M. M. *et al.* Silica nanoparticles: A promising platform for enhanced oral delivery of macromolecules. *Journal of Controlled Release* **326**, 544-555, doi:https://doi.org/10.1016/j.jconrel.2020.07.021 (2020).

141 Karnati, S. R., Agbo, P. & Zhang, L. Applications of silica nanoparticles in glass/carbon fiber-reinforced epoxy nanocomposite. *Composites Communications* **17**, 32-41, doi:https://doi.org/10.1016/j.coco.2019.11.003 (2020).

142 Yuan, J., Zhou, S., You, B. & Wu, L. Organic Pigment Particles Coated with Colloidal Nano-Silica Particles via Layer-by-Layer Assembly. *Chemistry of Materials* **17**, 3587-3594, doi:10.1021/cm048000b (2005).

143 Khajeh, M., Laurent, S. & Dastafkan, K. Nanoadsorbents: Classification, Preparation, and Applications (with Emphasis on Aqueous Media). *Chemical Reviews* **113**, 7728-7768, doi:10.1021/cr400086v (2013).

144 Bravo, J., Zhai, L., Wu, Z., Cohen, R. E. & Rubner, M. F. Transparent Superhydrophobic Films Based on Silica Nanoparticles. *Langmuir* **23**, 7293-7298, doi:10.1021/la070159q (2007).

145 Nguyen, N.-T. in *Micromixers (Second Edition)* (ed Nam-Trung Nguyen) 113-161 (William Andrew Publishing, 2012).

146 Wu, X. *et al.* Preparation of superamphiphobic polymer-based coatings via spray- and dip-coating strategies. *Progress in Organic Coatings* **90**, 463-471, doi:https://doi.org/10.1016/j.porgcoat.2015.08.008 (2016).

147 Amokrane, G., Falentin-Daudré, C., Ramtani, S. & Migonney, V. A Simple Method to Functionalize PCL Surface by Grafting Bioactive Polymers Using UV Irradiation. *IRBM* **39**, doi:10.1016/j.irbm.2018.07.002 (2018).

148 Strawbridge, I. & James, P. F. Thin silica films prepared by dip coating. *Journal of Non-Crystalline Solids* **82**, 366-372, doi:https://doi.org/10.1016/0022-3093(86)90153-5 (1986).

149 Neacşu, I. A., Nicoară, A. I., Vasile, O. R. & Vasile, B. Ş. in *Nanobiomaterials in Hard Tissue Engineering* (ed Alexandru Mihai Grumezescu) 271-295 (William Andrew Publishing, 2016).

150 Avrămescu, R.-E., Ghica, M. V., Dinu-Pîrvu, C., Prisada, R. & Popa, L. Superhydrophobic Natural and Artificial Surfaces-A Structural Approach. *Materials (Basel, Switzerland)* **11**, 866, doi:10.3390/ma11050866 (2018).

151 Tasaltin, N., Sanli, D., Jonáš, A., Kiraz, A. & Erkey, C. Preparation and characterization of superhydrophobic surfaces based on hexamethyldisilazane-modified nanoporous alumina. *Nanoscale Research Letters* **6**, 487, doi:10.1186/1556-276X-6-487 (2011).

152 Neumann, A. W. & Good, R. J. in *Surface and Colloid Science: Volume 11: Experimental Methods* (eds Robert J. Good & Robert R. Stromberg) 31-91 (Springer US, 1979).

153 Vafaei, S. & Podowski, M. Z. Analysis of the relationship between liquid droplet size and contact angle. *Advances in Colloid and Interface Science* **113**, 133-146, doi:https://doi.org/10.1016/j.cis.2005.03.001 (2005).

154 Zholob, S. A., Makievski, A. V., Miller, R. & Fainerman, V. B. Optimisation of calculation methods for determination of surface tensions by drop profile analysis tensiometry. *Advances in Colloid and Interface Science* **134-135**, 322-329, doi:https://doi.org/10.1016/j.cis.2007.04.011 (2007).

155 McMullan, D. Scanning electron microscopy 1928–1965. *Scanning* **17**, 175-185, doi:10.1002/sca.4950170309 (1995).

156 McMullan, D. in *Biological Low-Voltage Scanning Electron Microscopy* (eds Heide Schatten & James B. Pawley) 1-25 (Springer New York, 2008).

157 Ryntz, R. A. & Britz, D. Scratch resistance behavior of automotive plastic coatings. *Journal of Coatings Technology* **74**, 77-81, doi:10.1007/BF02720152 (2002).

158 Browning, R. L., Jiang, H. & Sue, H.-J. in *Tribology and Interface Engineering Series* Vol. 55 (eds Klaus Friedrich & Alois K. Schlarb) 354-373 (Elsevier, 2008).

159 Heavens, O. S. Some factors influencing the adhesion of films produced by vacuum evaporation. *J. Phys. Radium* **11**, 355-360 (1950).

160 Randall, N. X. The current state-of-the-art in scratch testing of coated systems. *Surface and Coatings Technology* **380**, 125092, doi:https://doi.org/10.1016/j.surfcoat.2019.125092 (2019).

161 Drdácký, M. *et al.* Standardization of peeling tests for assessing the cohesion and consolidation characteristics of historic stone surfaces. *Materials and Structures* **45**, 505-520, doi:10.1617/s11527-011-9778-x (2012).

162 Slížková, Z. & Drdácký, M. Enhanced affordable methods for assessing material characteristics and consolidation effects on stone and mortar. *Journal of Geophysics and Engineering* **10**, doi:10.1088/1742-2132/10/6/064005 (2013).

163 Wang, X. *et al.* Superhydrophobic candle soot/PDMS substrate for one-step enrichment and desalting of peptides in MALDI MS analysis. *Talanta* **190**, 23-29, doi:https://doi.org/10.1016/j.talanta.2018.07.066 (2018).

164 Li, L., Zhu, J. & Zeng, Z. A sky-blue superhydrophobic coating and applications. *Progress in Organic Coatings* **147**, 105863, doi:https://doi.org/10.1016/j.porgcoat.2020.105863 (2020).

165 Hydrophobic Coating Market Size & Forecast by Property (Anti-Microbial, Anti-Icing/Wetting, Anti-Fouling, Anti-Corrosion, Self-Cleaning), by Application (Aerospace, Automotive, Construction, Medical, Optical), by Region and Trend Analysis from 2014 To 2025, 2016. Grand View Research. http://www.grandviewresearch.com/industry-analysis/hydrophobic-coating-market.

166 The Global Market for Anti-Microbial, Anti-Viral, and Anti-Fungal Nanocoatings 2021. Future Markets, Inc. https://www.globenewswire.com/news-release/2020/05/18/2034825/0/en/Demand-for-Antimicrobial-and-Anti-Viral-Nanocoatings-Post-COVID-19-Pandemic.html.

167 Antimicrobial Coatings Market Size, Share & Trends Analysis Report By Product (Surface Modification & Coatings, Antimicrobial Powder), By Application (Medical Devices, Mold Remediation), And Segment Forecasts, 2020 - 2027. Grand View Research. https://www.grandviewresearch.com/industry-analysis/antimicrobial-coatings-market.

168 *http://www.smartvase.unisa.it/*.

169 Russell, S. J. *Artificial intelligence: a modern approach*. (Pearson, 2016).

170 Rumelhart, D. E., Hinton, G. E. & Williams, R. J. Learning representations by back-propagating errors. *Nature* **323**, 533-536, doi:10.1038/323533a0 (1986).

171 Cort, J. W. & Kenji, M. Advantages of the mean absolute error (MAE) over the root mean square error (RMSE) in assessing average model performance. *Climate Research* **30**, 79-82 (2005).

172 Skovgaard, L. T. Applied regression analysis. 3rd edn. N. R. Draper and H. Smith, Wiley, New York, 1998. No. of pages: xvii+706. Price: £45. ISBN 0-471-17082-8. *Statistics in Medicine* **19**, 3136-3139, doi:https://doi.org/10.1002/1097-0258(20001130)19:22<3136::AID-SIM607>3.0.CO;2-Q (2000).

173 Heinisch, O. Steel, R. G. D., and J. H. Torrie: Principles and Procedures of Statistics. (With special Reference to the Biological Sciences.) McGraw-Hill Book Company, New York, Toronto, London 1960, 481 S., 15 Abb.; 81 s 6 d. *Biometrische Zeitschrift* **4**, 207-208, doi:https://doi.org/10.1002/bimj.19620040313 (1962).

174 *SPSS tutorials, Kent State University. https://libguides.library.kent.edu/SPSS.*

175 *https://gmdhsoftware.com/ Copyright 2009-2021 © GMDH Inc.*

176 Anastasakis, L. & Mort, N. The development of self-organization techniques in modelling: a review of the group method of data handling (GMDH). *RESEARCH REPORT-UNIVERSITY OF SHEFFIELD DEPARTMENT OF AUTOMATIC CONTROL AND SYSTEMS ENGINEERING* (2001).

177 Ivakhnenko, A. G. & Ivakhnenko, G. A. The Review of Problems Solvable by Algorithms of the Group Method of Data Handling (GMDH). *Pattern Recognition and Image Analysis* **5**, 527-535 (1995).

178 Schmidhuber, J. Deep learning in neural networks: An overview. *Neural Networks* **61**, 85-117, doi:https://doi.org/10.1016/j.neunet.2014.09.003 (2015).

179 Ikeda, S., Sawaragi, Y. & Ochiai, M. Sequential GMDH Algorithm and Its Application to River Flow Prediction. *IEEE Transactions on Systems, Man and Cybernetics* **6**, 473-479, doi:10.1109/TSMC.1976.4309532 (1976).

180 Kondo, T. in *Proceedings of the SICE Annual Conference.* 1143-1148.

181 Kondo, T. & Ueno, J. Multi-layered GMDH-type neural network self-selecting optimum neural network architecture and its application to 3-dimensional medical image recognition of blood vessels. *International Journal of Innovative Computing, Information and Control* **4**, 175-187 (2008).

182 Witczak, M., Korbicz, J., Mrugalski, M. & Patton, R. J. A GMDH neural network-based approach to robust fault diagnosis: Application to the DAMADICS benchmark

problem. *Control Engineering Practice* **14**, 671-683, doi:https://doi.org/10.1016/j.conengprac.2005.04.007 (2006).

183 Kordik, P., Naplava, P., Snorek, M. & Berezovskyj, M. Modified GMDH method and models quality evaluation by visualization. *Control Systems and Computers* **2**, 68-75 (2003).

184 *https://www.softmining.it/*.

185 Sierra, J. M., Fusté, E., Rabanal, F., Vinuesa, T. & Viñas, M. An overview of antimicrobial peptides and the latest advances in their development. *Expert Opinion on Biological Therapy* **17**, 663-676, doi:10.1080/14712598.2017.1315402 (2017).

186 Li, S. *et al.* The structure-mechanism relationship and mode of actions of antimicrobial peptides: A review. *Trends in Food Science & Technology* **109**, 103-115, doi:https://doi.org/10.1016/j.tifs.2021.01.005 (2021).

187 Liu, Y. *et al.* The revitalization of antimicrobial peptides in the resistance era. *Pharmacological Research* **163**, 105276, doi:https://doi.org/10.1016/j.phrs.2020.105276 (2021).

188 Morris, A., Kellner, J. D. & Low, D. E. The superbugs: evolution, dissemination and fitness. *Current Opinion in Microbiology* **1**, 524-529, doi:https://doi.org/10.1016/S1369-5274(98)80084-2 (1998).

189 Piotto, S. P., Sessa, L., Concilio, S. & Iannelli, P. YADAMP: yet another database of antimicrobial peptides. *Int J Antimicrob Agents* **39**, 346-351, doi:10.1016/j.ijantimicag.2011.12.003 (2012).

190 Huang, Y. *et al.* Role of helicity of α-helical antimicrobial peptides to improve specificity. *Protein Cell* **5**, 631-642, doi:10.1007/s13238-014-0061-0 (2014).

191 McKinnon, P. S. & Davis, S. L. Pharmacokinetic and Pharmacodynamic Issues in the Treatment of Bacterial Infectious Diseases. *European Journal of Clinical Microbiology and Infectious Diseases* **23**, 271-288, doi:10.1007/s10096-004-1107-7 (2004).

192 *https://www.ebi.ac.uk/patentdata/*.

193 Jayachandran, G., Shirts, M. R., Park, S. & Pande, V. S. Parallelized-over-parts computation of absolute binding free energy with docking and molecular dynamics. *The Journal of Chemical Physics* **125**, 084901, doi:10.1063/1.2221680 (2006).

194 Griffen, E. J., Dossetter, A. G., Leach, A. G. & Montague, S. Can we accelerate medicinal chemistry by augmenting the chemist with Big Data and artificial intelligence? *Drug Discov Today* **23**, 1373-1384, doi:10.1016/j.drudis.2018.03.011 (2018).

195 Sai Prasad, K., Subhash Chander, O., Prabhakar Reddy, G. & Gururaj, S. Artificial Intelligence approach for Classifying Molecular Dataset using Density based technique with appropriate Euclidean Distance measure. *Materials Today: Proceedings* **4**, 8827-8836, doi:https://doi.org/10.1016/j.matpr.2017.07.233 (2017).

196 García-Godoy, M. J. *et al.* Bio-inspired optimization for the molecular docking problem: State of the art, recent results and perspectives. *Applied Soft Computing* **79**, 30-45, doi:https://doi.org/10.1016/j.asoc.2019.03.044 (2019).

197 Kumar, S., Rulhania, S., Jaswal, S. & Monga, V. Recent advances in the medicinal chemistry of carbonic anhydrase inhibitors. *European Journal of Medicinal Chemistry* **209**, 112923, doi:https://doi.org/10.1016/j.ejmech.2020.112923 (2021).

**List of Abbreviations**

| | |
|---|---|
| aa | Amino acid |
| ABS | Acrylonitrile Butadiene Styrene |
| AHEW | Amine hydrogen equivalent weight |
| AI | Artificial Intelligence |
| AI | Artificial Intelligence |
| AMP | Antimicrobial peptide |
| ANN | Artificial Neural Network |
| CA | Contact Angle |
| CSV | Comma separated values |
| DCM | Dichloromethane |
| DGEBA | Bisphenol-A diglycidyl ether |
| DL | Deep Learning |
| DMAC | Dimethylacetamide |
| EEW | Epoxy equivalent weight |
| GMDH | Group Method of Data Handling |
| MAE | Mean absolute error |
| MIC | Minimal inhibitory concentration |
| ML | Machine Learning |
| PC/ABS | Polycarbonate/Acrylonitrile Butadiene Styrene |
| PDMS | Polydimethylsiloxane |
| phr | Parts per hundred of resin |
| PLA | Polylactic Acid |
| PS | Polystyrene |
| $R^2$ | Coefficient of determination |
| SH | Superhydrophobic |
| SNPs | Silica Nanoparticles |
| THF | Tetrahydrofuran |